ABSORBENT FIBERS MANUFACTURED FROM POLYACRYLONITRILE AND SILK

LEE KA I

Ph.D

The Hong Kong Polytechnic University

2016

The Hong Kong Polytechnic University

Institute of Textiles and Clothing

Absorbent Fibers Manufactured from Polyacrylonitrile and Silk

Lee Ka I

A thesis submitted in partial fulfillment of the requirements

for the degree of Doctor of Philosophy

September 2015

CERTIFICATION OF ORIGINALITY

I hereby declare that this thesis is my own work and that, to the best of my knowledge and belief, it reproduces no material previously published or written, nor material that has been accepted for the award of any other degree or diploma, except where due acknowledgement has been made in the text.

(Signed)

Lee Ka I (Name of student)

Abstract

Nowadays, textile materials are used as clothing as well as other advanced applications. For an example, polyacrylonitrile (PAN) is the main component of acrylic fibers and the main precursor for carbon fibers. Inspired by this concept, various preparation methods were explored to improve the water absorbency of textile materials and hence widen their applications.

PAN, which is the main component of acrylic fibers, was selected to prepare the superabsorbent hydrogel. Facile and versatile electrospinning was employed to fabricate the PAN nanofibers as a nonwoven web. Further oxidative heat treatment was applied to stabilize the structure of PAN nanofibers. This stabilized structure was studied in depth by several characterization methods. The relative rate of three main reactions—dehydrogenation, cyclization and carbonylation—was investigated and revealed by Fourier transform infrared spectroscopy. The resultant PAN nanofibers were crosslinked that was confirmed by the gel fraction obtained from soxhlet extraction in DMF and the fiber integrity retained after alkaline hydrolysis. The heated PAN electrospun web was subsequently hydrolyzed in an alkaline solution to produce hydrogel. Oxidative stabilization plays a crucial role in maintaining the integrity of PAN nanofibers under harsh alkaline hydrolysis condition. The resultant hydrogel with highly interconnected three-dimensional pore network was obtained. Due to the

formation of solubilizing groups and porous structure, the obtained hydrogel achieved both remarkable water absorption ratio and rate. The optimized hydrogels absorbed over 100 g/g within 1 min, making them to be useful in drug delivery systems and personal care products.

Silk, which is another common natural textile fiber, was modified by in situ polymerization of two monomers acrylamide and sodium acrylate after swelling in 4.65 M lithium bromide solution. Because of its high swelling degree in LiBr as observed under optical microscope, these two synthetic monomers were able to penetrate into silk yarn. X-ray diffraction suggested the conformational changes of silk in 4.65 M LiBr, while dissolution test and Fourier transform infrared spectroscopy confirmed the formation of interpenetrating synthetic polymer network. An interesting ladder structure was observed in between the adjacent filaments of modified silk yarns. These modified silk yarns showed improvement in water absorption and mechanical property in both dry and wet states. The water absorption ratio of silk yarn modified by sodium acrylate achieved 7.6 g/g that was 9 times higher than that of raw silk yarn. This novel modified silk also showed low cytotoxicity towards skin keratinocytes, being promising in biomedical textiles such as wound dressings and sutures.

Moreover, another effective approach to modify silk fiber via environmentally friendly photoredox catalysis was introduced. In this study, the photocatalyst tris(2,2′-bipyridyl)dichlororuthenium(II) hexahydrate was

employed. This green chemical reaction was able to induce the crosslinking of the tyrosyl in silk protein under visible light at room temperature; meanwhile, it was found to be useful in initiating the polymerization of sodium acrylate. This photocatalyst system is beneficial to silk fiber modification through crosslinking and polymerization. The modified silk fibers displayed enhancement in water absorption that achieved at least 4 times higher than that of the control silk fiber. These modified silks were ready to be woven or knitted into fabrics, having potentials in biomedical textiles like wound dressings and dermal sealants.

To conclude, the water absorbency of two common textile materials PAN and silk has been successfully improved via various routes demonstrated in this study. These modification methods can be fully utilized in the textile materials which their applications are hence broadened.

Publications

Academic Journal Papers

1. Lee, K. I; Li, J. H.; Fei, B.; Xin, J. H. Mechanism study of heat stabilization of polyacrylonitrile nanofibers against alkaline hydrolysis. *Polym. Degrad. Stabil.* **2014**, 105, 80-85.
2. Lu, X. K.; Chan, C. Y.; Lee, K. I.; Ng, P. F.; Fei, B.; Xin, J. H.; Fu, J. Super-tough and thermo-healable hydrogel – promising for shape-memory absorbent fiber. *J. Mater. Chem. B* **2014**, 2, 7631-7638.
3. Li, J. H.; Lee, K. I; Lu, X. K.; Bao, S. P.; Hua, T.; Xin, J. H.; Fei, B. In-situ growth of pine-needle-like tungsten oxide nanowire arrays on carbon nanofibers. *Mater. Lett.* **2013**, 99, 131-133.
4. Lee, K. I; Cheng, H. M.; Yung, K. F.; Fei, B.; Xin, J. H. Structures and properties of fast swelling superabsorbent hydrogels converted from nanofibers (submitted)
5. Highly water-absorbing silk yarn with interpenetrating network via in situ polymerization (in preparation)

Conference Papers

1. Lee, K. I; Li, J. H.; Fei, B.; Xin, J. H. Superabsorbent nanofibers from PAN. In *The 41st Textile Research Symposium*, Guimaraes, Portugal, September 2012.

2. Lu, X. K.; Lee, K.I; Li, J. H.; Ng, P. F.; Fei, B.; Xin, J. H. Highly elastic and tough hydrogels for absorbent fibers. In *Proceedings of 12th Asian Textile Conference*, Shanghai, China, October 2013.
3. Lee, K. I; Lu, X. K.; Fei, B.; Xin, J. H. Absorbent yarns from silk by in situ polymerization. In *Textile Bioengineering and Informatics Symposium*, Hong Kong, August 2014.

Acknowledgements

I would like to express my sincerest gratitude to my chief supervisor Dr. Bin Fei for providing a precious opportunity for my Ph.D. study. Without his constant guidance, invaluable advice, and patience, this study would not have been completed. He has taught me how to develop the research from inspiration into action and provided me an invaluable research experience.

I would like to thank my co-supervisors Prof. John H. Xin and Dr. Ka-fu Yung for their constructive feedback, technical support, and encouragement throughout my research work.

I am very grateful to all my colleagues, Dr. Sijie Shao, Dr. Liang He, Dr. Liping Si, Mr. Xinkun Lu, Mr. Jianhua Li, Mr. Xiaowen Wang, Mr. Lin Luo, Miss Joanne Ng, Miss Heman Cheng and Miss Vicky Chan for their kindly help. Thanks for my friends Miss Supannee Boonroeng, Miss Christie Ng, Miss Car Tsang and Miss Vicky So who also fought for their Ph.D. study. Thanks for all your kindness and friendly support during the tough time.

Last but not least, I would like to give my sincere thanks to my parents and family members for their understanding, love, and support throughout my life so that I can overcome all the difficulties.

Table of Contents

CHAPTER 4

Preparation of superabsorbent hydrogel from polyacrylonitrile nanofibers

CHAPTER 6

Photo-induced crosslinking of silk fibers

CHAPTER 7

Photo-induced crosslinking and sodium acrylate polymerization on silk fiber

List of Figures

List of Schemes

List of Tables

List of Symbols and Abbreviations

AFM	atomic force microscope
Am	acrylamide
APS	ammonium persulfate
DI	deionized
DMF	dimethylformamide
FE-SEM	field-emission scanning electron microscope
FTIR	Fourier transform infrared
HPAN	hydrolyzed polyacrylonitrile
HSPAN	hydrolyzed starch-*graft*-polyacrylonitrile
IPN	interpenetrating polymer network
LiBr	Lithium bromide
MBAAm	*N,N'*-methylene bisacrylamide
MLCT	metal-to-ligand charge transfer
M_W	molecular weight
NaA	sodium acrylate
NaOH	sodium hydroxide
OM	optical microscope
PAN	polyacrylonitrile
PTFE	polytetrafluoroethylene
Q	absorption ratio
$Ru(bpy)_3^{2+}$	tris(2,2′-bipyridyl)dichlororuthenium(II) hexahydrate
SAF	superabsorbent fiber
SAP	superabsorbent polymer
semi-IPN	semi-interpenetrating network
SF	silk fibroin
TGA	thermogravimetric analyzer

Tyr	tyrosine
wt%	weight percentage
XRD	X-ray diffraction
p	capillary pressure
r	rocking
δ	bending
η	fluid viscosity
L	wetted length of the tubes
t	time
γ	surface tension of the liquid
θ	contact angle at the liquid at the liquid-solid-air interface
r_c	capillary radius/ pore size

Chapter 1

Introduction

1.1 Research background

Thousands of years ago, natural fibers from plants and animals have been widely used as textile materials for keeping us warm and protecting our body. As time goes on, these textile materials are inadequate to meet our needs. Hence, man-made and regenerated fibers have been invented to compensate the deficiencies of these natural fibers. Technology keeps moving forward, for an example, the common textile material polyacrylonitrile (PAN) is the main precursor to produce the lightweight and high tensile strength carbon fiber. Therefore, an idea of producing functional and advanced materials from the common textile materials is suggested in order to raise their functionality that favors wider applications.

Two common textile materials—man-made acrylic fiber and natural silk fiber—have been selected for this study. An acrylonitrile is a commercially available and low-cost raw material for acrylic fiber that is light-weighted, soft handle, and capable of keeping warm. In the textile industry, it is one of the important synthetic polymers since it has a vast range of applications like clothing and upholster. Besides textiles, it is also another intriguing raw material for preparing the superabsorbents. During 1970s, the Northern Regional Research

Laboratory of U.S. Department of Agriculture developed a superabsorbent from the hydrolyzed starch-*g*-polyacrylonitrile that finally aroused the interests of the public. Afterward, this superabsorbent has been gradually modified and further processed into commercial products including baby diapers, adult incontinence products, surgical dressings, food packaging, performance textiles, and agriculture applications.

Up-to-date, the superabsorbents produced from PAN have been prepared mainly by three methods including graft polymerization, physical blending and direct alkaline hydrolysis on the surface. However, these prepared superabsorbents are mainly in granular form and only partially hydrolyzed. It is difficult to process into commercial products and highly limits the water absorption performance. In order to accelerate the reaction rate and shorten the processing time, electrospinning has been chosen to prepare the PAN nanofibers with exceedingly high surface-area-to-volume ratio. The as-electrospun PAN nanofibers are a nonwoven web that can be easily assembled into products. The heat treatment in the presence of oxygen enables the stabilization and crosslinking of the PAN electrospun web. Fine control of this oxidative stabilization stage is crucial for the success of the post-treatment, that is, alkaline hydrolysis. The stabilization kinetics of PAN nanofibers have been studied in depth and compared with that of PAN microfibers. Fully alkaline hydrolysis on this stabilized PAN nanofibers web can highly enhance the water absorbency. The water absorption

performances, including water absorption ratio and swelling kinetic, of the fully hydrolyzed sample have also been evaluated.

In addition, silk, which is another important textile fiber with more than 1.5 million tons annual production around the world, is another promising candidate for enhancing its water absorption performance. It is a natural protein with remarkable mechanical property, good oxygen and vapor permeability, and biocompatibility. Since silk has a smooth surface with a considerable amount of hydroxyl groups, it can adsorb water immediately but cannot retain water. Many methods like oxygen plasma treatment and graft polymerization have been applied to improve its hydrophilicity and wickability; however, the water retention value of these modified silk remains low, limiting its applications. As it has desirable biological and mechanical properties, it is a promising material for textiles and biomaterials uses. Therefore, modifications are required to overcome its shortcomings especially water absorbency to expand its applications like biomedical textiles.

In this study, the silk has been modified via two approaches. The first approach is based on high swelling degree of silk in low concentration of lithium bromide (i.e., 4.65 M LiBr). The silk has been modified through in situ polymerization of acrylamide and sodium acrylate at its swollen state. The second approach is to perform photo-induced crosslinking of silk protein and polymerization of sodium acrylate using the photocatalyst

tris(2,2′-bipyridyl)dichlororuthenium(II) hexahydrate. These approaches are to develop the interpenetrating network or the double network from synthetic polymer and natural silk. Hence, they can provide an additional functionalization of the silk, having potentials in preparing functional textiles like wound dressings, dermal sealants, and surgical dressings.

1.2 Significance and originality

This study starts from a different viewpoint from the previous studies. It focuses on full utilization of textile materials by extending their fields of use. The preparation and modification methods on two common textile materials have been explored.

In this study, PAN nanofiber, having ten times smaller fiber diameter than the common textile fiber, is fabricated by electrospinning. Oxidative stabilization, which is an important process to stabilize and crosslink the PAN, has been studied in depth. This oxidative stabilization mechanism of PAN nanofiber is firstly studied and differs from that of PAN microfiber reported in literatures. Majority of research focuses on hydrolysis of PAN graft copolymer, physical blending with hydrolyzed PAN, and partially hydrolysis of PAN. The heated PAN nanofibers prepared in this study have been fully hydrolyzed in alkaline solution in order to obtain the fast superabsorbent hydrogel with highly interconnected pore structure.

Moreover, the modified silks reported in previous research have low water

absorption after modification; however, our modified silks achieve delightful water absorption of at least four times higher than that of the raw silk. Modification of silk is mainly conducted in water. In this work, lithium bromide solution, which is a good dissolution agent of silk, is used as a medium to swell the silk before polymerization so that the monomers can penetrate into it for development of the synthetic polymer network in an individual silk fibroin fiber. In addition, another environmental friendly system using the photocatalyst tris(2,2′-bipyridyl)dichlororuthenium(II) hexahydrate is introduced. This system can initiate both the crosslinking of silk and the polymerization of sodium acrylate. The aim of these two modification techniques is to create the interpenetrating network from natural silk protein and synthetic polymer, instead of modifying the silk surface, for a long-term effect. The improvement of water absorbency of silk is essential in some biomedical textiles, for example, wound dressings require high absorbency to prevent the accumulation of exudates at the wound area and keep the wound at optimal microenvironment for cell proliferation, migration, and differentiation.

1.3 Objectives

In order to prepare the functional and useful materials from the common textile materials including both man-made and natural materials, followings are the objectives to achieve:

(1) To establish a series of methods to improve the water absorbency of the common textile materials;

(2) To prepare the superabsorbent hydrogels from PAN nanofibers by oxidative stabilization and alkaline hydrolysis;

(3) To develop new approach to improve the water absorption of silk via in situ polymerization and photo-induced dual reactions;

(4) To characterize the hydrolyzed PAN hydrogels and modified silks, and quantify their water absorption performance; and

(5) To investigate the relationship between their chemical structures and physical properties, and explore their potential applications.

1.4 Research methodology

Followings are the general research methodology employed, and the details will be discussed in each chapter.

1.4.1 Preparation of superabsorbent PAN hydrogels

PAN nanofibers were prepared by electrospinning. The conditions of oxidative stabilization were finely controlled to stabilize and crosslink the PAN electrospun web. The stabilized PAN electrospun web was further hydrolyzed in the alkaline solution to obtain the hydrogel.

1.4.2 Modification of silk via in situ polymerization

Silk was immersed into 10 wt% monomer solutions (acrylamide or sodium acrylate) in 4.65 M lithium bromide solution with ammonium persulfate and *N,N'*-methylene bisacrylamide as initiator and crosslinker respectively. The swollen silk was then collected from the swelling solution, sealed and heated for polymerization. The resultant silk was rinsed by deionized water to remove the remaining residues and dried.

1.4.3 Modification of silk using photocatalyst

Silk was immersed into the solution of tris(2,2′-bipyridyl)dichlororuthenium(II) hexahydrate, ammonium persulfate, sodium acrylate, and *N,N'*-methylene bisacrylamide in deionized water with various combinations. The sample was then irradiated under light at room temperature to induce crosslinking of silk protein and polymerization of sodium acrylate. The resultant silk was rinsed by deionized water to remove residues and dried.

1.4.4 Characterizations

The morphologies, chemical structures and physical properties of the samples were characterized and analyzed with different techniques including field-emission scanning electron microscopy, optical microscopy, Fourier transform infrared (FTIR) spectroscopy, X-ray diffraction, and thermogravimetry.

Mechanical property was measured by means of the universal material testing machine with 2 cm distance between the clamps and 1 cm clamp width, at a strain speed of 5 mm/min under the room temperature (25 ℃).

To measure the water absorption ratio *Q* (g/g) and absorption rate, the dried sample was immersed in DI water for various periods and weighed sequentially. The excess water was removed by centrifuging. The value of *Q* was calculated based on the dry weight and wet weight of the sample.

1.5 Thesis outline

This thesis is composed of eight chapters focusing on enhancing water absorption performance of the common textile materials. Chapter 1 introduces the research background, significance, objectives, research methodology, and structure of this dissertation.

Chapter 2 reviews the limitations on water absorption performance of the common textiles and summarizes the literatures on preparation methods of PAN hydrogels and modification methods of silk.

Chapter 3 presents a method to stabilize the PAN nanofibers. The oxidative stabilization mechanism is deducted from FTIR analysis, and the stability of stabilized PAN electropsun webs against alkaline hydrolysis is also studied.

Chapter 4 focuses on the preparation and characterization of the fast superabsorbent hydrogels prepared from alkaline hydrolysis of the stabilized PAN

electropsun webs.

Chapter 5 presents the preparation and characterization of the modified silk with interpenetrating network structure via in situ polymerization of acrylamide or sodium acrylate after swelling in 4.65 M lithium bromide solution.

Chapter 6 investigates the photo-induced crosslinking effect on silk and polymerization of sodium acrylate by using the photocatalyst tris(2,2′-bipyridyl)dichlororuthenium(II) hexahydrate.

Chapter 7 further examines and characterizes the modified silk prepared from the dual reactions of photo-induced crosslinking and sodium acrylate polymerization on silk using the photocatalyst.

Chapter 8 summarizes the work of this thesis and provides some suggestions for future work.

Chapter 2

Literature review

2.1 Water absorbent materials

Water is vital for all life. It plays an important role in the absorption process. Its polar nature leads to good solvating power. Its properties also determine the characteristics of absorbent materials to be effective in absorption.

Traditional absorbent fibers such as cotton, wood pulp, and rayon, have been used for commercial products, ranging from daily uses (e.g., diapers) to medical uses (e.g., surgical sponges). Water is mainly transported by capillarity with limited fiber swelling in the traditional absorbents, so their maximum water absorbency is only 10 times of their weight with poor water retention. Since 1970s, superabsorbent polymers (SAPs), which have higher water absorbency than the traditional absorbent fibers, have been developed. Their unique structure enables them to swell without dissolution after absorbing a large amount of water and retain the water under external pressure.

In early 1990s, the specialty superabsorbent fibers (SAFs) were developed. SAF was firstly prepared by esterification or etherification reaction of the hydroxyl groups of cellulosic fibers with crosslinking such as crosslinked sodium carboxymethylcellulose [1]. Nowadays, many other synthetic SAFs are also manufactured. For an example, Lanseal® F developed by Japan Exlan Company

(now Toyobo Co., Ltd.) is consisted of a double-layer structure that has an acrylic fiber as core and a superabsorbent material at outer layer [2]. Another superabsorbent fiber prepared from crosslinked terpolymers based on acrylic acids called SAF^{TM} has been developed by Technical Absorbents Limited (TAL) [3]. It is claimed to absorb up to 200 times of water. The commercial SAF has been widely used in many products such as agrotextiles, filtration, geotextiles, and food packaging. Therefore, the water absorbent materials are important and necessary in our daily life.

2.1.1 Mechanisms for water absorption

Transportation of water through the absorbent materials is a complicated process. This absorption phenomenon is affected by many factors. The main driving force of absorption is the intrinsic liquid attraction. Moreover, an externally imposed force like gravity or pressure also influences the absorption process. Generally, two main mechanisms are responsible for the water absorption process [4].

(1) Physical absorption: capillarity owing to their physical structure

(2) Chemical absorption: partial dissolution and swelling owing to their chemical structure

2.1.1.1 Capillarity

Capillary pressure is the most common driving force for bulk water being absorbed into the absorbents via porous or capillary medium. It is due to surface

tension on fiber surface and in the capillary space between fiber surfaces [4]. The movement of fluid along fiber owing to capillarity is illustrated in the linear wicking model as shown in Figure 2.1. For traditional absorbent materials, a common feature is that they contain open spaces or pores within their structure so that they can absorb water mainly via this physical absorption [5]. However, their chemical structure limits their absorption capacity. An example is the fluff pulp that draws aqueous fluids into its porous structure by the capillary suction pressure with limited swelling.

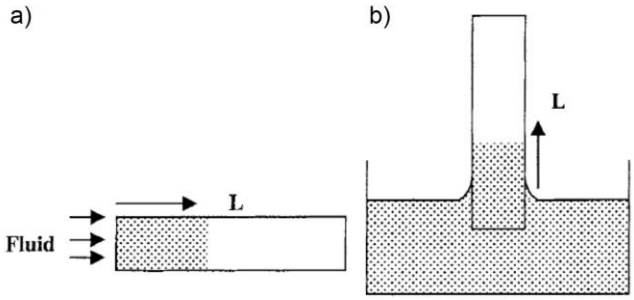

Figure 2.1 Schematic illustrations of linear wicking models in (a) horizontal and (b) vertical directions [6].

The physical absorption depends on pore radius and length, surface tension, contact angle, and fluid viscosity. The magnitude of the capillary pressure (p) is commonly given by Laplace equation (idealized capillary tubes) [7]:

$$p = \frac{2\gamma \cos\theta}{r_c} \qquad \text{(Equation 2.1)}$$

where γ is the surface tension of the liquid, θ is the contact angle at the liquid–solid–air interface, and r_c is the capillary radius or pore size. From equation 2.1, when the fiber diameter or pore size of fibers is smaller, the capillary pressure

becomes higher. Moreover, the movement of the liquid front through linear wicking effect along fibers is measured by Washburn model. Assuming that the rate of evaporation is equal to the rate of absorption [7]:

$$L = [\frac{r_c \gamma \cos\theta}{2\eta}]^{1/2} t^{1/2} \qquad \text{(Equation 2.2)}$$

where L is the wetted length of fibers, η is the fluid viscosity and t is the time. According to equation 2.2, the movement of the liquid front is proportional to the square root of time. In other words, the flow rate decreases as the time increases. The flow rate is also affected proportionally by capillary radius or pore size, surface tension, and contact angle at fixed length. The water absorption by capillarity is faster than by swelling; however, this capillary pressure provides limited water absorption capacity [7].

2.1.1.2 Partial dissolution and swelling

Another important aspect for water absorption is the partial dissolution and the swelling ability of the absorbent materials. The natural textile fibers have limited swelling. Cotton fiber is an example. When a lot of water molecules come in contact with cotton fibers, the fibrillary unzipping happens in the fibers. The hydroxyl groups of fibers become accessible to accommodate the incoming water molecules in the amorphous regions but not in the crystalline regions throughout the absorption process. For the SAPs, the polymer chains with high molecular weight are lightly crosslinked so that they can provide the large space for swelling

while remain connected together. As a result, a large amount of water is kept in their highly expanded network without dissolution. The balance between swelling ability and crosslinking density determines the water absorption capacity. When the crosslinks finally constrain the dissipation of polymer chains, equilibrium swelling is said to be reached [7].

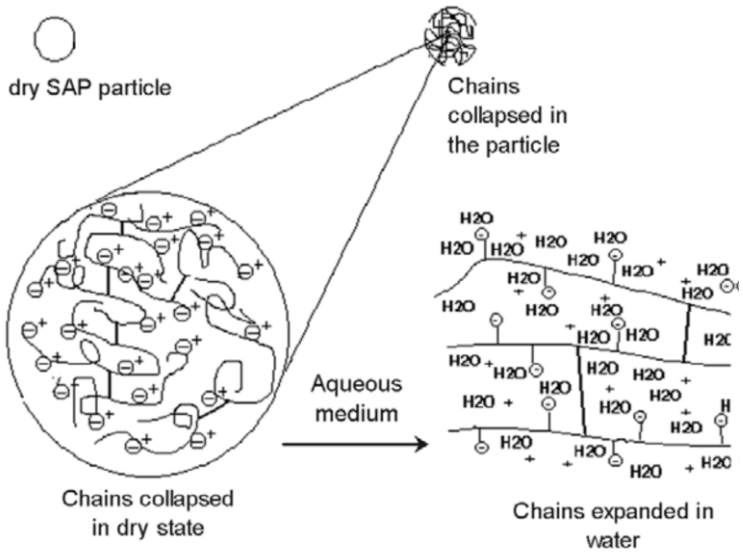

Figure 2.2 Illustration of swelling of acrylic-based anionic polymer in aqueous medium [8].

In general, four types of SAPs are classified according to their charges along the polymer chains including amphoteric, ionic, non-ionic, and zwitterionic types [4, 8]. The acrylic based anionic polymer is the most common among them and its absorption mechanism is illustrated in Figure 2.2. The dry polymer collapses and shrinks as its interior structure has low water activity. By immersing in water, water molecules move into the polymer chains and hence the carboxylate groups on the polymer chains are highly solvated by water

molecules. Because of the accumulation of similarly charged groups along the polymer chains, these charged polymer chains repel each other and expand the network; finally, the volume of wet polymer increases. The lightly crosslinked polymer allows swelling of its three-dimensional network without dissolution in water [7, 9]. An equilibrium swelling is said to be reached when the diffusion of water stops.

2.2 Synthetic superabsorbents

Synthetic superabsorbents, which are one of the special hydrogel members, occupy a very important position in commercial areas [10]. The global superabsorbent production of the main companies (e.g., Nippon Shokubai, BASF and LG Chemical Company) will reach 2.7 million tons by the end of 2015 and increase to 2.8 million tons by the end of 2016 [11]. Applications of superabsorbents are mainly in disposable hygiene areas including baby diapers, feminine napkins, and adult incontinence products. The annual growth of these products keeps increasing, especially adult incontinence products (retail sales of 8% in volume terms) [12].

Two main characteristics of superabsorbents are: (1) they can absorb a large amount of aqueous liquid, and (2) they can hold and retain the aqueous liquid from being squeezed under external pressure [1]. They can imbibe 1,000–100,000% (i.e., 10–1000 g/g) deionized water while general hydrogels absorb

less than 100% (i.e., 1 g/g) [8]. These two unique characteristics lead them to become important in commercial uses.

2.2.1 Development of synthetic superabsorbents

In 1938, the first water absorbent polymer was synthesized from the thermal polymerization of acrylic acid and divinylbenzene in aqueous medium [13]. A breakthrough in absorbent technology came in 1960s. The polymeric aqueous gelling agents or hydrogels that are well known as absorbent polymers or superabsorbents were discovered [4]. They were mainly based on hydroxyalkyl methacrylate and related monomers, having a swelling capacity of 40–50% [14]. During 1970s, the SAP developed from hydrolysis of starch-*g*-polyacrylonitrile, which was invented at the Northern Regional Research Laboratory of the United States Department of Agriculture, finally aroused the interests of the public. The first commercial superabsorbent product—feminine napkin—was introduced in 1978 at Japan. In 1983, the SAP was also used in manufacturing thin diapers [13]. Afterward, the products prepared from SAP widely spread over the world.

2.2.2 Superabsorbents prepared from polyacrylonitrile

In 1893, the synthesis of acrylonitrile and the production of polyacrylonitrile (PAN) were recorded by French chemist, C. Mourea. PAN was not popular at first because it is insoluble in common solvents and decomposes before its melting point [14]. Before the World War II started, several suitable spinning solvents

were discovered by I. G. Farbenindustrie in Germany and DuPont Co. in the United States [15]. As the production of PAN became more feasible, it was further commercialized to manufacture acrylic fibers and also produce carbon fibers [16, 17, 18].

Acrylonitrile (vinyl cyanide), CH_2=CHCN, is the monomer of PAN. PAN is one of the most important synthetic polymers especially the textile materials (i.e., acrylic fibers). According to the content of acrylonitrile, the acrylic fibers can be classified into acrylic fibers (85% acrylonitrile unit) and modacrylic fibers (35–85% acrylonitrile unit). They provide a wool-like appearance at a relatively low-cost. They have high tensile strength, resistance to abrasion, and good resistance to insects. Therefore, their fascinating properties lead them to occupy a prominent position among the synthetic fibers. They have a wide range of textile applications like clothing and upholsters [19, 20]. The world production of PAN fiber reached 1.95 million tons in 2013 [21].

PAN has high potential in preparing the superabsorbents because of its chemical properties. The common method is the alkaline hydrolysis that converts the nitrile groups of PAN into the solubilizing groups like carboxamide and alkali metal carboxylate to enhance its water absorption performance. The reaction mechanisms for hydrolysis at the nitrile groups and along the PAN polymer chains were proposed as shown in Figure 2.3.

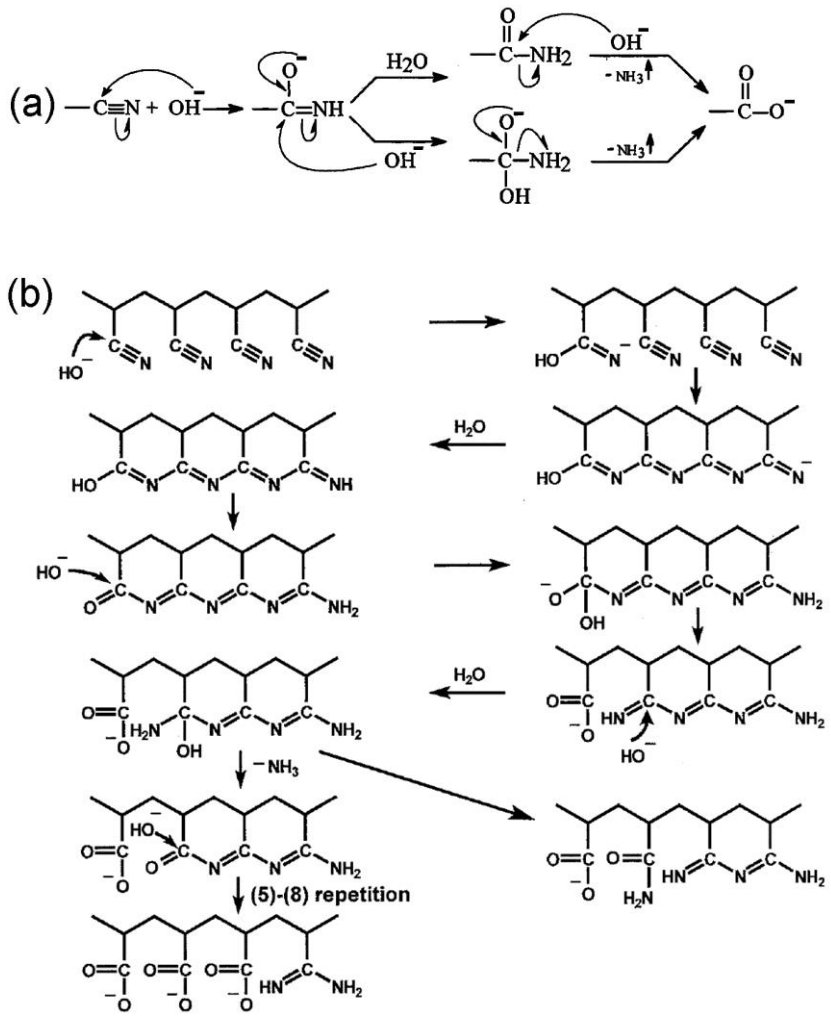

Figure 2.3 Illustration of proposed mechanisms for hydrolysis reactions (a) at nitrile groups to carboxamide and carboxylate [22], and (b) along the PAN polymer chain [23].

Three approaches to prepare superabsorbents from PAN have been extensively studied—graft polymerization, physical blending and direct hydrolysis.

2.2.2.1 Graft polymerization

Synthetic superabsorbent material was firstly described at the Northern laboratory of the U.S. Department of Agriculture. Since then, extensive research has been

conducted on graft polymerization of PAN or other synthetic water-absorbing polymers such as polyacrylamide and poly(acrylic acid) with natural polymers.

The superabsorbents prepared from graft polymerization of PAN with polysaccharides have been widely studied. Starch is the most common source among them [24, 25, 26, 27]. Various synthesis routes were developed to graft starch with PAN such as the ceric (Ce^{4+}) ammonium nitrate initiation system and manganic (Mn^{3+}) pyrophosphate complex initiation system [28, 29, 30]. The resultant starch-*g*-PAN was then hydrolyzed to achieve water absorption capacity up to 500 g/g [31]. The chitosan-*g*-PAN was also synthesized through the ceric-initiated system and then underwent hydrolysis to yield a smart hydrogel having superabsorbency, salt- and pH-sensitive for drug carriers [22, 32, 33]. However, these superabsorbents are in granular form that is difficult to be processed into commercial products.

On the other hand, other materials can also act as the backbone. Acrylonitrile monomers were directly grafted onto the wood pulp fiber or gray cotton yarn to impart high water absorption [34, 35]. PAN was also grafted on carboxymethylcellulose sodium salt to obtain a superabsorbent having pH-responsive behavior [36]. This graft polymerization provides a great versatility in attaching PAN onto different sources including agar [37], sodium alginate [38], guar gum [39], and tragacanth gum [40], via various polymerization approaches.

2.2.2.2 Physical blend polymer

The polysaccharides, such as like carboxymethylcellulose [41], alginates [38], kappa carrageenan (κC) [42], and chitosan [43], were physically blended with PAN. The mixture underwent alkaline hydrolysis to produce hydrogels. The as-prepared hydrogels also equipped with high water absorption, pH-responsive and pH-reversible properties.

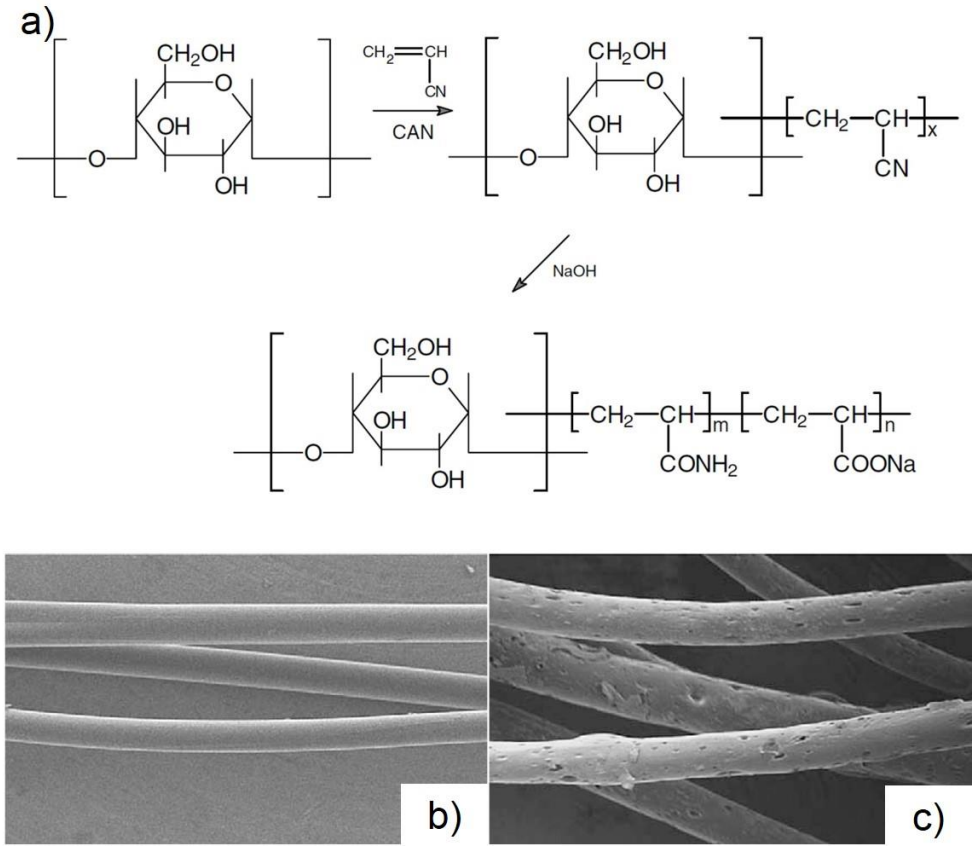

Figure 2.4 (a) Reaction mechanism of preparing the hydrolyzed starch-*g*-PAN (HSPAN); SEM images of (b) pure lyocell fiber and (c) lyocell fiber with 5 wt% HSPAN [44].

This physical blend can also be prepared in the fiber shape. Firstly, the hydrolyzed starch-*g*-PAN (HSPAN) was synthesized and ground into powder;

then, this powder was dispersed into cellulose solution to spin the lyocell fibers by dry jet-wet spinning as shown in Figure 2.4 [44]. The as-spun lyocell fiber with 5 wt% HSAPN had a rough and porous surface and increased its water absorption capacity from 1.94 g/g (pure lyocell fiber) to 8.21 g/g.

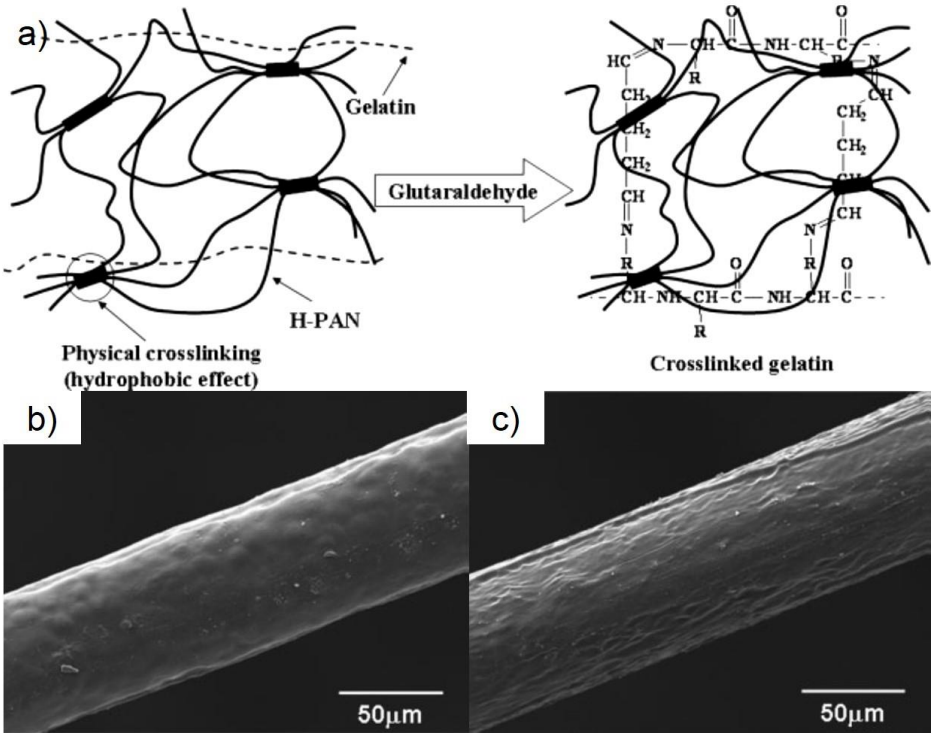

Figure 2.5 (a) Schematic illustration of formation of hydrolyzed PAN (HPAN)-*blend*-gelatin hydrogel; SEM images of HPAN/gelatin hydrogel fiber (with 3:7 weight ratio) in (b) acidic solution (pH = 1) and (c) alkaline solution (pH = 13) [45].

Apart from polysaccharides, another family of natural polymers—proteins were also commonly used to blend with the hydrolyzed PAN (HPAN), such as soy protein [46, 47] and gelatin [45, 48]. For example, in the hydrolyzed PAN-*blend*-gelatin system, the gelatin was crosslinked by glutaraldehyde, while the HPAN was physically crosslinked via hydrophobic effect as illustrated in

Figure 2.5a [45]. The hydrogel fiber was prepared by wet spinning method. It was sensitive to pH that it swelled in alkaline medium and shrank in acidic solution as shown in Figures 2.5b and 2.5c. Through the physical mixing, the absorbent hydrogel fiber in micro-scale can be prepared easily.

2.2.2.3 Direct alkaline hydrolysis

Extensive studies have been conducted on the direct alkaline hydrolysis of PAN fibers. Staple PAN fibers [49], hollow PAN fibers [50], PAN nanofibers [51], and PAN-based fibers [52] were mildly hydrolyzed in an alkaline solution to obtain the superabsorbent fibers. The smooth surface of PAN microfiber became rough after hydrolysis was shown in Figure 2.6 [49]. Apart from using PAN as the only starting material, copolymer of acrylonitrile-*co*-acrylamide was hydrolyzed to achieve high water absorption [53]. Using this method, the fibers are only partially hydrolyzed so that its surface swells and its core retains the mechanical strength. However, these hydrolyzed fibers have limited water absorption rate and ratio.

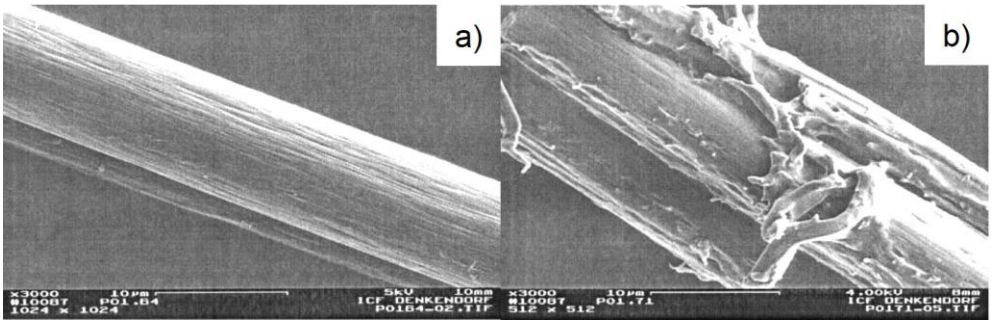

Figure 2.6 SEM images of PAN microfiber (a) untreated and (b) treated by 10% sodium hydroxide for 2 h [49].

The hydrophilicity of PAN was also improved using various hydrolysis methods such as thermal hydrolysis, alkaline hydrolysis and acidic hydrolysis [54, 55, 56]; however, their reaction mechanisms have not been fully discovered [23, 56, 57, 58, 59, 60]. The thermal hydrolysis changed the hydrophilicity of the PAN electrospun web by heating at 200 °C in air as shown in Figure 2.7 [54]. A biphasic Janus fabric having both superhydrophilic and superhydrophobic surface was then prepared. Since the direct hydrolysis is a simple method to manufacture the PAN fibers with high water absorption, it is advantageous for industrial production. Therefore, extensive studies are on the direct hydrolysis.

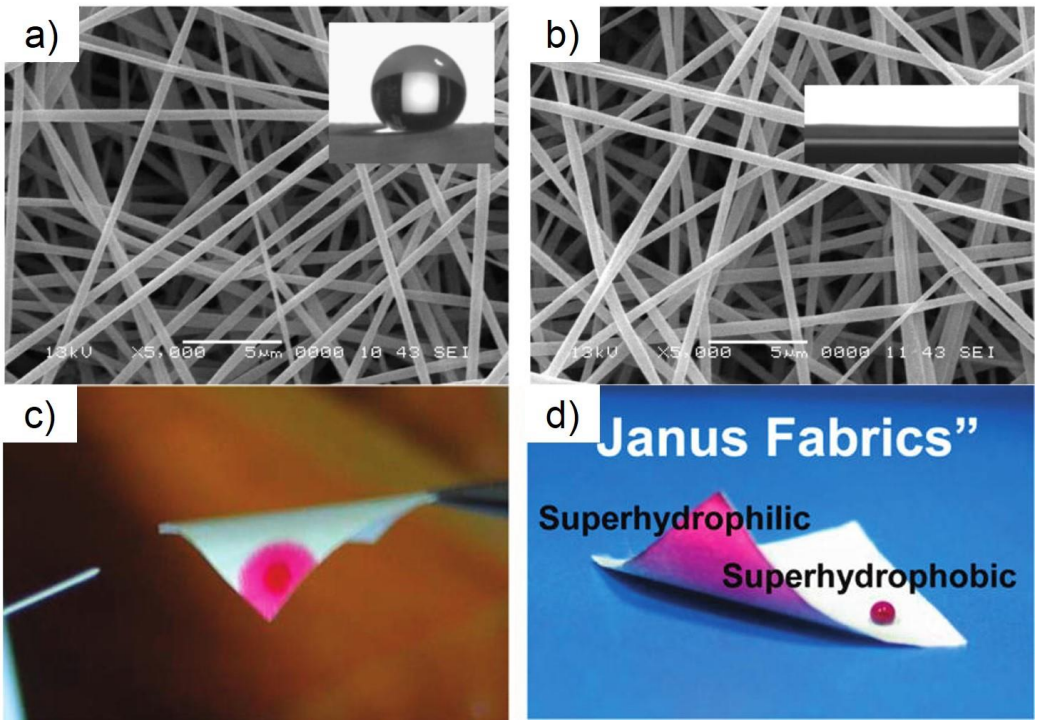

Figure 2.7 SEM images and contact angles of PAN electrospun webs (a) before and (b) after hydrolysis at 200 °C in air; photos of free-standing biphasic Janus fabric showing its (c) superhydrophilicity and (d) superhydrophobicity [54].

To conclude, the HPAN enhances its water absorption and has reversible pH- and salt-responsiveness. These novel properties enable the HPAN to become a suitable candidate as a smart hydrogel for artificial actuators [62, 63] and artificial muscles [61, 62, 63, 64]. The mechanisms of elongation and contraction of HPAN fiber are depicted as illustrated in Figure 2.8. The main driving force is the osmotic pressure. In the basic solution, the OH^- groups draw the H^+ from the –COOH groups of HPAN fiber so the resultant $–COO^-$ ions between polymer chains have strong repulsive forces developed. Cations (e.g., Na^+) and water molecules diffuse into the polymer chains in order to compensate the negative charge. As a result, the HPAN fiber elongates. Under the environmental SEM and AFM, its pH- responsiveness were observed as shown in Figure 2.9.

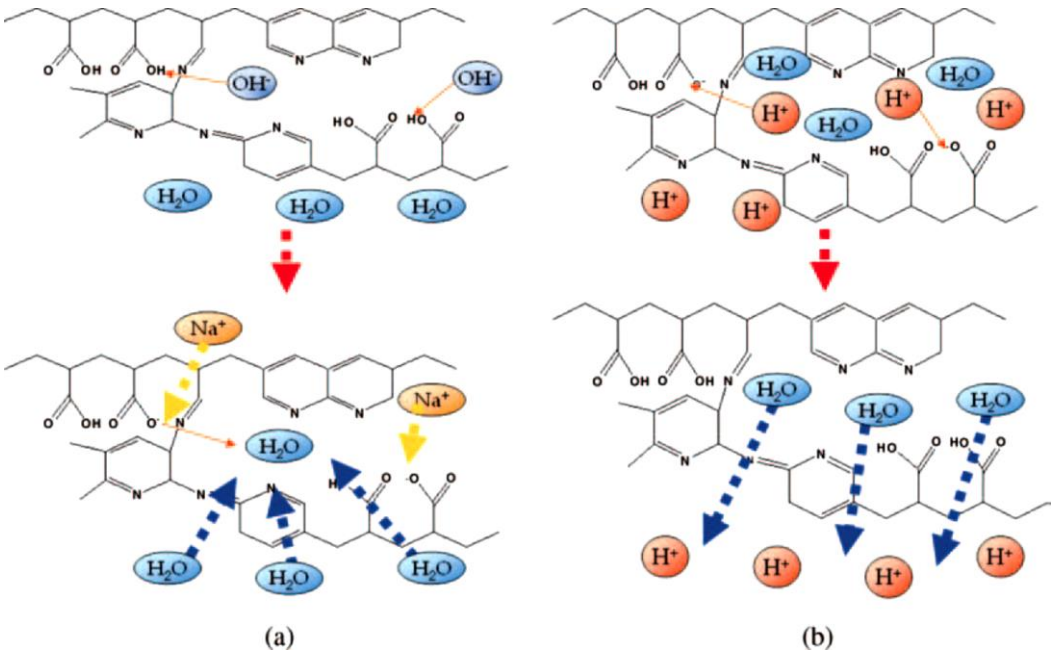

Figure 2.8 Proposed mechanisms of HPAN fiber (a) elongation in basic solution and (b) contraction in acidic solution [61].

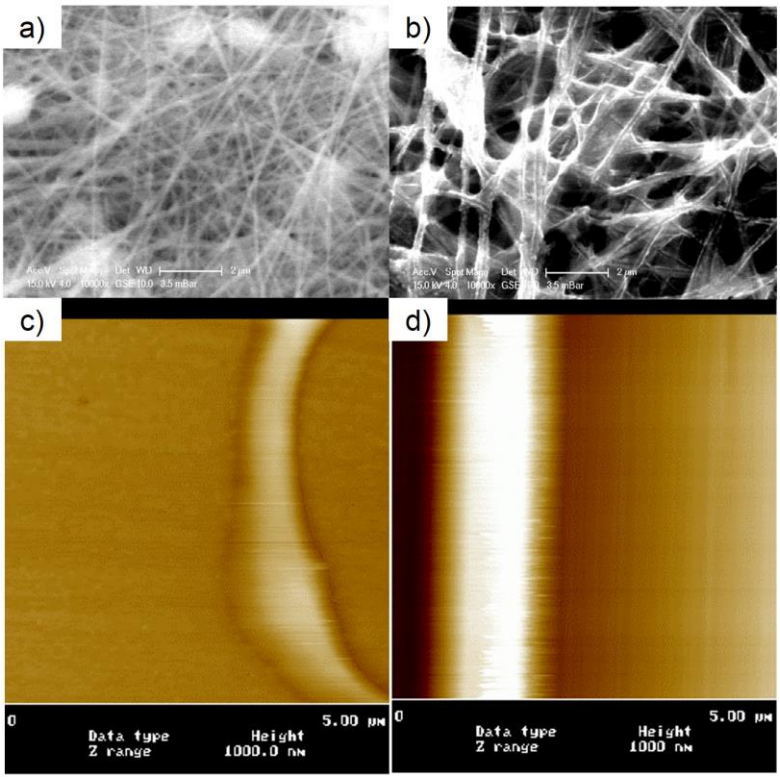

Figure 2.9 Environment SEM images and AFM images of HPAN nanofibers in (a, c) acidic solution and (b, d) basic solution respectively [65].

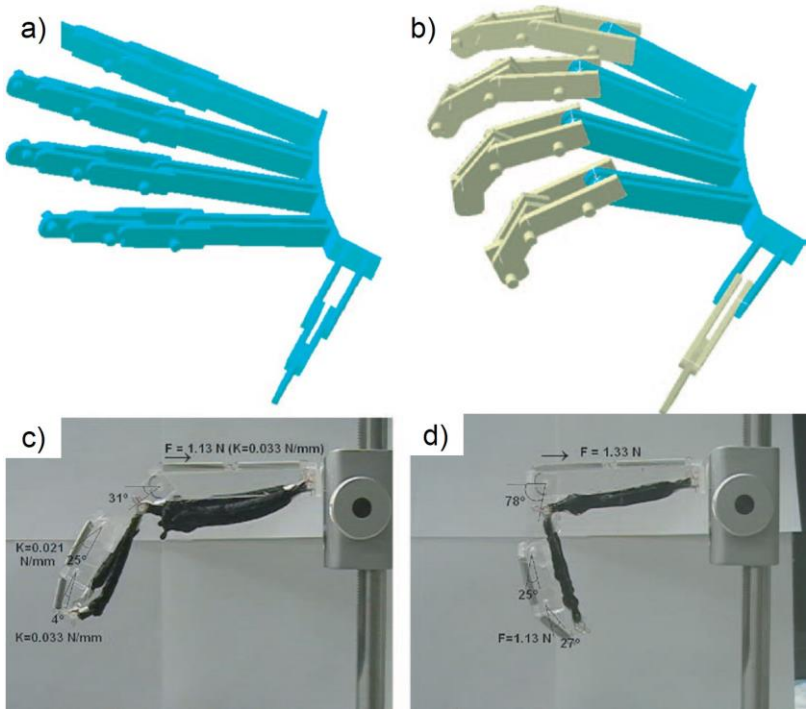

Figure 2.10 Schematic illustrations and photos of PAN robotic hand at (a, c) relaxed (elongated) position and (b, d) grab (contracted) motion [61].

Because of the pH-responsiveness of HPAN fiber, a PAN robotic hand was suggested by Chloe [61]. Figure 2.10 illustrates the application of HPAN fiber as a muscle actuator equipped with two tubes that deliver acid and basic solutions for fiber shrinking and elongation. Therefore, the HPAN achieves high water absorption and can be used as smart materials.

2.2.3 Applications of superabsorbents

Since the superabsorbents can be blended with other materials to make nonwoven or woven fabrics, high versatility provides them a wide range of applications. Generally, they can be divided into two categories—hygienic and non-hygienic applications [1, 4, 13, 66].

For hygienic uses, especially the personal care applications, the superabsorbents account for about 80% of the overall hydrogel production [67]. They include the disposable baby diapers, feminine care products, adult incontinence products, and hospital disposables. In order to achieve satisfactory properties with reasonable cost, most of them are blended with other fibers like cotton. For non-hygienic applications, the superabsorbents can be used in different fields such as agriculture and horticultural applications, water treatment, fibers and textile, food packaging, electrical applications, and geotextiles. A comprehensive review on non-hygienic applications has been conducted by Zohuriaan-Mehr [67].

2.3 Natural fibers

2.3.1 Water absorbent properties of textile fibers

As mentioned previously, capillary pressure traps water in between the adjacent fibers. The simple centrifugal method has been suggested by Preston and his colleagues to remove the excess water. When a bundle of fibers experiences high field of force by centrifuging, the water rapidly drains out from it. Table 2.1 shows the amount of water retained by different textile materials. It should be noted that centrifuging does not remove all the water held in the capillary spaces but reduces it in an acceptable amount [68].

Table 2.1 Water retained by centrifuging and swelling of fibers in water. (Values were reported by different authors and collected by Preston and Nimkar.) [68, 69]

Materials	Water retention value by centrifuging (%)	Diameter swelling (%)	Volume swelling (%)
Cotton yarn	48	20, 23, 7	
Mercerized cotton		17	
Viscose rayon yarn	103	25, 35, 52	109, 117, 115, 74
Acetate yarn	31	9, 11, 14	
Wool	45	14, 8, 17	36, 37, 41
Silk yarn	52	16.5, 16.3, 18.7	30, 32
Nylon yarn	16	1.9, 2.6	8.1, 11.0

When the fibers absorb water, they swell transversely and axially. Swelling also leads to the interchanging of position between fiber molecules and water molecules but in a limited extent. It can be expressed in terms of increment in diameter, area, length, or volume. The fiber diameter change can be easily examined by optical microscope. As seen in Table 2.1, the reported diameter and volume swelling percentages of some common textile fibers are quite low [68, 69]. Among all these textile materials, viscose rayon yarn obtains the highest water retention of 103% and volume swelling of 117%. The silk yarn only achieves water retention of 52% and volume swelling of 32%. From the water retention value and the swelling percentage, it can be seen that these common textile fibers have poor water absorption capacity.

2.3.2 Silk fibers

The use of silk fibers as textile materials existed in the Far East over 4000 years ago. The commercial production was firstly reported during the Chinese emperor Huang Ti in 2640 B.C. The techniques of sericulture and weaving silk were spread over the world starting from Korea to Japan and India. Because of its sheen, soft handle and draping qualities, silk becomes the important and valuable textile fibers [70]. Silk is an extracellular continuous filament that can be produced by many different species in the phylum Arthropoda such as *Nematus ribesii*, *Bombyx mori*, and *Antherae* from the class of *Insecta*. Among them, the most commercially

available silk in the textile industry is mainly produced by domestic silkworm, that is, *Bombyx mori*. Other cheaper synthetic and regenerated fibers also provide similar properties; however, the availability of their raw material crude oil and the environmental impact of their production are the main concerns. More than 1.5 million tons of silk are produced annually around the world [71]. High production enables the silk fibers to be one of the important raw materials in the textile industry [72].

2.3.3 Composition of silk fibers

Silk is a natural protein with remarkable mechanical properties, good oxygen and water vapor permeability, and biocompatibility. It is mainly proteinaceous materials—sericin and fibroin.

2.3.3.1 Silk sericin

For sericin, it is a glue-like protein that contributes 25–30% of silk protein to cement two silk fibroin fibers together during cocoon formation to protect the growing worm [73]. Its molecular weight ranges from 10 to above 300 kDa. It is consisted of 18 amino acids in which most of them contain highly polar side groups such as hydroxyl, carboxyl, and amino groups [74, 75]. It is constituted of 33.4% of serine (Ser, S) and 16.7% of aspartic acid (Asp, D). Therefore, the sericin is highly hydrophilic in nature and water-soluble, especially in alkaline solution [76].

For the low molecular weight sericin peptides (≤20 kDa) and its hydrazates, they have excellent moisture absorption and a lot of biological activities such as antioxidant action [77], inhibition of colon tumors development [78], and cryoprotective activity [79]. For the high molecular weight (≥20 kDa) sericin peptides, they are soluble in hot water but poorly soluble in cold water. They are useful in degradable biomaterials, biomedical materials, functional biomembrane materials, hydrogels, and functional fibers. For example, it can act as a support for the enzyme *L*-asparaginase immobilization [80].

Some previous studies were on the sericin-based hydrogels. For example, an elastic silk sericin hydrogel with porous structure was prepared by adding ethanol to induce gelation. This hydrogel shrank in ethanol and swelled again in water back to its original size [81]. The flexible sericin gel film prepared without chemical crosslinking had high potential use for wound dressings [82]. Moreover, by using crosslinking agents, silk sericin and poly(N-isopropylacrylamide) composed the interpenetrating network (IPN) hydrogels. This porous IPN hydrogel was sensitive to temperature and pH of the buffer solutions [83]. The fast pH-responsive IPN hydrogel prepared by silk sericin/ poly(methacrylic acid) could be used as drug delivery [84]. The hydrogel formed by physical blending of methacrylated sericin and poly(vinyl alcohol) was also able to enhance the cellular interactions [85]. However, the mechanical property of sericin-based hydrogels is poor.

2.3.3.2 Silk fibroin

For silk fibroin (SF), it is mainly consisted of one heavy (H-) chain (M_W 350,000) and one light (L-) chain (M_W 25,000) linked by disulfide bonds [86, 87]. The H-chain has a repetitive amino acid sequence and contains mainly four types of amino acids—alanine (Ala, A), glycine (Gly, G), serine (Ser, S), and tyrosine (Tyr, Y). The L-chain does not have repetitive sequence and contains mainly the glutamic acid (Glu, E) and asparatic acid (Asp, D) [88]. The primary amino acid sequence of H-chain has a pattern of hydrophobic and hydrophilic blocks including large hydrophilic blocks at the two chain ends, six small hydrophilic internal blocks, and seven large hydrophobic internal blocks along the H-chain as illustrated in Figure 2.11 [89, 90].

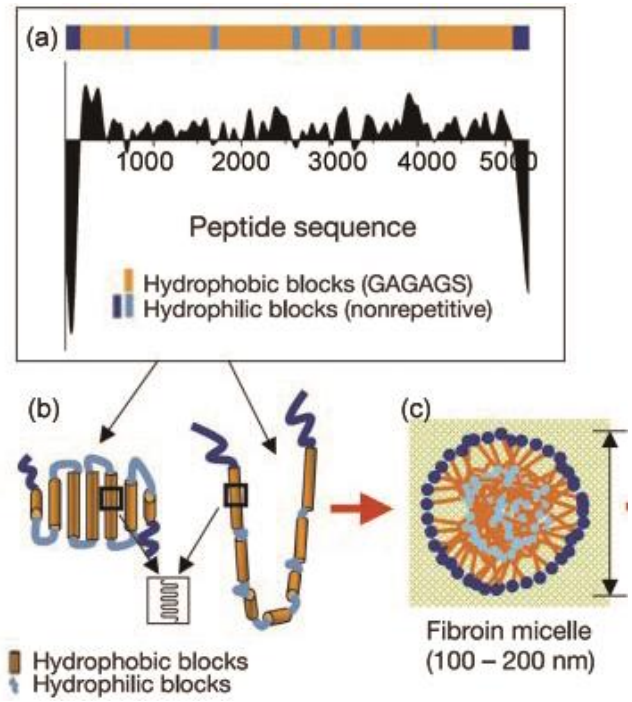

Figure 2.11 The illustration of (a) the model of fibroin chain; (b) the model of chain folding due to hydrophobic effect and (c) micelle assembly in water [89].

For the secondary structure, SF has two major conformation states—silk I and silk II. Silk I has random coil and alpha helical structure. It is soluble in water and metastable in the silk gland [74, 91]. Silk II has β-sheet structure that is thermodynamically stable. It is found in the spun silk fiber in form of solid hydrophobic silk fibroin. By exposure to heat, humidity, organic solvents, physical stretching, or shear stress, they can trigger the formation of insoluble crystallized structure of silk fibroin [92].

2.3.4 Modifications of silk fibers

Silk is still widely used as fibers in the textile industry as well as biomaterials in the medical area. They have many desirable biological properties such as biodegradability, good oxygen and water vapor permeability, and minimal inflammatory reaction [93, 94, 95, 96, 97, 98]. However, silk has several drawbacks such as its low water retention, wrinkling, photo-yellowing, and deformation and degradation caused by microorganisms that highly limit its applications [99, 100, 101]. Therefore, modifications of silk fibers have been extensively studied to enhance its performance and hence widen its applications. Three types of modification techniques and methods on silk fibers are classified as follow.

2.3.4.1 Physical techniques

Three main physical principles are introduced for silk fiber modification–UV

treatment, plasma treatment and gas treatment.

UV treatment is the use of excimer lamps that can generate intense and nearly monochromatic light in the vacuum ultraviolet (VUV) region via dielectric barrier discharges [102]. High-energy photons can break the molecular chains of silk fibroin surface and create roughness on its surface to enhance wettability and wickability. The nanopores (~190 nm) appeared after irradiation with excimer lamp for 30 min as shown in Figure 2.12 [103]. In addition, when the high-energy VUV irradiation was applied on one side of the fluorocarbon-based hydrophobic pretreated silk fabric, it removed the fluorocarbon finish and the fabric became hydrophilic. Hence, the silk fabric contained both hydrophobic and hydrophilic surfaces [104]. This treatment had negligible effects on silk fiber like weight loss, crystallinity, and mechanical strength [103, 104, 105, 106].

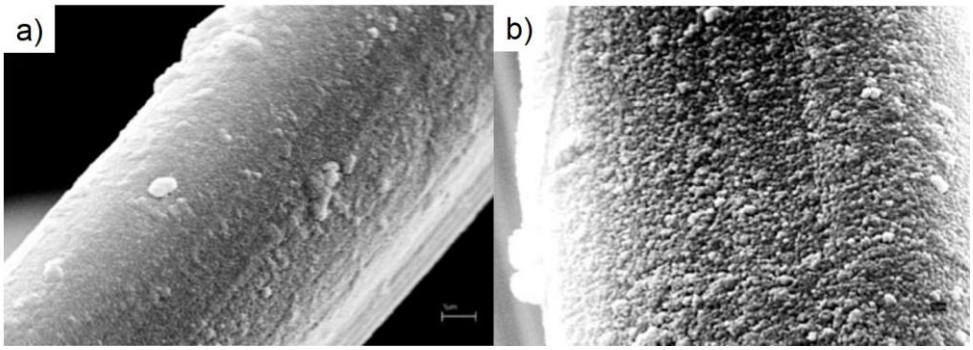

Figure 2.12 SEM images of silk fiber irradiated with excimer lamp (a) untreated and (b) 30 min [103].

Plasma is consisted of negatively charged electrons, positively charged ions, and neutral atoms and molecules. The medium is electrically conductive

and neutral because of the equilibrium between electrons, positively and negatively charged excited ions [107]. Since the raw silk fiber has a smooth surface with many hydroxyl groups, it can adsorb water immediately but cannot retain water. Therefore, it is treated by various types of plasma treatments to enhance their hydrophilicity or hydrophobicity. In previous studies, the fluorine-containing compound plasma treatment, such as hexafluoropropene (C_3F_6) and sulphur hexafluoride (SF_6), greatly improved the hydrophobicity of silk [108, 109]. As seen in Figure 2.13, the silk fiber had a rough surface after SF_6 treatment and the water droplet rested on its surface with contact angle of 140° [108]. On the other hand, oxygen plasma treatment on silk enhanced its hydrophilicity and wickability through increasing surface roughness as well as introducing polar groups like –OH and –COOH [110, 111]. The improved hydrophilicity increased the adsorption capacity of dyes during the dyeing process so it exhibited a deeper color shade and enhanced the pattern sharpness in inkjet printing [112, 113, 114].

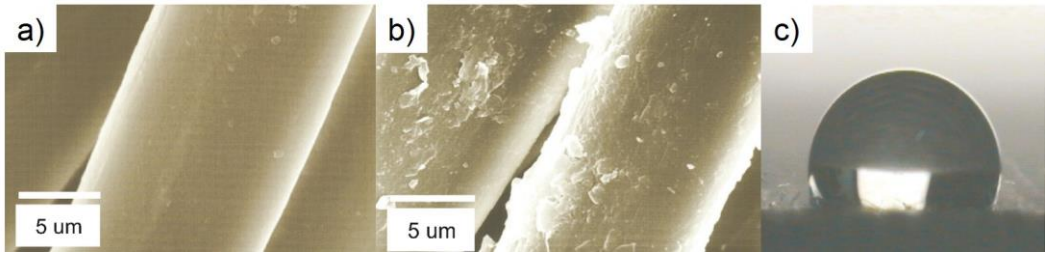

Figure 2.13 SEM images of silk fibers (a) before treatment and (b) after treatment with 0.05 Torr of SF_6 for 1 min; (c) photo of water droplet resting on treated silk fabric [108].

Some other gas treatments are also used for imparting different properties to silk such as ammonia gas treatment. This treatment only improved its soft handle property [115]. Although these methods impart some desirable properties on silk, the lifetime of the treated samples may not meet the standard of textile products such as washing fastness, light fastness and perspiration fastness.

2.3.4.2 Chemical methods

In order to impart the permanent desirable properties on silk, chemical approach is applied. It is because the main peptide chains and the side chains of silk fibroins have many active sites for modification. One of the common approaches is the graft polymerization. Graft polymerization is a method to modify silk fibers by creating branches of side chains onto the main silk fibroin chains. It can impart some desirable properties to the silk fibers without altering their fundamental properties. Several vinyl monomer and initiator systems have been applied to improve silk fibers properties such as thermal stability, photo yellowing resistance, water repellency, and wrinkle recovery.

Vinyl monomers like methyl methacrylate and acrylamide were extensively studied. Grafting silk with methyl methacrylate enhanced its mechanical properties, crease recovery, resistance to chemical, thermal stability, and dyeability [116, 117, 118, 119, 120]. Grafting with acrylamide mainly improved its tensile strength [121, 122, 123]. The mechanism of graft

polymerization using Ce^{4+} initiation system is shown in Figure 2.14. The initiator attacks some functional groups on main peptide chains to form the macro-radicals for further free radical polymerization with acrylamide monomers.

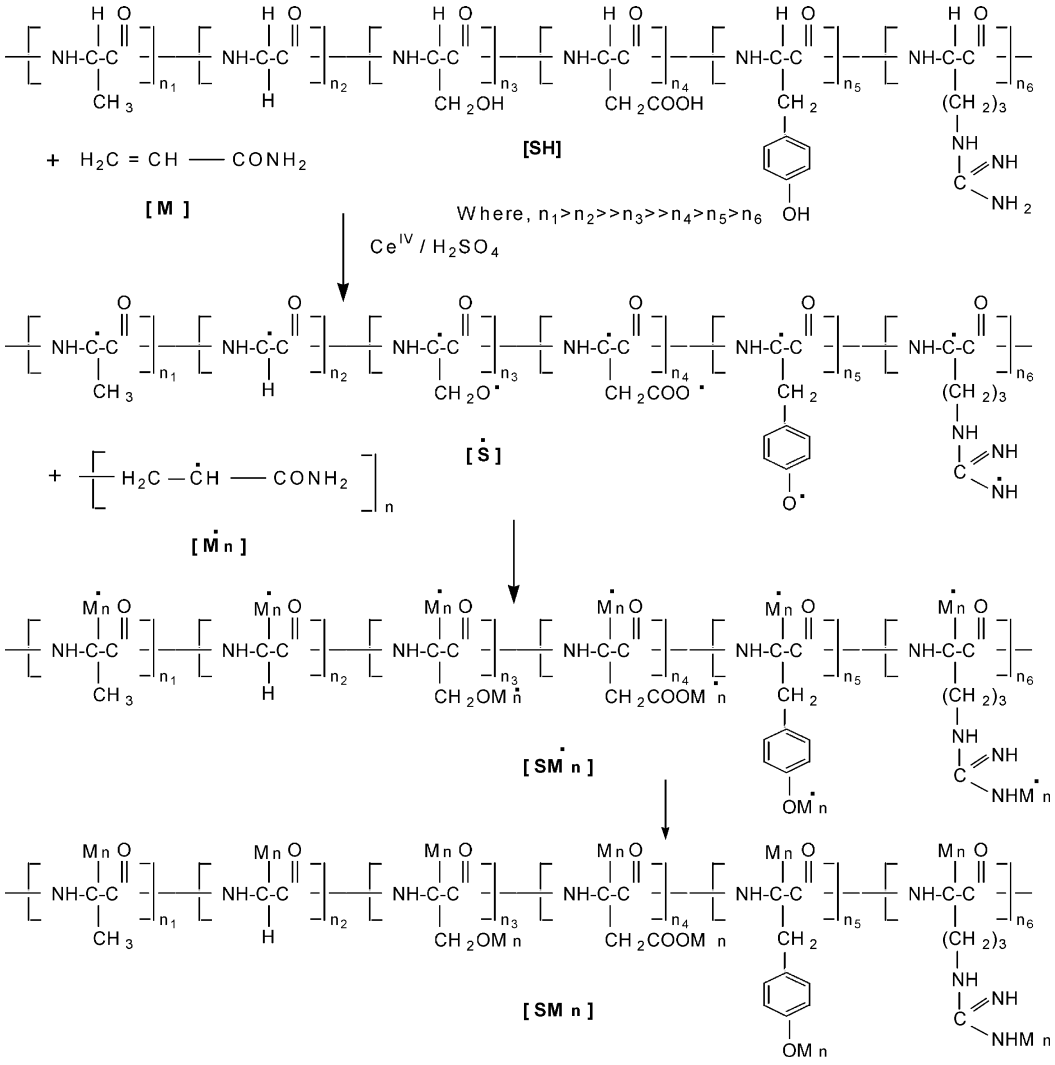

Figure 2.14 Schematic representation of acrylamide grafting reaction mechanism on silk using Ce^{4+} / H_2SO_4 as initiator [121].

Furthermore, some other vinyl monomers, such as methacryloyloxyethyl diphenyl phosphate [123], dimethyl(methacryloyloxyethyl) phosphoramidate [124], and vinyltrimethoxysilane [125], were grafted onto silk to enhance its

flame retardancy; acrylate fluoride was grafted via atom transfer radical polymerization to improve its water repellency [126].

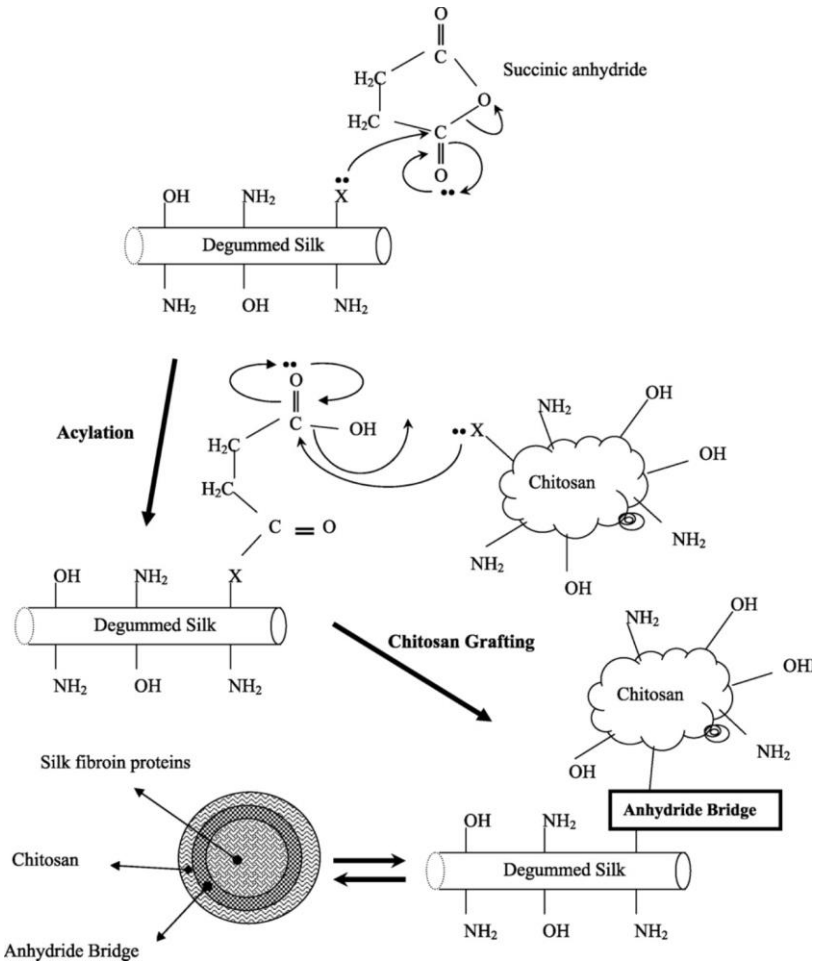

Figure 2.15 Illustration of grafting silk with chitosan using succinic anhydride as a bridge (X = OH and NH_2) [127].

Besides vinyl monomers, chitosan was also grafted onto silk because of its anti-bacterial property [128]. Several methods have been applied such as using succinic anhydride as the bridge to connect silk and polysaccharide chitosan as illustrated in Figure 2.15 [127] and using enzyme tyrosinase to oxidize tyrosyl residues resulting in activated *o*-quinone residue for grafting chitosan as shown in Figure 2.16 [129].

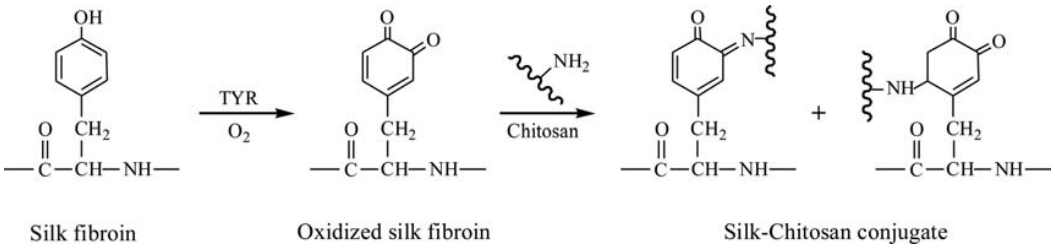

Figure 2.16 Scheme of tyrosinase-catalyzed grafting of chitosan on silk fibers [129].

Even though various chemicals have been grafted onto silk, the water retention values of these modified silks are still lower than that of raw silk. Especially when the grafting efficiency increases, the water retention value decreases, limiting the applications.

2.3.4.3 Functionalization with nanomaterials

Functionalization with nanomaterials like metal nanoparticles and quantum dots on silk enhanced its end-use performance. Deposition of silver nanoparticles was extensively studied because of its effective anti-bacterial property [130]. To reduce silver ions (Ag^+) to silver metal (Ag), some hazardous chemicals like sodium borohydride and hydrazine were used [131, 132]. Therefore, other methods like layer-by-layer method [132], γ-irradiation [133], ultrasound irradiation [134, 135], and UV irradiation [136, 137] were suggested. In addition, silk can act as biotemplate for preparing Ag nanoparticles as its tyrosine residues have strong electron donating properties. As seen in the Figure 2.17, tyrosine residues were distributed along the protein chains and they attracted the Ag^+ ions through coulombic interactions. The Ag nuclei and tyrosine residues developed a

chemically reducing environment for further reduction of Ag^+ ions to form Ag nanoparticles (~45 nm) [138].

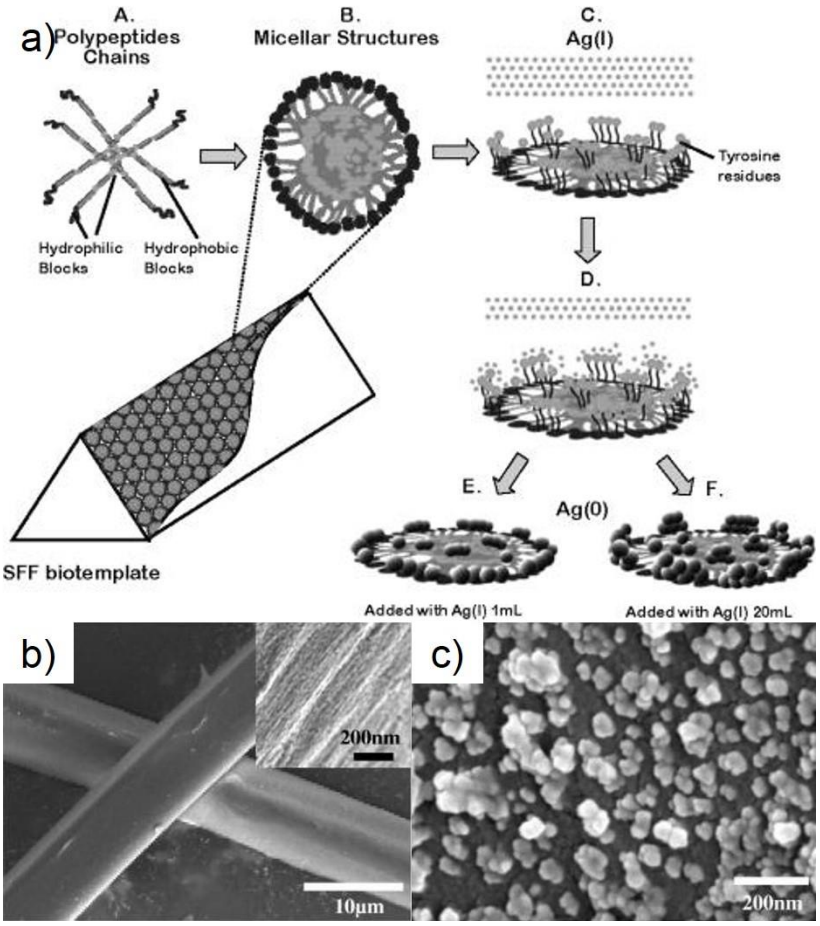

Figure 2.17 (a) Illustration of deposition of Ag nanoparticles on silk as biotemplate with different Ag^+ ions; SEM images of (b) original silk and (c) silk prepared with 20 mL 0.01 M $AgNO_3$ reagent [138].

Hydroxyapatite (HAp) has high affinity to many cells and tissues such as bone, tooth and skin tissue. Bone bonding is easily developed between the implanted HAp and the host bone tissue. It has been widely used as bone graft biomaterials and dental applications [139, 140]. Since silk has high mechanical strength and biocompatibility, it is used as a support of HAp for biological

applications like bone reconstruction surgery and bone regeneration scaffold [141, 142]. The chemically bonded HAp/silk composites were prepared as shown in Figure 2.18. The silk was grafted with vinyl monomers followed by ring opening using aqueous potassium hydroxide to generate carboxylate groups. Cationic HAp was then adsorbed by carboxylate groups on silk via ionic interaction [143].

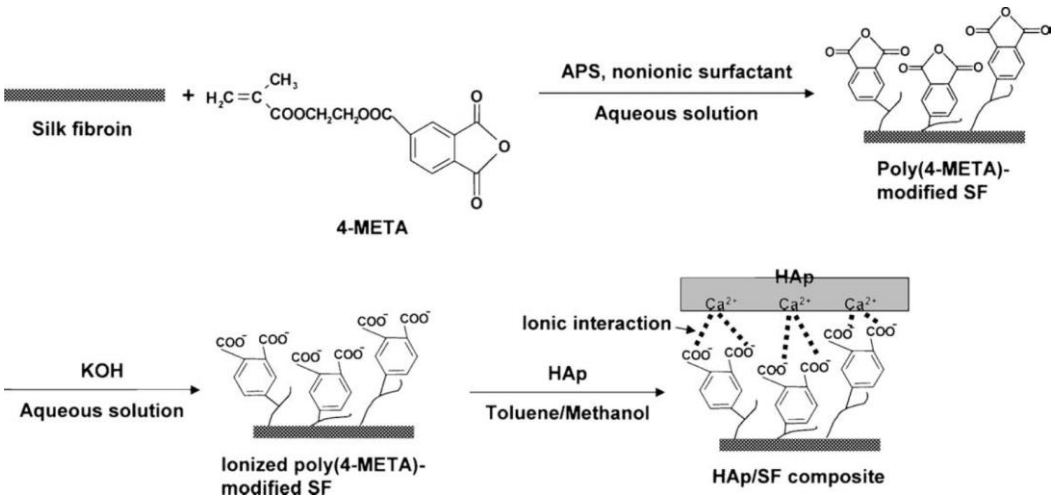

Figure 2.18 Schematic illustration of HAp/ SF composite synthesis [143].

To conclude, silk has desirable mechanical property and biological properties such as biodegradability, good oxygen and water vapor permeability, and minimal inflammatory reaction. However, silk has several drawbacks such as low water retention, and deformation and degradation caused by microorganisms. Even though many modification methods have been studied, its water absorption performance remains poor. When this performance is improved, it will become a promising material in preparing biomedical textiles.

References

[1] Cooke, T. F. Fibers: Superabsorbent. In *Encyclopedia of Materials: Science and Technology*; Jürgen Buschow, K. H., Cahn, R. W., Flemings, M. C., Ilschner, B., Kramer, E. J., Mahajan, S., Veyssière, P., Eds.; Elsevier: Amsterdam; New York, 2001, Vol. 4, pp. 3146-3150.

[2] Lanseal® F. http://www.toyobo-global.com/seihin/ap/lanseal_f/lanseal_f.html (accessed 20/6/2016).

[3] Technical Absorbents. http://techabsorbents.com (accessed 30/7/2015).

[4] Gross, J. R. The Evolution of Absorbent Materials. In *Absorbent polymer technology*; Brannon-Peppas, L., Harland, R. S., Eds.; Elsevier: Amsterdam, 1990; Chapter 1, pp. 3-22.

[5] Buchholz, F. L. Absorbency and Superabsorbency. In *Modern Superabsorbent Polymer Technology*; Buchholz, F. L., Graham, A. T., Eds.; Wiley-VCH: New York, 1998, Chapter 1, pp 1-17.

[6] Chatterjee, P. K., Gupta, B. S. Porous structure and liquid flow models. In *Absorbent Technology*; Chatterjee, P. K., Gupta, B. S.,Eds.; Elsevier: Amsterdam, 2002; Chapter 1, pp. 2-55.

[7] Staples, T. L. Synthetic Superabsorbents. In *Absorbent Technology*; Chatterjee, P. K., Gupta, B. S.,Eds.; Elsevier: Amsterdam, 2002; Chapter 8, pp. 283-322.

[8] Zohuriaan-Mehr, M. J.; Kabiri, K. Superabsorbent polymer materials: A review. *Iran. Polym. J.* **2008**, 17(6), 451-477.

[9] Albrecht, W. Other raw materials. In *Nonwoven Fabrics: Raw Materials, Manufacture, Applications, Characteristics, Testing Processes*; Albrecht, W., Fuchs, H., Kittelmann, W., Eds.; Wiley-VCH: Weinheim, 2003, Chapter 2, pp 87-118.

[10] Dewsbury, M. E. Market opportunities with Superabsorbent Fibers. *Tappi J.* **1991**, 74(2), 146-148.

[11] Mclntyre K. SAP Market Report. *Nonwovens industry*, April 7, 2015.

[12] Uduslivaia S. From Shame to Fame: Adult Incontinence Continues In Global Advance. *Nonwovens industry*, March 9, 2015.

[13] Masuda, F. Trends in the Development of Superabsorbent Polymers for Diapers. In *Superabsorbent Polymers: Science and Technology*; Buchholz, F. L., Peppas, N. A., Eds.; ACS symposium series 573; American Chemical Society: Washington, DC, 1994; Chapter 7, pp 88-98.

[14] Frushour, B. G.; Knorr, R. S. Acrylic fibers. In *Handbook of fiber science and technology;* Lewin, M., Sello, S. B., Eds; International fiber science and technology series; New York, 1983, Vol. IV, pp 171-344.

[15] Simitzis, J. C. Polyacrylonitrile. In *Handbook of thermoplastics;* Olabisi, O., Eds.; Plastics engineering; Marcel Dekker: New York, N.Y., 1997, Vol. 41, pp 177-201.

[16] Chand, S. Carbon fibers for composites. *J. Mater. Sci.* **2000**, 35(6), 1303-1313.

[17] Rahaman, M. S. A.; Ismail, A. F.; Mustafa, A. A review of heat treatment on polyacrylonitrile fiber. *Polym. Degrad. Stab.* **2007,** 92(8), 1421-1432.

[18] Zussman, E.; Chen, X.; Ding, W.; Calabri, L.; Dikin, D. A.; Quintana, J. P.; Ruoff, R.S. Mechanical and structural characterization of electrospun PAN-derived carbon nanofibers. *Carbon* **2005**, 43(10), 2175-2185.

[19] Collier, B. J.; Tortora P. G. Acrylics. In *Understanding Textiles*, 6th ed.; Upper Saddler River, N. J.: Prentice Hall, 2001, pp 190-199.

[20] Joseph, M. L. Acrylic and Modacrylic Fibers. In *Introductory textile science*, 5th ed.; Holt, Rinehart, and Winston: New York, 1986; Chapter 12, pp 124-134.

[21] 60 years of Dralon polyacrylic fibers. *Chemical Fibers International*, Dec, 2014, p121.

[22] Mahdavinia, G. R.; Zohuriaan-Mehr, M. J.; Pourjavadi, A. Modified chitosan III, superabsorbency, salt- and pH-sensitivity of smart ampholytic hydrogels from chitosan-g-PAN. *Polym. Adv. Technol.* **2004**, 15(4), 173-180.

[23] Litmanovich, A. D.; Platé, N. A. Alkaline hydrolysis of polyacrylonitrile: on the reaction mechanism. *Macromol. Chem. Phys.* **2000**, 201(16), 2176-2180.

[24] Castel, D.; Ricard, A.; Audebert, R. Swelling of anionic and cationic starch-based superabsorbents in water and saline solution. *J. Appl. Polym. Sci.* **1990**, 39(1), 11-29.

[25] Lim, D.; Whang, H.; Yoon, K.; Ko, S. Synthesis and absorbency of a superabsorbent from sodium starch sulfate-g-polyacrylonitrile. *J. Appl. Polym. Sci.* **2001**, 79(8), 1423-1430.

[26] Sadeghi, M.; Hosseinzadeh, H. Synthesis and swelling behavior of starch-poly(sodium acrylate-co-acrylamide) superabsorbent hydrogel. *Turk. J. Chem.* **2008**, 32(3), 375-88.

[27] Weaver, M. O.; Gugliemelli, L. A.; Doane, W. M.; Russell, C. R. Hydrolyzed starch–polyacrylonitrile graft copolymers: Effect of structure on properties. *J. Appl. Polym. Sci.* **1971**, 15(12), 3015-3024.

[28] Fanta, G.; Burr, R. C.; Doane, W. M. Saponified starch-g-polyacrylonitrile. Variables in the Ce^{4+} initiation of graft polymerization. *J. Appl. Polym. Sci.* **1982**, 27(7), 2731-2737.

[29] Zohuriaan-Mehr, M. J.; Pourjavadi, A. Superabsorbent hydrogels from starch-g-PAN: Effect of some reaction variables on swelling behavior. *J. Polym. Mater.* **2003**, 20(1), 113-120.

[30] Ranby, B.; Rodehed, C.; Rånby, B. Structure and molecular properties of saponified starch-graft-polyacrylonitrile. *J. Appl. Polym. Sci.* **1986**, 32(1), 3323-3333.

[31] Sadeghi, M.; Hosseinzadeh, H. Synthesis of starch-poly(sodium acrylate-co-acrylamide) superabsorbent hydrogel with salt and pH-responsiveness properties as a drug delivery system. *J. Bioact. Compatible Polym.* **2008**, 23(4), 381-404.

[32] Pourjavadi, A.; Mahdavinia, G. R.; Zohuriaan-Mehr M. J. Modified chitosan. II. H-chitoPAN, a novel pH-responsive superabsorbent hydrogel. *J. Appl. Polym. Sci.* **2003**, 90(11), 3115-3121.

[33] Mahdavinia, G. R.; Pourjavadi, A.; Zohuriaan-Mehr, M. J. A convenient one-step preparation of chitosan-poly(sodium acrylate-co-acrylamide) hydrogel hybrids with super-swelling properties. *J. Appl. Polym. Sci.* **2006**, 99(4), 1615-1619.

[34] Rezai, E.; Warner, R. R. Polymer-grafted cellulose fibers. I. enhanced water absorbency and tensile strength. *J. Appl. Polym. Sci.* **1997**, 65(8), 1463-1469.

[35] Deo, H. T.; Gotmare, V. D. Acrylonitrile monomer grafting on gray cotton to impart high water absorbency. *J. Appl. Polym. Sci.* **1999**, 72(7), 887-894.

[36] Pourjavadi, A.; Zohuriaan-Mehr M. J.; Ghasernpoori, S. N.; Hossienzadeh, H. Modified CMC. V. synthesis and super-swelling behavior of hydrolyzed CMC-g-PAN hydrogel. *J. Appl. Polym. Sci.* **2007**, 103(2), 877-883.

[37] Chhatbar, M. U.; Meena, R.; Prasad, K.; Siddhanta, A. K. Agar/sodium alginate-graft-polyacrylonitrile, a stable hydrogel system. *Indian J. Chem. A* **2009**, 48(8), 1085-1090.

[38] Marandi, G. B.; Sharifnia, N.; Hosseinzadeh, H. Synthesis of an Sadeghi alginate–poly(sodium acrylate-co-acrylamide) superabsorbent hydrogel with low salt sensitivity and high pH sensitivity. *J. Appl. Polym. Sci.* **2006**, 101(5), 2927-2937.

[39] Lokhande, H. T.; Varadarajan, P. V.; Iyer, V. Water-superabsorbent polymers through gamma radiation-induced graft-copolymerization of acrylonitrile on guargum. *J. Appl. Polym. Sci.* **1992**, 45(11), 2031-2036.

[40] Mohamadnia, Z.; Zohuriaan-Mehr, M. J.; Kabiri, K.; Razavi-Nouri M. Tragacanth gum-graft-polyacrylonitrile: Synthesis, characterization and hydrolysis. *J. Polym. Res.* **2008**, 15(3), 173-180.

[41] Sadeghi, M.; Hosseinzadeh, H. Synthesis and superswelling behavior of carboxymethylcellulose–poly(sodium acrylate-co-acrylamide) hydrogel. *J. Appl. Polym. Sci.* **2008**, 108(2), 1142-1151.

[42] Savoji, M. T.; Pourjavadi, A. Partially hydrolyzed kappa carrageenan—polyacrylonitrile as a novel biopolymer-based superabsorbent hydrogel: Synthesis, characterization, and swelling behaviors. *Polym. Eng. Sci.* **2006**, 46(12), 1778-1786.

[43] Nam, C. W.; Kim, Y. H.; Ko, S. W. Blend fibers of polyacrylonitrile and water-soluble chitosan derivative prepared from sodium thiocyanate solution. *J. Appl. Polym. Sci.* **2001**, 82(7), 1620-1629.

[44] Lim, K. Y.; Yoon, K. J.; Kim, B. C. Highly absorbable lyocell fiber spun from celluloses/hydrolyzed starch-g-PAN solution in NMMO monohydrate. *Eur. Polym. J.* **2003**, 39(11), 2115-2120.

[45] Yu, L.; Gu, L. Effects of microstructure, crosslinking density, temperature and exterior load on dynamic pH-response of hydrolyzed polyacrylonitrile-blend-gelatin hydrogel fibers. *Eur. Polym. J.* **2009**, 45(6), 1706-1715.

[46] Yu, L.; Yan, D.; Sun, G.; Gu, L. Preparation and characterization of pH-sensitive hydrogel fibers based on hydrolyzed-polyacrylonitrile/soy protein. *J. Appl. Polym. Sci.* **2008**, 108(2), 1100-1108.

[47] Yu, L.; Gu, L. Hydrolyzed polyacrylonitrile-blend-soy protein hydrogel fibers: A study of structure and dynamic pH response. *Polym. Int.* **2009**, 58(1), 66-73.

[48] Yu, L.; Xu, J.; Gu, L. Preparation, morphology and pH sensitivity of hybrid hydrolyzed polyacrylonitirile-blend-gelatin hydrogel fibers. *Polym. Int.* **2008**, 57(9), 1017-1026.

[49] Gupta, M. L.; Gupta, B.; Oppermann, W.; Hardtmann, G. Surface modification of polyacrylonitrile staple fibers via alkaline hydrolysis for superabsorbent applications. *J. Appl. Polym. Sci.* **2004**, 91(5), 3127-3133.

[50] Yang, M. C.; Tong, J. H. Loose ultrafiltration of proteins using hydrolyzed polyacrylonitrile hollow fiber. *J. Membr. Sci.* **1997**, 132(1), 63-71.

[51] Liu, H.; Hsieh, Y. L. Preparation of water-absorbing polyacrylonitrile nanofibrous membrane. *Macromol. Rapid Commun.* **2006**, 27(2), 142-145.

[52] Hu, X.; Xiao, C. Study on superabsorbent polyacrylonitrile-based fibre. *Indian J. Fibre Text.* **2005**, 30(2), 207-210.

[53] Pourjavadi, A.; Hosseinzadeh, H. Synthesis and properties of partially hydrolyzed acrylonitrile-co-acrylamide superabsorbent hydrogel. *B. Kor. Chem. Soc.* **2010**, 31(11), 3163-3172.

[54] Lim, H. S.; Park, S. H.; Koo, S. H.; Kwark, Y. J.; Thomas, E. L.; Jeong, Y.; Cho, J. H. Superamphiphilic Janus Fabric. *Langmuir* **2010**, 26(24), 19159-19162.

[55] Chemat, F.; Poux, M.; Berlan, J. "Dry" hydrolysis of nitriles effected by microwave heating. *J. Chem. Soc. Perkin. Trans. 2* **1994**, 12, 2597-2602.

[56] Lövy, J.; Janout, V.; Hrudkovă, H. C-13 NMR-study of hydrolyzed poly(acrylonitrile). *Collect. Czech. Chem. Commun.* **1984**, 49(2), 506-512.

[57] Bajaj, P.; Chavan, R. B.; Manjeet, B. Saponification kinetics of acrylonitrile terpolymer and polyacrylonitrile. *J. Macromol. Sci. Chem.* **1985**, A22(9), 1219-1239.

[58] Bajaj, P.; Kumari, M. S. Structural investigations on hydrolyzed acrylonitrile terpolymers. *Eur. Polym. J.* **1988**, 24(3), 275-279.

[59] Choi, Y. H.; Choi, C. M.; Choi, D. H.; Paik, Y.; Park, B. J.; Joo, Y. K.; Kim, N. J. Time dependent solid-state ^{13}C NMR study on alkaline hydrolysis of polyacrylonitrile hollow fiber ultrafiltration membranes. *J. Membr. Sci.* **2011**, 371(1-2), 84-89.

[60] Krentsel, L. B.; Kudryavtsev, Y. V.; Rebrov, A. I.; Litmanovich, A. D.; Platé, N. A. Acidic hydrolysis of polyacrylonitrile: effect of neighboring groups. *Macromolecules* **2001**, 34(16), 5607-5610.

[61] Choe, K. Y.; Kim, K. J.; Kim, D. Y.; Manford, C.; Heo, S.; Shahinpoor M. Performance Characteristics of electro-chemically Driven Polyacrylonitrile Fiber bundle actuators. *J. Intell. Mater. Syst. Struct.* **2006**, 17, 563-576.

[62] Bao, Y.; Ma, J. Z.; Li, N. Synthesis and swelling behaviors of sodium carboxymethyl cellulose-g-poly(AA-co-AM-co-AMPS) / MMT superabsorbent hydrogel. *Carbohydr. Polym.* **2011**, 84(1), 76-82.

[63] O' Grady, M. L.; Kuo, P. L.; Parker, K. K. Optimization of electroactive Hydrogel Actuators. *ACS Appl. Mater. Inter.* **2010**, 2(2), 343-346.

[64] Lee, D.Y.; Kim, Y.; Lee S. J.; Lee, M. H.; Lee, J. Y.; Kim, B. Y.; Cho N. I. Characteristics of chemo-mechanically driven polyacrylonitrile fiber gel actuators. *Mat. Sci. Eng. C-Biomim.* **2008**, 28, 294-298.

[65] Samatham, R.; Park, I. S.; Nam, J. D.; Whisman, N.; Adams, J. Electrospun nanoscale polyacrylonitrile artificial muscle. *Smart Mater. Struct.* **2006**, 15, N152-N156.

[66] Mark, H. F. Superabsorbent Polymers. In *Encyclopedia of polymer science and technology*, 4th ed.; Chichester: Wiley-Blackwell, 2014.

[67] Zohuriaan-Mehr, M.J.; Omidian, H.; Doroudiani, S.; Kabiri, K. Advances in non-hygienic applications of superabsorbent hydrogel materials. *J. Mater. Sci.* **2010**, 45(21), 5711-5735.

[68] Hearle, J. W. S.; Morton, W. E. The retention of liquid water. In *Physical Properties of Textile Fibers*, 4th ed.; Woodhead publishing in Textiles no. 468; Cambridge: Textile Institute: Woodhead Pub.; Boca Raton, Fla.: CRC Press, 2008; Chapter 10, pp. 229-236.

[69] Hearle, J. W. S.; Morton, W. E. Swelling. In *Physical Properties of Textile Fibers*, 4th ed.; Woodhead publishing in Textiles no. 468; Cambridge: Textile Institute: Woodhead Pub.; Boca Raton, Fla.: CRC Press, 2008; Chapter 11, pp. 237-242.

[70] Otterburn, M. S. The chemistry and reactivity of silk. In *Chemistry of natural protein fibers*; Asquith, R. S., Eds.; Plenum Press: New York, 1977; pp 53-80.

[71] International Sericultural Commission – Industry Statistics. http://inserco.org/en/?q=statistics (accessed 30/7/2015).

[72] Li, G.; Liu, H.; Li T. D.; Wang, J. Surface modification and functionalization of silk fibroin fibers-fabric toward high performance applications. *Mat. Sci. Eng. C-Biomim.* **2012**, 32(4), 627-636.

[73] Ltman, G. H.; Diaz, F.; Jakuba, C.; Calabro, T.; Horan, R. L.; Chen, J.; Lu, H.; Richmond, J.; Kaplan, D. L. Silk-based biomaterials. *Biomaterials* **2003**, 24(3), 401-416.

[74] Hakimi, O.; Knight, D.; Vollrath, F.; Vadgama, P. Spider and mulberry silkworm silks as compatible biomaterials. *Compos. Part B-Eng.* **2007**, 38(3), 324-337.

[75] Zhang Y. Q. Applications of natural silk protein sericin in biomaterials. *Biotechnol. Adv.* **2002**, 20(2), 91-100.

[76] Altman, G. H.; Horan, R. L.; Lu, H. H.; Moreau, J.; Martin, I.; Richmond, J. C.; Kaplan, D. L. Silk matrix for tissue engineered anterior cruciate ligaments. *Biomaterials* **2002**, 23(20), 4131-4141.

[77] Kato, N.; Sato, S.; Yamanaka, A.; Yamada, H.; Fuwa, N.; Nomura, M. Silk protein, sericin, inhibits lipid peroxidation and tyrosinase activity. *Biosci. Biotechnol. Biochem.* **1998**, 62(1), 145-147.

[78] Zhaorigetu, S.; Sasaki, M.; Watanabe, H.; Kato, N. Supplemental silk protein, sericin, suppresses colon tumorigenesis in 1, 2-dimethylhydrazine-treated mice by reducing oxidative stress and cell proliferation. *Biosci. Biotechnol. Biochem.* **2001**, 65(10), 2181-2186.

[79] Tsujimoto, K.; Takagi, H.; Takahashi, M.; Yamada, H.; Nakamori, S. Cryoprotective effect of the serine-rich repetitive sequence in silk protein sericin. *J. Biochem.* **2001**, 129(6), 979-986.

[80] Zhang, Y. Q.; Tao, M. L.; Shen, W. D.; Zhou, Y. Z.; Ding, Y.; Ma, Y.; Zhou, W. L. Immobilization of L-asparaginase on the microparticles of the natural silk sericin protein and its characters. *Biomaterials* **2004**, 25(17), 3751-3759.

[81] Teramoto, H.; Nakajima, K.; Takabayashi, C. Preparation of elastic silk sericin hydrogel. *Biosci. Biotechnol. Biochem.* **2005**, 69(4), 845-847.

[82] Teramoto, H.; Kameda, T.; Tamada, Y. Preparation of gel film from bombyx mori silk sericin and its characterization as a wound dressing. *Biosci. Biotechnol. Biochem.* **2008**, 72(12), 3189-3196.

[83] Wu, W.; Li, W.; Wang, L. Q.; Tu, K.; Sun, W. Synthesis and characterization of pH- and temperature- sensitive silk sericin/poly(N-isopropylacrylamide) interpenetrating polymer networks. *Polym. Int.* **2006**, 55(5), 513-519.

[84] Wu, W.; Wang, D. S. A fast pH-responsive IPN hydrogel: Synthesis and controlled drug delivery. *React. Funct. Polym.* **2010**, 70(9), 684-691.

[85] Lim, K. S.; Kundu, J.; Reeves, A.; Poole-Warren, L. A.; Kundu, S. C.; Martens, P. J. The influence of silkworm species on cellular interactions with novel PVA/silk sericin hydrogels. *Macromol. Biosci.* **2012**, 12(3), 322-332.

[86] Oyama, F.; Mizuno, S.; Shimura, K. Studies on immunological properties of fibroin heavy and light chains. *J. Biochem.* **1984**, 96(6), 1689-1694.

[87] Takei, F.; Kikuchi, Y.; Kikuchi, A.; Mizuno, S.; Shimura, K. Further evidence for importance of the subunit combination of silk fibroin in its efficient secretion from the posterior silk gland cells. *J. Cell. Biol.* **1987**, 105(1), 175-180.

[88] Tanaka, K.; Mori, K.; Mizuno, S. Immunological identification of the major disulfide-linked light component of silk fibroin. *J. Biochem.* **1993**, 114(1), 1-4.

[89] Jin, H. J.; Kaplan, D. L. Mechanism of silk processing in insects and spiders. *Nature* **2003**, 424(6952), 1057-1061.

[90] Zhou, C. Z.; Confalonieri, F.; Medina, N.; Zivanovic, Y.; Esnault, C.; Yang, T.; Jacquet, M.; Janin, J.; Duguet, M.; Perasso, R.; Li, Z. G. Fine organization of *bombyx mori* fibroin heavy chain gene. *Nucleic Acids Res.* **2000**, 28(12), 2413-2419.

[91] Agostini de Moraes, M.; Beppu, M. M. Silk fibroin hydrogels: A review under biomaterials perspective. In *Hydrogels: Synthesis, characterization and applications*, Câmara, F. V., Ferreira, L. J. Eds.; Biochemistry Research Trends: Pharmacology - Research, Safety Testing and Regulation; Nova Science Publishers, Inc., 2012; pp 209-226.

[92] Matsumoto, A.; Chen, J.; Collette, A. L.; Kim, U. J.; Altman, G. H.; Cebe, P.; Kaplan, D. L. Mechanisms of silk fibroin sol-gel transitions. *J. Phys. Chem. B* **2006**, 110, 21630-21638.

[93] Arai, T.; Freddi, G.; Innocenti, R.; Tsukada, M. Biodegradation of *Bombyx mori* Silk Fibroin Fibers and Films. *J. Appl. Polym. Sci.* 2004, 80, 2383-2390.

[94] Horan, R. L.; Antle, K.; Collette, A. L.; Huang, Y. Z.; Huang, J.; Moreau, J. E.; Volloch, V.; Kaplan, D. L.; Altman, G. H. In vitro degradation of silk fibroin. *Biomaterials* **2005**, 26(17), 3385-3393.

[95] Hu, K.; Lv, Q.; Cui, F. Z.; Feng, Q. L.; Kong, X. D.; Wang, H. L.; Huang, L. Y.; Li, T. Biocompatible fibroin blended films with recombinant human-like collagen for hepatic tissue engineering. *J. Bioact. Compat. Polym.* **2006**, 21(1), 23-37.

[96] Minoura, N.; Tsukada, M.; Nagura, M. Fine structure and oxygen permeability of silk fibroin membrane treated with methanol. *Polymer* **1990**, 31(2), 265-269.

[97] Santin, M.; Motta, A.; Freddi, G.; Cannas, M. In vitro evaluation of the inflammatory potential of the silk fibroin. *J. Biomed. Mater. Res.* **1999**, 46(3), 382-389.

[98] Vasconcelos, A.; Freddi, G.; Cavaco-Paulo, A. Biodegradable materials based on silk fibroin and keratin. *Biomacromolecules* **2008**, 9, 1299-1305.

[99] Baltova, S.; Vassileva, V.; Valtvheva, E. Photochemical behaviour of natural silk—I. Kinetic investigation of photoyellowing. *Polym. Degrad. Stabil.* **1998**, 60, 53-60.

[100] Lu, Y. H.; Lin, H.; Chen, Y. Y.; Wang, C.; Hua, Y. R. Structure and performance of Bombyx mori silk modified with nano-TiO_2 and chitosan. *Fiber. Polym.* **2007**, 8(1), 472-478.

[101] Park, D. J.; Lee, M. H.; Woo, Y. I.; Han, D. W.; Choi, J. B.; Kim, J. K.; Hyun, S. O.; Chung, K. H.; Park, J. C. Sterilization of microorganisms in silk fabrics by microwave-induced argon plasma treatment at atmospheric pressure. *Surf. Coat. Technol.* **2008**, 202 (22-23), 5773-5778.

[102] Gellert, B.; Kogelschatz, U. Generation of excimer emission in dielectric barrier discharges. *Appl. Phys., B Photophys. Laser Chem.* **1991**, 52, 14-21.

[103] Periyasamy, S.; Gupta, D.; Gulrajani, M. L. Nanoscale surface roughening of mulberry silk by monochromatic VUV excimer lamp. *J. Appl. Polym. Sci.* **2007**, 103, 4102-4106.

[104] Periyasamy, S.; Gulrajani, M. L.; Gupta, D. Preparation of a multifunctional mulberry silk fabric having hydrophobic and hydrophilic surfaces using VUV excimer lamp. *Surf. Coat. Technol.* **2001**, 201, 7286-7291.

[105] Elsner, C.; Lenker, M.; Prager, L.; Mehnert. R. Windowless argon excimer source for surface modification. *Appl. Surf. Sci.* **2006**, 252, 3616-3624.

[106] Ramgopal, G.; Ramani, R.; Ramachandra, P.; Ranganathaiah, C. UV degradation of bivoltine silk fiber: a positron annihilation study. *Eur. Polym. J.* **1998**, 34, 1423-1427.

[107] Long, J. J.; Wang, H. W.; Lu, T. Q.; Tang, R. C.; Zhu, Y. W. Application of Low-Pressure Plasma Pretreatment in Silk Fabric Degumming Process. *Plasma Chem. Plasma Process.* **2008**, 28, 701-713.

[108] Hodak, S. K.; Supasai, T.; Paosawatyanyong, B.; Kamlangkla, K.; Pavarajarn, V. Enhancement of the hydrophobicity of silk fabrics by SF6 plasma. *Appl. Surf. Sci.* **2008**, 254, 4744-4749.

[109] Shen, L.; Dai, J. Improvement of hydrophobic properties of silk and cotton by hexafluoropropene plasma treatment. *Appl. Surf. Sci.* **2007**, 253, 5051-5055.

[110] Borcia, G.; Anderson, C. A.; Brown N. M. D. Surface treatment of natural and synthetic textiles using a dielectric barrier discharge. *Surf. Coat. Technol.* **2006**, 201, 3074-3081.

[111] Molina, R.; Espinós, J. P.; Yubero, F.; Erra, P.; González-Elipe, A. R. XPS analysis of down stream plasma treated wool: Influence of the nature of the gas on the surface modification of wool. *Appl. Surf. Sci.* **2005**, 252, 1417-1429.

[112] Boonla, K.; Saikrasun, S. Influence of silk surface modification via plasma treatments on adsorption kinetics of lac dyeing on silk. *Text. Res. J.* **2013**, 83, 288-297.

[113] Fang, K.; Wang, S.; Wang C.; Tian, A. Inkjet printing effects of pigment inks on silk fabrics surface-modified with O2 plasma. *J. Appl. Polym. Sci.* **2008**, 107, 2949-2955.

[114] Iriyama, Y.; Mochizuki, T.; Watanabe, M.; Utada, M. Plasma Treatment of Silk Fabrics for Better Dyeability. *J. Photopolym. Sci. Tec.* **2002**, 15, 299-306.

[115] Lee, M. S.; Lee, M.; Tokuyama, T.; Wakida, T.; Inoue, G.; Ishida, S. Ammonia-gas and liquid ammonia treatments of silk fabric. *J. Appl. Polym. Sci.* **2006**, 101, 3487-3492.

[116] Das, A.; Saikia, C. N.; Hussain, S. Grafting of methyl methacrylate (MMA) onto Antheraea assama silk fiber. *J. Appl. Polym. Sci.* **2001**, 81(11), 2633-2641.

[117] Maji, T. K.; Basu, D.; Datta, C.; Banerjee, A. Studies of mechanical and moisture regain properties of methyl methacrylate grafted silk fibers. *J. Appl. Polym. Sci.* **2002**, 84(5), 969-974.

[118] Ojah, R.; Dolui, S. K. Graft copolymerization of vinyl monomers onto silk fibers initiated by a semiconductor-based photocatalyst. *J. Appl. Polym. Sci.* **2007**, 105(4), 2164-2175.

[119] Prachayawarakorn, J.; Boonsawat, K. Physical, chemical, and dyeing properties of *Bombyx mori* silks grafted by 2-hydroxyethyl methacrylate and methyl methacrylate. *J. Appl. Polym. Sci.* **2007**, 106(3), 1526-1534.

[120] Shang, S.; Zhu, L.; Chen, W.; Yi, L.; Qi, D.; Yang, L. Reducing silk fibrillation through MMA graft method. *Fiber. Polym.* **2009**, 10(6), 807-812.

[121] Das, A. M.; Chowdhury C. N.; Saikia, C. N.; Rao, P. G. Some Physical Properties and Structure Determination of Vinyl Monomer-Grafted *Antheraea assama* Silk Fiber. *Ind. Eng. Chem. Res.* **2009**, 48, 9338-9345.

[122] Das, A. M.; Chowdhury, P. K.; Saikia, C. N.; Rao, P. G. Silk fibre modification through graft copolymerization using vinyl monomer. *Indian J. Fibre Text.* **2010**, 35, 107-114.

[123] Paosawatyanyong, B.; Jermsutjarit, P.; Bhanthumnavin, W. Graft copolymerization coating of methacryloyloxyethyl diphenyl phosphate flame retardant onto silk surface. *Prog. Org. Coat.* **2014**, 77, 1585-1590.

[124] Guan, J.; Chen, G. Performance of flame retardancy silk modified with water-soluble vinyl phosphoamide. *J. Appl. Polym. Sci.* **2013**, 129, 2335-2341.

[125] Tsukada, M; Arai, T.; Winkler, S.; Freddi, G. Physical properties of silk fibers grafted with vinyltrimethoxysilane. *J. Appl. Polym. Sci.* **2001**, 79(10), 1764-1770.

[126] Li, S.; Xing, T.; Li, Z.; Chen, G. Structure and properties of silk grafted with acrylate fluoride monomers by ATRP. *Appl. Surf. Sci.* **2013**, 268, 92-97.

[127] Davarpanah, S.; Mahmoodi, N. M.; Arami, K.; Bahrami, H.; Mazaheri, F. Environmentally friendly surface modification of silk fiber- Chitosan grafting and dyeing. *Appl. Surf. Sci.* **2009**, 255, 4171-4176.

[128] Ferrero, F.; Periolatto, M.; Burelli, S.; Carletto, R. A. Silk grafting with chitosan and crosslinking agents. *Fiber. Polym.* **2010**, 11, 185-192.

[129] Wang, P.; Yu, M.; Cui, L.; Yuan, J.; Wang, Q.; Fan, X. Modification of *Bombyx mori* silk fabrics by tyrosinase- catalyzed grafting of chitosan. *Eng. Life Sci.* **2014**, 14, 211-217.

[130] Li, G.; Liu, H.; Zhao, H.; Gao, Y.; Wang, J.; Jiang, H.; Boughtin, R. I. Chemical assembly of TiO_2 and TiO_2@Ag nanoparticles on silk fiber to produce multifunctional fabrics. *J. Colloid Interface Sci.* **2011**, 358, 307-315.

[131] Dubas, S. T.; Kumlangdudsana, P.; Potiyaraj, P. Layer-by-layer deposition of antimicrobial silver nanoparticles on textile fibers. *Colloids Surf., A* **2006**, 289, 105-109.

[132] Gulrajani, M. L.; Gupta, D.; Periyasamy, S.; Muthu, S. G. Preparation and application of silver nanoparticles on silk for imparting antimicrobial properties. *J. Appl. Polym. Sci.* **2008**, 108, 614-623.

[133] Chang, S.; Kang, B.; Dai, Y.; Chen, D. Synthesis of Antimicrobial Silver Nanoparticles on Silk Fibers Via gamma-Radiation. *J. Appl. Polym. Sci.* **2009**, 112, 2511-2515.

[134] Abbasi, A. R.; Morsali, A. Synthesis and properties of silk yarn containing Ag nanoparticles under ultrasound irradiation. *Ultrason. Sonochem.* **2011**, 18, 282-287.

[135] Abbasi, A. R.; Morsali, A. Ultrasound-assisted coating of silk yarn with silver chloride nanoparticles. *Colloids Surf., A* **2010**, 371, 113-118.

[136] Lu, Z.; Meng, M.; Jiang, Y.; Xie,J. UV-assisted in situ synthesis of silver nanoparticles on silk fibers for antibacterial applications. *Colloids Surf., A* **2014**, 447, 1-7.

[137] Wang, X.; Gao, W.; Xu, S.; Xu, W. Luminescent fibers: *In situ* synthesis of silver nanoclusters on silk via ultraviolet light-induced reduction and their antibacterial activity. *Chem. Eng. J.* **2010**, 210, 585-589.

[138] Dong, Q.; Su, H.; Zhang, S. *In Situ* Depositing Silver Nanoclusters on Silk Fibroin Fibers Supports by a Novel Biotemplate Redox Technique at Room Temperature. *J. Phys. Chem. B* **2005**, 109, 17429-17434.

[139] Wang, L.; Nemoto, R.; Senna, M. Microstructure and chemical states of hydroxyapatite/ silk fibroin nanocomposites synthesized via a wet-mechanochemical route. *J. Nanopart. Res.* **2002**, 4, 535-540.

[140] Yang, M.; He, W.; Shuai, Y.; Min, S.; Zhu, L. Nucleation of hydroxyapatite crystals by self-assembled *Bombyx mori* silk fibroin. *J. Polym. Sci. Pol. Phys.* **2013**, 51, 742-748.

[141] Kim, H. H.; Park, J. B.; Kang, M. J.; Park, Y. H. Surface-modified silk hydrogel containing hydroxyapatite nanoparticle with hyaluronic acid–dopamine conjugate. *Int. J. Biol. Macromol.* **2014**, 70, 516-522.

[142] Tanaka, T.; Hirose, M.; Kotobuki, N.; Ohgushi, H.; Furuzono, T.; Sato, J. Nano-scaled hydroxyapatite-silk fibroin sheets support osteogenic differentiation of rat bone marrow mesenchymal cells. *Mater. Sci. Eng. C* **2007**, 27, 817-823.

[143] Korematsu, A.; Furuzono, T.; Yasuda, S.; Tanaka, J.; Kishida, A. Nano-scaled hydroxyapatite/ polymer composite III. Coating of sintered hydroxyapatite particles on poly(4-methacryloyloxyethyl trimellitate anhydride)-grafted silk fibroin fibers. *J. Mater. Sci.-Mater. M.* **2005,** 16, 67-71.

Chapter 3
Study on heat stabilization of polyacrylonitrile (PAN) nanofibers

3.1 Introduction

Polyacrylonitrile (PAN) is an important synthetic polymer of producing acrylic fiber and also a common precursor for manufacturing carbon fiber [1, 2]. The production of carbon fiber involves two major procedures: (1) heat stabilization below 300 ℃ under air, and (2) carbonization and graphitization by heating up over 1000 ℃ under inert atmosphere [3, 4]. During oxidative stabilization at suitable temperatures, cyclization of the nitrile (–CN) side groups on the polymer backbones occur simultaneously, resulting in conjugated structure within chains and crosslink structure between chains [5-10]. These structural changes of PAN enable further carbonization process to manufacture carbon fiber or hydrolysis to prepare hydrogel. Therefore, fine control of the first heat stabilization stage is crucial for the success of those post-treatments. As reported by previous research, stabilization rate is mainly controlled by oxygen diffusion into the precursor fiber [11, 12]. Hence, the fiber diameter casts an important effect on the heat stabilization reaction. The decrease in fiber diameter by 10 times may significantly change the fiber stabilization kinetics and increase the conversion yield. However, previous studies on oxidative stabilization were mainly focused

on the microfiber, whereas the heat treatment performance on the nanofiber has not been fully investigated.

Electrospinning is an effective and versatile method for producing continuous fiber of nanometric-scale [13]. The principle of electrospinning is to apply a strong electrical field in between a syringe filled with polymer solution and a collector to generate nanofibers. As the electrostatic repulsion force is high enough to overcome the surface tension of the droplet at needle tip, the electrically charged polymer solution is ejected out of the droplet to create a Taylor cone. Eventually, the droplet is stretched into nanofiber, and the nanofiber is collected on the grounded collector [14]. Because of the flexibility of electrospinning, electrospun nanofibers have been applied in different fields such as filtration membranes [15], scaffolds for cells and catalysts [16-18], electronic and optical devices [19], and functional textiles [20].

PAN undergoes hydrolysis in an alkaline aqueous solution to produce solubilizing groups such as amide ($–CONH_2$) and carboxylic acid (–COOH) [21, 22]. If PAN fiber is firstly crosslinked, superabsorbent fiber would be obtained by further alkaline hydrolysis, as patented by Toyobo [23, 24]. In this study, PAN nanofiber, which has a smaller fiber diameter than the traditional absorbent resins, is fabricated via electrospinning in order to prepare the superabsorbent with high water absorption rate.

Although the oxidative stabilization is an important process for

crosslinking PAN fiber and maintaining its integral structure, only a few studies have been conducted on the stabilization of PAN nanofibers [25]. In this chapter, the relative rates of reactions (i.e., dehydrogenation, cyclization, and carbonylation) occurred during stabilization process were investigated in depth by Fourier transform infrared (FTIR) spectroscopy. The resultant crosslink structure, which is significant for maintaining integrity of hydrogel, was further examined by extraction in dimethylformamide (DMF) and hydrolysis in aqueous alkaline solution.

3.2 Experimental

3.2.1 Materials

Polyacrylonitrile (PAN, M_w = 150,000), dimethylformamide (DMF), and sodium hydroxide (NaOH) were all purchased from Sigma-Aldrich Co. and used without further purification. 10 wt% PAN was dissolved in DMF by stirring at room temperature until a clear yellowish solution was obtained.

3.2.2 Electrospinning

PAN solution of 10 wt% was loaded into a syringe, and electrospun into nanofibers collected by a rolling substrate, using a commercial electrospinning device (Kato Tech Co., Ltd.). The schematic illustration electrospinning setup is shown in Figure 3.1. The distance and voltage between the needle tip and the cylindrical collector were 15 cm and 25 kV respectively. The speeds of target

rotation, syringe pump, and transverse movement were set as 2.0 m/min, 0.05 mm/min, and 10.0 cm/min, respectively. The as-prepared PAN electrospun web was heated up to 100 ℃ in a vacuum oven (Shel Lab) to remove DMF till a constant weight.

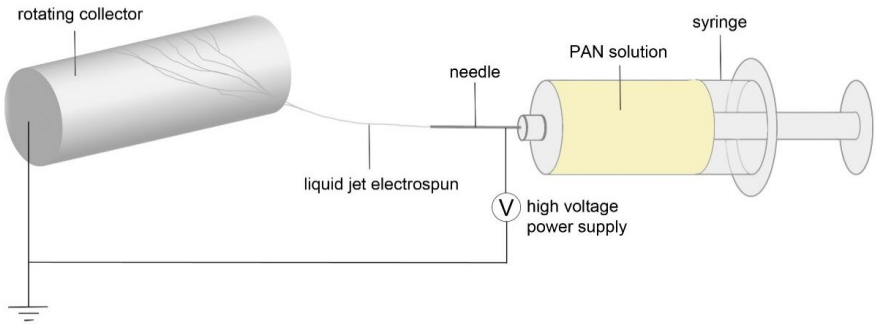

Figure 3.1 Schematic illustration of electrospinning setup.

3.2.3 Heat treatment and alkaline hydrolysis

The PAN electrospun webs were heated in a muffle oven (Carbolite Co., Ltd.) at 220 or 260 °C for 30 or 120 min in the presence of air. These samples were denoted as “heating temperature (℃)-heating time (min)”, for example, 220-120 and 260-30 representing heating at 220 °C for 120 min and 260 °C for 30 min respectively. The alkaline hydrolysis of PAN webs was carried out in a 1.0 N NaOH aqueous solution at 85 ℃ with stirring. The specimens were then collected by a nickel net filter and rinsed by deionized water till neutral pH.

3.2.4 Characterizations

The samples were fully swollen in DI water and then freeze-dried (Christ Alpha 1-4 LD). The surface morphologies of the samples were observed under a

field-emission scanning electron microscope (FE-SEM, JEOL JSM-6335F) with 5 or 8 kV and another SEM (JEOL JSM-6490) with 20 kV, after being coated with gold sputtering.

The PAN electrospun webs were analyzed by thermogravimetric analyzer (Mettler Toledo TGA 1) under air atmosphere. The samples were heated at 10 °C/min until the designated temperature at 220, 260, or 320 °C was reached and then maintained at that particular temperature for further 120 min.

Fourier transform infrared (FTIR) spectra were obtained by PerkinElmer Spectrum 100 equipped with a beam condenser in a spectral region of 4000–650 cm^{-1} with 16 scans at 4 cm^{-1} resolution.

To measure the gel fraction of heated PAN samples, they were extracted by soxhlet extraction using DMF at 100 ℃ for 24 h as illustrated in Figure 3.2 and then dried in a vacuum oven at 100 ℃ to remove the remaining solvent. The extraction procedure was repeated for several times until the specimen weight became constant. Weight remain (%) is calculated by

$$\text{Weight remain} = \frac{\text{dry weight of residue}}{\text{dry weight of sample}} \times 100\% \qquad \text{(Equation 3.1)}$$

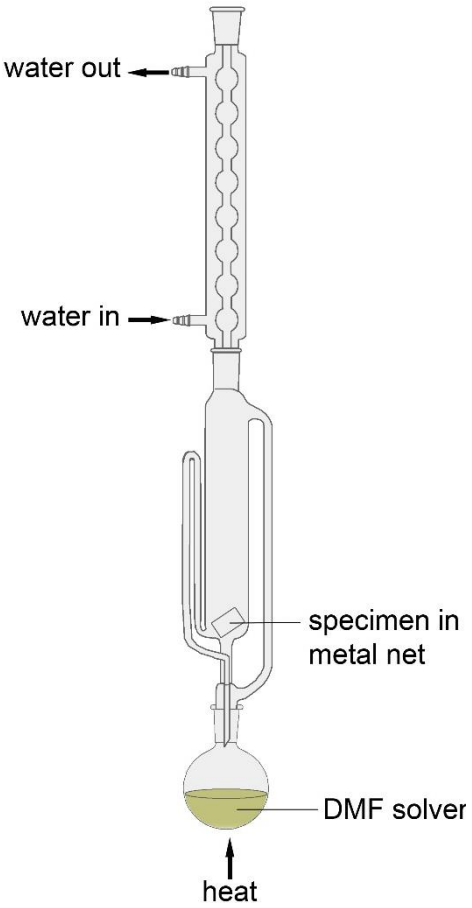

Figure 3.2 Experimental setup of the soxhlet extraction.

3.3 Results and discussion

3.3.1 Surface morphology

PAN nanofibers were prepared by electrospinning as described previously. As shown in Figure 3.3a, the as-electrospun PAN nanofibers were smooth, straight, and overlapped as observed clearly under SEM. The diameter of these nanofibers was about 400–1000 nm that was 10 times smaller than that of common textile fibers. Therefore, this fineness feature is expected to enable fast modification in following heating and alkaline hydrolysis treatments.

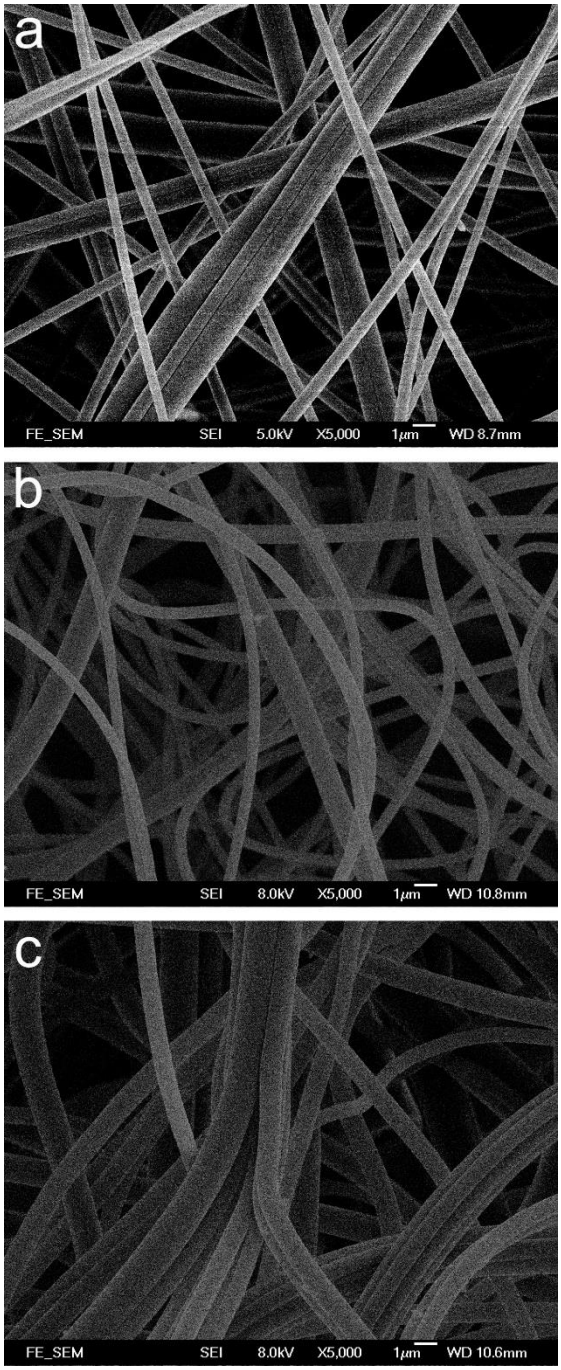

Figure 3.3 SEM images of PAN webs: (a) as-electrospun, (b) 220-120, and (c) 260-120.

3.3.2 TG analysis

Figure 3.4a shows the TG curve of PAN powder heated from 30 to 900 ℃ under air atmosphere at 10 ℃/min. Its decomposition began at around 308 ℃, and its

weight loss was around 16% of its original weight. It further decomposed as the temperature reached around 329 ℃, and its weight dramatically decreased by 82%. Thus, the temperature of heat treatment on PAN in air should be below 329 ℃ to avoid decomposition.

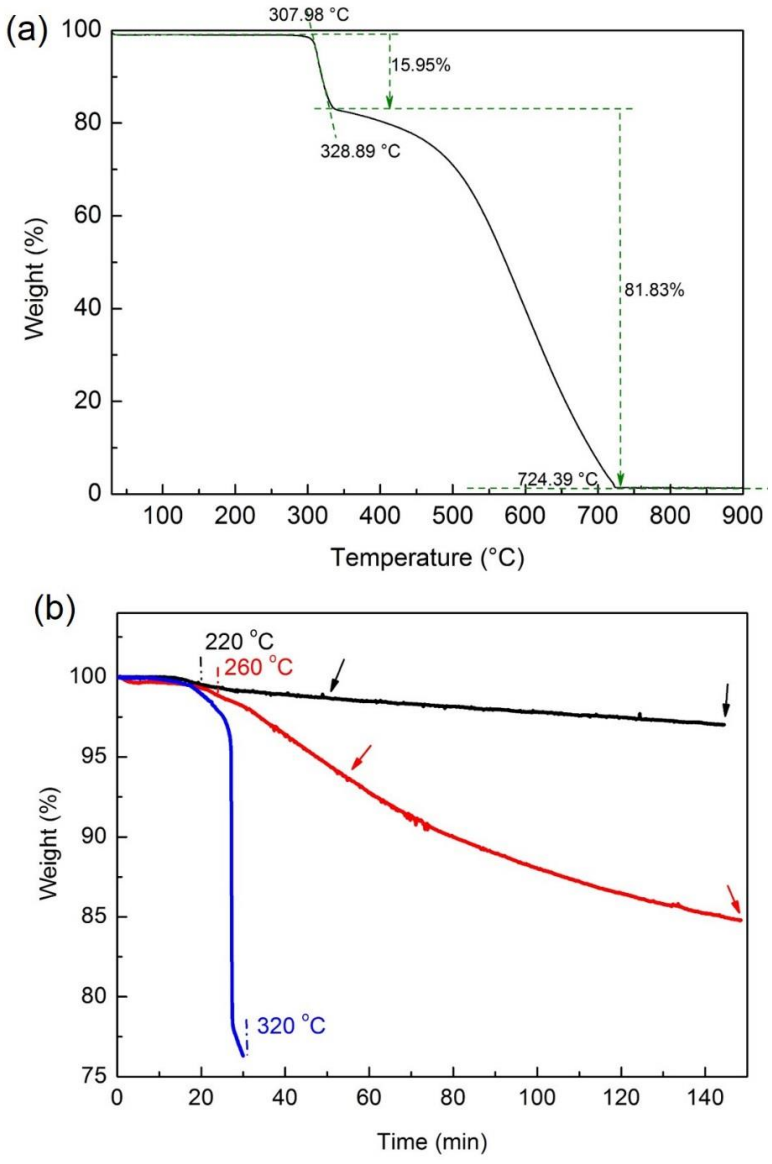

Figure 3.4 TG curves of (a) PAN powder, and (b) PAN nanofibers: section before the dash-line was the heating up stage with 10 ℃/min, section after the dash-line was at constant temperature, arrows pointed to the period selected to treat PAN nanofibers.

Color change from white to yellow or even brown was visually observed, when the PAN electrospun web was heated over 200 ℃ in the presence of oxygen. Increasing temperature and time led to a darker color. In order to observe the effect of temperature on stabilizing the PAN nanofibers without decomposition, further experiments on isothermal TG analysis of PAN nanofibers at 220, 260, and 320 ℃ were conducted so that the suitable oxidation temperature for the PAN webs could be determined. As seen in Figure 3.4b, when the web was heated up to 320 ℃ at 10 ℃/min, a sharp and significant weight loss occurred at 300 ℃. This high weight loss of 23 wt% implies a severe damage to the PAN chains that is owing to an intense heat released from the exothermic reaction during heat stabilization [5]. This breakout should be avoided in a controllable oxidative stabilization treatment. Conversely, by heating at constant temperatures at 220 and 260 ℃ for 120 min, weight losses of only 3 wt% and 15 wt% were observed respectively. As a result, two representative temperatures below 300 ℃, 220 and 260 ℃ are selected to mildly treat PAN nanofibers.

After the heat treatment in a muffle oven at the selected temperatures of 220 and 260 ℃, relaxation and cohesion of PAN nanofibers were noticed under SEM that many straight nanofibers became curved shapes and adhered to adjacent ones as shown in Figures 3.3b and 3.3c. However, their fiber diameters remained similar to that of as-electrospun PAN nanofibers, in contrast to another

PAN copolymer nanofibers that their fiber diameter decreased by 20% at 250 ℃ as reported by Esrafilzadeh's group [26]. It should be noted that the heat treatment environments in TG analyzer and muffle oven may not match exactly because of different sample amount and atmosphere.

3.3.3 FTIR analysis

To achieve a deeper insight into the oxidative stabilization process of PAN nanofibers, the chemical changes of samples were analyzed with FTIR spectra. As shown in Figure 3.5, several noticeable changes were observed after heat treatment. As the heating temperature and time increased, the intensity of the characteristic peak of nitrile (–CN) group stretching at 2242 cm^{-1} decreased, implying the cyclization reaction occurs between the adjacent –CN groups. Moreover, the peaks at 2940 and 1450 cm^{-1}, corresponding to $–CH_2$ stretching and $–CH_2$ bending respectively, also decreased obviously. It indicates the dehydrogenation occurs on PAN polymer chains. As the heat treatment proceeded, a weak shoulder peak appeared at 2211 cm^{-1}. It is due to the conjugation of –CN with the adjacent vinyl –C=CH– resulted from dehydrogenation reaction. Concurrently, a significant change at 1622 cm^{-1} after heat treatment was also observed. This small peak in the as-electrospun PAN nanofibers is possibly attributed to low amount of vinyl –C=CH– group present in the raw material. It became more intense after being heated over 220 ℃. New

peaks at 1712 and 1658 cm^{-1} appeared in the IR spectra of 260 ℃ samples. These absorptions are assigned to two newborn –C=O and –C=N– groups. Furthermore, as the absorptions of –C=C–, –C=N–, and –C=O groups increased, their corresponding peaks shifted to lower wavenumbers gradually. It is due to the occurrence of conjugation between these densely distributed double bonds. In contrast to our FTIR results, Sun's work on PAN nanofibers only reported cyclization and dehydrogenation occurred during stabilization at 250 ℃ [27].

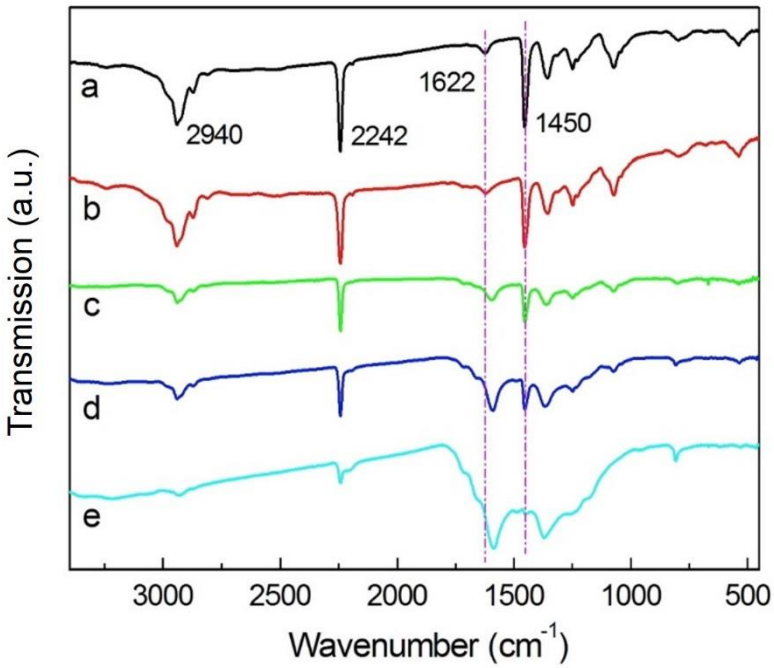

Figure 3.5 FTIR spectra of PAN webs: (a) as-electrospun nanofibers, (b) 220-30, (c) 220-120, (d) 260-30, and (e) 260-120.

In conclusion, FTIR spectra reveal that three types of reactions occur during PAN oxidative heat treatment: 1) dehydrogenation to eliminate hydrogen and form –C=C– in the PAN backbone; 2) cyclization between adjacent –CN groups along the PAN chain to form six-membered ring; and 3) carbonylation to

embed –C=O group in the polymer chain. Their relative speeds are clarified by carefully monitoring the changes in their corresponding peak areas. To facilitate the comparison, all FTIR spectra of samples are normalized by the peak of –CN group stretching at 2242 cm^{-1}, in which area is set at constant value. The intensities of several representative peaks are then traced from various heat treatment conditions. Assuming the width of each individual peak remains the same at each treatment, its intensity can be used directly to represent its area. As shown in Figure 3.6, in comparison to –CN peak, the peaks at 2940 and 1450 cm^{-1} kept lowering, indicating that dehydrogenation is faster than cyclization during the heat treatment, and this difference became more apparent at a higher temperature. Through the comparison between peaks at 1622, 1658, and 1712 cm^{-1}, it confirms that the amount of –C=C– group (dehydrogenation) increases faster than that of –C=N– group (cyclization) while the amount of –C=O group (carbonylation) increases the slowest.

These three groups were also reported on the oxidative stabilization of 12 μm PAN microfibers; however, they were not separated and compared their relative increasing intensity [27]. Their peak assignments were also in the same sequence as ours, although the wavenumbers were slightly shifted. Another research on PAN microfibers did differentiation on these three peaks, where the allocation of corresponding groups was contrary [28]. The authors also claimed that the reaction rate of dehydrogenation was about equal to cyclization, different

from our results on nanofibers. This difference is possibly due to the slow oxygen diffusion in microfibers.

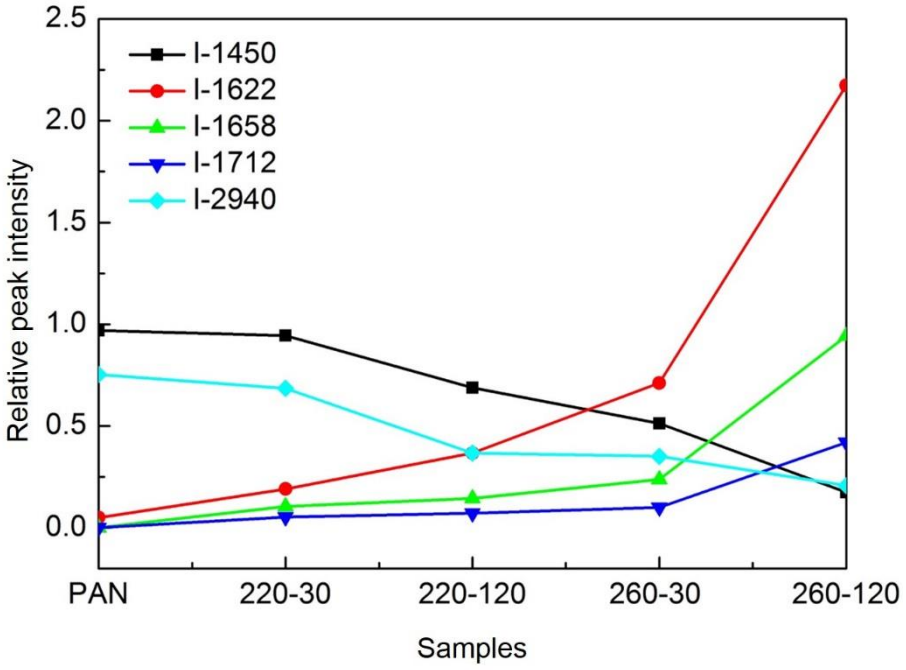

Figure 3.6 The relative peak intensity of five representative FTIR peaks change of PAN webs after various heat treatments, with all spectra normalized to the peak area at 2242 cm^{-1}.

In previous literatures, the peak intensities at 1600 and 2240 cm^{-1} are used to calculate the extent of nitrile conversion, assuming the 1600 cm^{-1} peak as –C=N– stretching absorption [7, 25, 29]. Based on our results, the peak at 1600 cm^{-1} also involves the contributions from –C=O and –C=C– groups, since these three group peaks are quite close and even overlap significantly because of their conjugation with each other. Therefore, the previous equation "conversion extent = $I_{1600}/ (I_{CN} + I_{1600})$" is unreliable, especially for sample being treated at high temperature for a long period [29].

The conversion extent in references 7 and 29 had been overestimated and resulted in an unreasonable value that was even higher than that of our nanofibers. The peak at 1600 cm^{-1} is mainly attributed to –C=C– rather than –C=N– absorption. In order to obtain a more reliable value, these three overlapped peaks should be separated by suitable curve fitting process [30, 31], and the revised equation for conversion index is as following:

$$\text{Conversion index} = \frac{I_{C=N}}{I_{C\equiv N} + I_{C=N}} \qquad \text{(Equation 3.2)}$$

With the consideration of these three reactions, including dehydrogenation, cyclization and carbonylation, this modified conversion index expresses the extent of cyclization precisely.

3.3.4 Heat stabilization mechanism

Based on these FTIR results, a possible mechanism is proposed to demonstrate the gradual chemical changes of PAN nanofibers during heat treatment as shown in Figure 3.7. It involves dehydrogenation to form –C=C–, cyclization to form six-membered ring, and carbonylation to embed –C=O group at initial stage. Moreover, another change worth to notice is that crosslinks are formed via inter-chain cyclization of nitrile groups. Increasing crosslinks will result in high gel content in the heat-treated PAN nanofibers. This crosslink is important to maintain the fiber integrity against alkaline hydrolysis.

According to the above mechanism, weight loss of PAN in the selected heat treatments at 220 and 260 ℃ should be less than 3 wt%. However, much higher weight loss of 15 wt% was found at 260 ℃ in the previous TG results. Therefore, the mechanism derived from FTIR results only is incomplete. Degradation by eliminating –C=O groups and releasing carbon dioxide are possibly the main reason of high weight loss at 260 ℃. In this circumstance, FTIR measurement is not able to confirm this reaction.

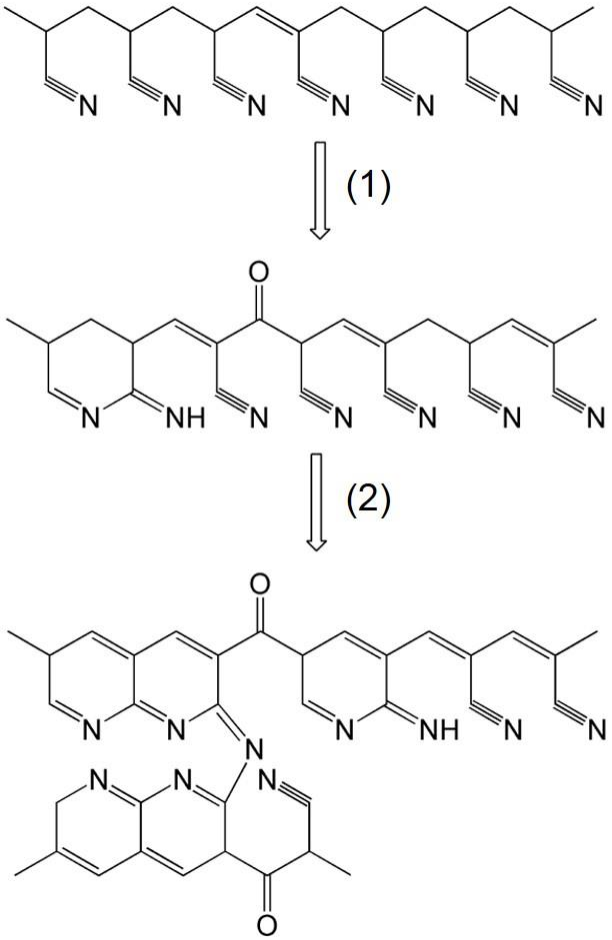

Figure 3.7 Schematic illustration of PAN stabilization mechanism in nanofibers: (1) initial stage; (2) deep stage.

3.3.5 Weight remain

The extraction results of heated samples in DMF are shown in Figure 3.8. The weight remain of extracted samples shows strong dependence on their heat treatment conditions. The amount of residue increases with temperature and heat treatment duration. The weight remain is attributed to the crosslink structure formed by heat treatment and defined as gel fraction. The sample 260-120 had the highest weight remain of 95% among all samples. Since no crosslink was formed in the sample 220-30, it totally dissolved into DMF without residue. In comparison to the gel fraction of 61% from the sample 220-120, the sample 260-30 obtained a higher gel fraction of 72%.

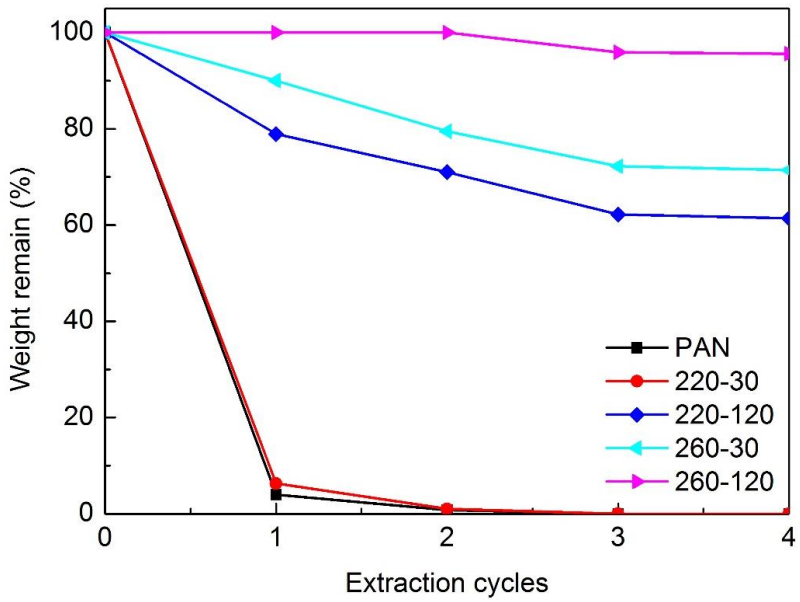

Figure 3.8 The extraction of PAN webs after various heat treatments in hot DMF.

The resultant trend of gel fraction agrees with the previous FTIR spectroscopic results of the heat-treated PAN webs. In a literature, a gel fraction

of ~90% from a PAN copolymer being heated at 210 ℃ for 2 h was also reported [32]. This result is unreliable because gel fraction was measured by immersing melt-spun fiber samples in DMF at room temperature only for 3 days. This mild extraction could not completely remove all those uncrosslinked polymers, based on our experimental results.

3.3.6 Surface morphology after hydrolysis

In Figure 3.9a, both as-electrospun and heat-crosslinked PAN webs were hydrolyzed in aqueous alkaline solution for 120 min. The as-electrospun PAN web was completely dissolved and the solution remained transparent. On the contrary, the heat-crosslinked nanofibers had some remaining soft gels in dark brown color.

After being rinsed and dried at room temperature, the typical gel residues were freeze-dried and observed under SEM. The residue of sample 220-120 had a relatively smooth surface without fibrous texture, and layered texture was seen as shown in Figure 3.9b. Because of its low gel content and low crosslink density, the swollen soft fibers easily collapse and adhere to each other to form a continuous and flattened surface during drying. On the other hand, the residue of sample 260-120 gave a noticeable fibrous structure on surface as shown in Figure 3.9c. Owing to its high gel content and high crosslink density, its fibers adhere to each other very closely, and have diameters of about 1000 nm, evidently thicker

than that of original nanofibers. These features are resulted from the wetness and softness of swollen gel fibers. It also supports that a lot of nitrile groups remain and are ready to be hydrolyzed even after heating at 260 ℃ for 120 min.

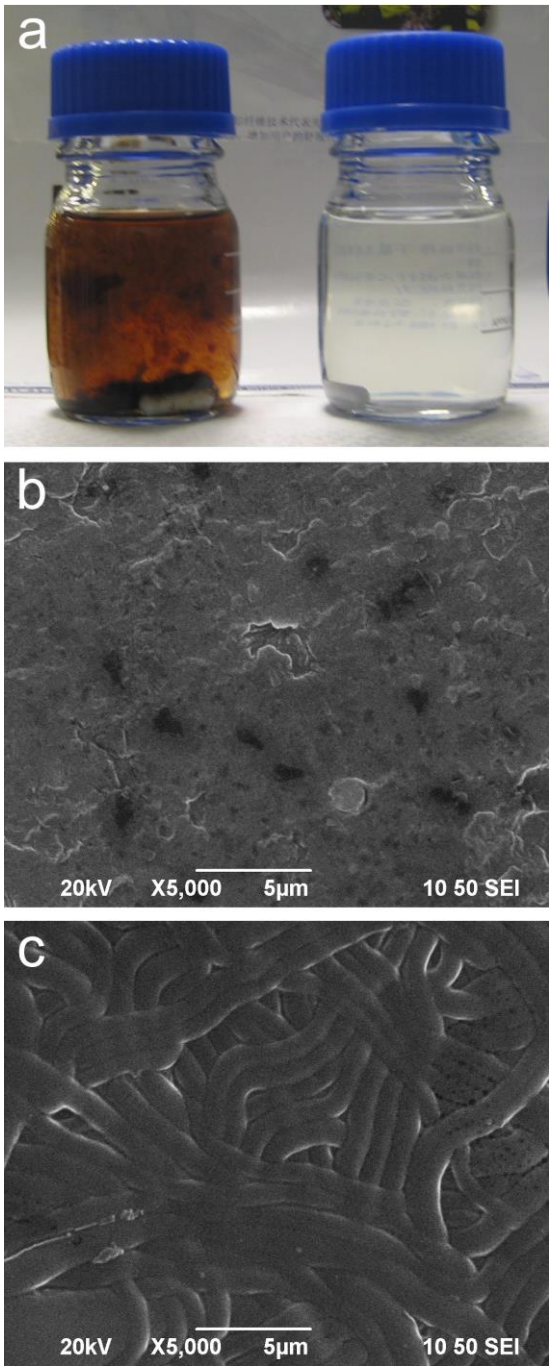

Figure 3.9 (a) Photo of PAN nanofibers after alkaline hydrolysis for 120 min: (right) as-electrospun and (left) heat-crosslinked; and SEM images of PAN nanofibers after hydrolysis: (b) 220-120 and (c) 260-120.

After all, the nanofiber integrity is well preserved against the alkaline hydrolysis through suitable heating pretreatment. It allows further exploration on the properties of resultant hydrogel that will be discussed in chapter 4. These finely modified PAN nanofibers have potential applications such as superabsorbent and artificial muscles responding to pH change and electrical voltage [33-35].

3.4 Summary

In this chapter, PAN electrospun webs were heated at various temperatures and time to observe their effects on stabilizing the PAN. From TG analysis, the heating temperature was found to be below 300 ℃ to avoid the rapid decomposition so 220 and 260 ℃ were selected to mildly treat PAN nanofibers. Some representative peaks of the PAN electrospun webs appeared in the FTIR spectra and were used to compare the rate of cyclization, dehydrogenation, and carbonylation in PAN nanofibers. By analyzing these peak intensities, which were normalized to the peak area at –CN group stretching quantitatively, relative rates were determined in the order of dehydrogenation, cyclization, and carbonylation. It also revealed the difference in stabilization kinetic rates between the microfibers and nanofibers, which was possibly due to oxygen diffusion rate. Further examining the crosslinking formed during heat treatment, the gel content was found to increase with heating temperature and time. The

fiber integrity against the alkaline hydrolysis was evaluated under SEM, showing the effect of heat treatment on fiber integrity. The proper heat treatment had successfully maintained the surface morphology of PAN electrospun webs by crosslinking. As a result, this crosslinking by heat treatment is vital for the preparation of the superabsorbent derived from PAN electrospun webs.

References

[1] Chand, S. Carbon fibers for composites. *J. Mater. Sci.* **2000**, 35, 1303-1313.

[2] Zhang, W.; Liu, J.; Wu, G. Evolution of structure and properties of PAN precursors during their conversion to carbon fibers. *Carbon* **2003**, 41, 2805-2812.

[3] Rahaman, M. S. A.; Ismail, A. F.; Mustafa, A. A review of heat treatment on polyacrylonitrile fiber. *Polym. Degrad. Stab.* **2007**, 92, 1421-1432.

[4] Kaburagi, M.; Bin, Y.; Zhu, D.; Xu, C.; Matsuo, M. Small angle X-ray scattering from voids within fibers during the stabilization and carbonization stages. *Carbon* **2003**, 41, 915-926.

[5] Avilés, M. A.; Ginés, J. M.; del Rio, J. C.; Pascual, J.; Pérez-Rodríguez J. L.; Sánchez-Soto, P. J. Thermal analysis of acrylonitrile polymerization and cyclization in the presence of *N,N-dimethylformamide*. *J. Therm. Anal. Calorim.* **2002**, 67, 177-188.

[6] Conley, R. T.; Bieron, J. F. Examination of the oxidative degradation of polyacrylonitrile using infrared spectroscopy. *J. Appl. Polym. Sci.* **1963**, 7, 1757-1773.

[7] Dalton, S.; Heatley, F.; Budd, P. M. Thermal stabilization of polyacrylonitrile fibers. *Polymer* **1999**, 40, 5531-5543.

[8] Fitzer, E.; Müller, D. J. The influence of oxygen on the chemical reactions during stabilization of PAN as carbon fiber precursor. *Carbon* **1975**, 13, 63-69.

[9] Kalfon-Cohen, E.; Harel, H.; Saadon-Yechezkia, M.; Timna, K.; Zhidkov, T.; Weinberg, A.; Marom, G. Thermal-crosslinked polyacrylonitrile fiber compacts. *Polym. Adv. Technol.* **2010**, 21, 904-910.

[10] Surianarayanan, M.; Vijayaraghavan, R.; Raghavan, K. Spectroscopic investigations of polyacrylonitrile thermal degradation. *J. Polym. Sci., Part A: Polym. Chem.* **1998**, 36, 2503-2512.

[11] Fennessey, S. F.; Farris, R. J. Fabrication of aligned and molecularly oriented electrospun polyacrylonitrile nanofibers and the mechanical behavior of their twisted yarns. *Polymer* **2004**, 45, 4217-4225.

[12] Fitzer, E.; Monocha, L. M. Carbon Fibers. In *Carbon reinforcements and carbon/ carbon composites*; Springer: New York, 1998; Chapter 1, pp. 3-70.

[13] Dzenis Y. Spinning continuous fibers for nanotechnology. *Science* **2004**, 304, 1917-1919.

[14] Reneker, D. H.; Chun I. Nanometre diameter fibers of polymer, produced by electrospinning. *Nanotechnology* **1996**, 7, 216-223.

[15] Krogman, K. C.; Lowery, J. L.; Zacharia, N. S.; Rutledge, G. C.; Hammond, P. T. Spraying asymmetry into functional membranes layer-by-layer. *Nat. Mater.* **2009**, 8, 512-518.

[16] Mo, X. M.; Xu, C. Y.; Kotaki, M.; Ramakrishna, S. Electrospun P(LLA-CL) nanofiber: A biomimetic extracellular matrix for smooth muscle cell and endothelial cell proliferation. *Biomaterials* **2004**, 25, 1883-1890.

[17] Jia, H.; Zhu, G.; Vugrinovich, B.; Kataphinan, W.; Reneker, D. Enzyme-carrying polymeric nanofibers prepared via electrospinning for use as unique biocatalysts. *Biotechnol. Prog*. **2002**, 18, 1027-1032.

[18] Demir, M. M.; Gulgun, M. A.; Menceloglu, Y. Z.; Erman, B.; Abramchuk, S. S.; Makhaeva, E. E.; Khokhlov, A. R.; Matveeva, V. G.; Sulman, M. G. Palladium nanoparticles by electrospinning from poly(acrylonitrile-co-acrylic acid)-$PdCl_2$ solutions. Relations between preparation conditions, particle size, and catalytic activity. *Macromolecules* **2004**, 37, 1787-1792.

[19] Norris, I. D.; Shaker, M. M.; Ko, F. K.; MacDiarmid, A. G. Electrostatic fabrication of ultrafine conducting fibers: Polyaniline/ polyethylene oxide blends. *Synthrtic Met.* **2000**, 114, 109-114.

[20] Schreuder-Gibson, H.; Gibson, P. W.; Senecal, K.; Sennett, M.; Walker, J.; Yeomans, W. Protective textile materials based on electrospun nanofibers. *J. Adv. Mater.* **2002**, 34, 44-55.

[21] Bajaj, P.; Surya Kumari, M. Structural investigations on hydrolyzed acrylonitrile terpolymers. *Eur. Polym. J.* **1988**, 24, 275-279.

[22] Lövy, J.; Janout, V.; Hrudková H. C-13 NMR-study of hydrolyzed poly (acrylonitrile). *Collect. Czech. Chem. Commun.* **1984**, 49, 506-512.

[23] Tanaka, K. Novel water-swellable fibers having a high degree of water swellability and excellent physical properties and process for producing the same. U.S. Patent 4, 366, 206, 1982.

[24] Tanaka K. Novel water-swellable fibers and process for producing the same. U.S. Patent 4, 374, 175, 1983.

[25] Duan, Q.; Wang, B.; Wang, H. Effects of stabilization temperature on structures and properties of polyacrylonitrile (PAN)-based stabilized electrospun nanofibers mats. *J. Macromol. Sci. Phys.* **2012**, 51, 2428-2437.

[26] Esrafilzadeh, D.; Morshed, M.; Tavanai, H. An investigation on the stabilization of special polyacrylonitrile nanofibers as carbon or activated carbon nanofibers precursor. *Synthetic Met.* **2009**, 159, 267-272.

[27] Sun, T.; Hou, Y.; Wang, H. Mass DSC/ TG and IR Ascertained Structure and Color Change of Polyacrylonitrile Fibers in Air/ Nitrogen during Thermal Stabilization. *J. Appl. Polym. Sci.* **2010**, 118, 462-468.

[28] Xue, Y.; Liu, J.; Liang, J. Correlative study of critical reactions in polyacrylonitrile based carbon fiber precursors during thermal-oxidative stabilization. *Polym. Degrad. Stab.* **2013**, 98, 219-229.

[29] Hou, Y.; Sun, T.; Wang, H.; Wu D. Thermal-shrinkage investigation of the chemical reaction during the stabilization of polyacrylonitrile fibers. *J. Appl. Polym. Sci.* **2009**, 114, 3668-3672.

[30] Fei, B.; Chen, C.; Wu, H.; Peng, S.; Wang, X.; Dong, L.; Xin, J. H. Modified poly(3-hydroxybutyrate-*co*-3-hydroxyvalerate) using hydrogen bonding monomers. *Polymer* **2004**, 45, 6275-6284.

[31] Fei, B.; Chen, C.; Wu, H.; Peng, S.; Wang, X.; Dong, L. Quantitative FTIR study of PHBV/ bisphenol A blends. *Eur. Polym. J.* **2003**, 39, 1939-1946.

[32] Deng, W.; Lobovsky, A.; Iacono, S. T.; Wu, T.; Tomar, N.; Budy, S. M.; Long, T.; Hoffman, W. P.; Smith Jr., D. W. Poly(acrylonitrile-co-1-vinylimidazole): A new melt processable carbon fiber precursor. *Polymer* **2011**, 52, 622-628.

[33] Choe, K; Kim K. J.; Kim, D. Y.; Manford, C.; Heo, S.; Shahinpoor, M. Performance Characteristics of electro-chemically Driven Polyacrylonitrile Fiber bundle actuators. *J. Intell. Mater. Syst. Struct.* **2006**, 17, 563-576.

[34] Lee, D. Y.; Kim, Y.; Lee, S. J.; Lee, M. H.; Lee, J. Y.; Kim, B. Y.; Cho, N. I. Characteristics of chemo-mechanically driven polyacrylonitrile fiber gel actuators. *Mat. Sci. Eng. C-Biomim.* **2008**, 28, 294-298.

[35] Samatham, R.; Park, I. S.; Kim, K. J.; Nam, J. D.; Whisman, N.; Adams, J. Electrospun nanoscale polyacrylonitrile artificial muscle. *Smart Mater. Struct.* **2006**, 15, 152-156.

Chapter 4

Preparation of superabsorbent hydrogel from polyacrylonitrile (PAN) nanofibers

4.1 Introduction

Superabsorbent polymer hydrogel is lightly crosslinked polymer with high molecular weight that can imbibe remarkable amount of water (over 10 g/g) by swelling into a much larger size. Its uniqueness is that it can retain the absorbed water even if under external pressure [1-4]. Because of these fascinating properties, a wide range of applications includes hygienic products [5], agricultural consumables [6], drug delivery systems [7], and wound dressings [8].

One of the important parameters for superabsorbent is the water absorption rate. Even though low absorption rate is enough for some specialties, high rate is preferable in many applications such as fast swelling hydrogel for gastric retention [9, 10]. To enhance the absorption rate of superabsorbent, capillarity is introduced to it. Highly interconnected pores provide an effective capillary space to draw in water faster than slow diffusion of water into the superabsorbent. As the pore size is smaller, the capillarity effect becomes stronger. These pores enable higher water absorption rate to reach the equilibrium state. The interconnected pores can be prepared by several methods, such as phase separation [11, 12], porogenation [13], gas foaming [14], and cryogelation [15].

However, these methods involve time-consuming and tedious steps. In contrast, electrospinning is a simple and versatile method to produce the fibrous and porous structure [16, 17]. This electrospun web has a large surface-to-volume ratio and a highly porous structure that supports a significant capillary effect. Some electrospun hydrogel nanofibers prepared from poly (acrylic acid) [18] and hyaluronic acid [19] have been reported. Their diameters were from 150 to 300 nm, having rapid water absorption; however, their chemical structures limited their absorption ratios (18–25 g/g) as well.

Polyacrylonitrile (PAN) was firstly reported as a raw material for superabsorbent by the US Department of Agriculture [20]. PAN was hydrolyzed in alkaline medium to convert its nitrile groups into solubilizing groups like amide and carboxylic acid [21]. From the previous research, staple PAN fibers [22, 23], hollow PAN fibers [24], and PAN nanofibers [25] were partially hydrolyzed in order to enhance water absorption; however, their water absorptions were still relatively low (2–50 g/g).

In previous chapter, proper heat treatment can retain the integral structure of electrospun PAN web against alkaline hydrolysis. The heat treatment provides effective crosslinking of PAN through inter-chain cyclization of nitrile groups, during which nanofibers have much different stabilization kinetics from microfibers. In this chapter, the evolvement of porous structure and solubilizing groups in the crosslinked PAN webs was investigated. The water absorption

performance and mechanical properties of the resultant hydrogels were also evaluated. Our optimized hydrogels achieved absorption ratio *Q* over 100 within 1 min.

4.2 Experimental

4.2.1 Materials

Polyacrylonitrile (PAN, Mw = 150,000), dimethylformamide (DMF), and sodium hydroxide (NaOH) were purchased from Aldrich Co.

4.2.2 Electrospinning

PAN solution of 10 wt% in DMF was electropsun into a web using the same parameters as mentioned in chapter 4. The collected electrospun PAN webs were heated up to 100 ℃ in a vacuum oven (Shel Lab) till a constant weight.

4.2.3 Heat treatment and alkaline hydrolysis

The electrospun PAN webs were heated in a muffle oven (Carbolite Co., Ltd.) at 220 and 260 ℃ for 30 and 120 min respectively in the presence of air. The heated samples were hydrolyzed in 1.0 N NaOH at 85 ℃ with stirring for 60 min, collected by nickel-net filter and neutralized by DI water. The samples were denoted as “heating temperature (℃)-heating time (min)-W/H”, -W for those webs treated by heating, and -H for those hydrogels resulted from heating and hydrolysis e.g. 220-120-W and 260-30-H.

4.2.4 Characterizations

The morphologies of fully swollen hydrolyzed and freeze-dried PAN samples were observed by field-emission scanning electron microscopes (FE-SEM, Hitachi S4800 and JEOL JSM-6335F).

Fourier transform infrared (FTIR) spectra were obtained by PerkinElmer Spectrum 100 equipped with a beam condenser in a spectral region of 4000–650 cm^{-1} with 16 scans at a resolution of 4 cm^{-1}.

Tensile strength was measured by the universal material testing machine (Instron 5566, USA) with 2 cm distance between the clamps and 1 cm clamp width, at a strain speed of 5 mm/min. The samples (1 cm in width and 5 cm in length) were conditioned at standard conditions (T = 25 ℃ and R.H. = 65%). Few samples were immersed in DI water till equilibrium.

4.2.5 Water absorption measurement

To measure the water equilibrium absorption ratio and absorption rate, the dried samples were immersed in DI water for various periods and weighed sequentially. The excess water was removed by centrifuging at 500 revolutions per min for 1 min. The water absorption ratio, Q (g/g), is calculated as following:

$$Q\ (t) = \frac{w_t - w_0}{w_0} \qquad \text{(Equation 4.1)}$$

where w_0 and w_t are the weight of sample at beginning and immersion time t, in g, respectively.

4.3 Results and discussion

4.3.1 Surface morphology

Surface morphologies of electrospun PAN webs after alkaline hydrolysis were freeze-dried and then observed under SEM.

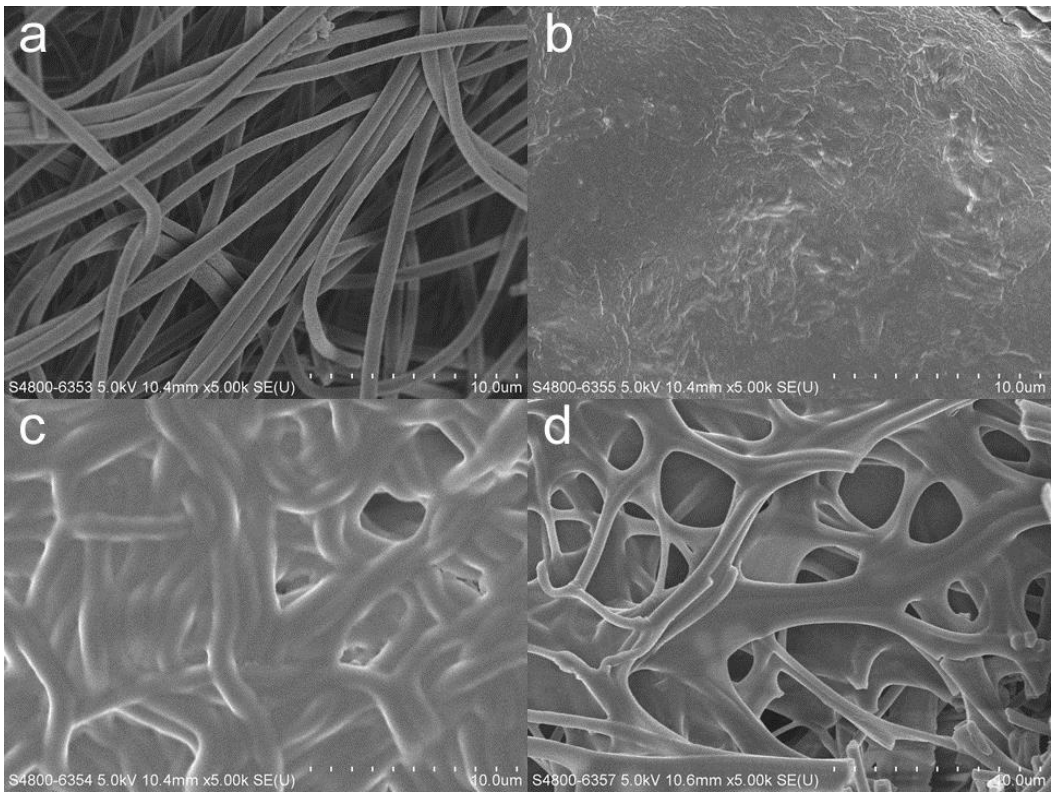

Figure 4.1 SEM images of electrospun PAN web samples: (a) as-electrospun, (b) 220-120-H, (c) 260-30-H, and (d) 260-120-H.

As shown in Figure 4.1a, the PAN nanofibers were distinctive. The heat-treated samples exhibited some notable changes after undergoing alkaline hydrolysis. As mentioned previously in chapter 3, the sample 220-30-W was not crosslinked so it was totally dissolved under harsh hydrolysis condition. On the contrary, the sample 220-120-H, which was heated for a longer time, had gel

residues left with relatively smooth surface (Figure 4.1b). As shown in Figures 4.1c and 4.1d, both of the 260-30-H and 260-120-H retained their fibrous texture with swollen nanofibers. Comparing to 260-30-H, 260-120-H had thinner fibers and more pores on surface because of its higher crosslink density. Thus, the heating temperature and time strongly affect the fiber integrity against alkaline hydrolysis.

The cross-sections of as-electrospun and hydrolyzed PAN samples were obtained from the fracture of freeze-dried samples and observed under SEM as shown in Figure 4.2. The as-electrospun PAN nanofibers were distinctive from each other forming a layer of fibers. On the other hand, the 220-120-H demonstrated a thin layer of membrane with many tiny pores, and the pore size was about 100 nm as shown in the high magnification (× 40,000) image (Figure 4.2c). The nanoparticles of about 100 nm were interconnected with each other to form a network. As reported in previous chapter, the 220-120-W had low gel fraction and crosslink density. Thus, some uncrosslinked parts were dissolved in alkaline solution while some parts swelled so pores were formed. This result is similar to Hu's report that the alkaline hydrolysis destroyed the wet-spun PAN fiber surface [23]. This fully hydrolyzed sample is possibly able to absorb a large amount of water at high absorption rate.

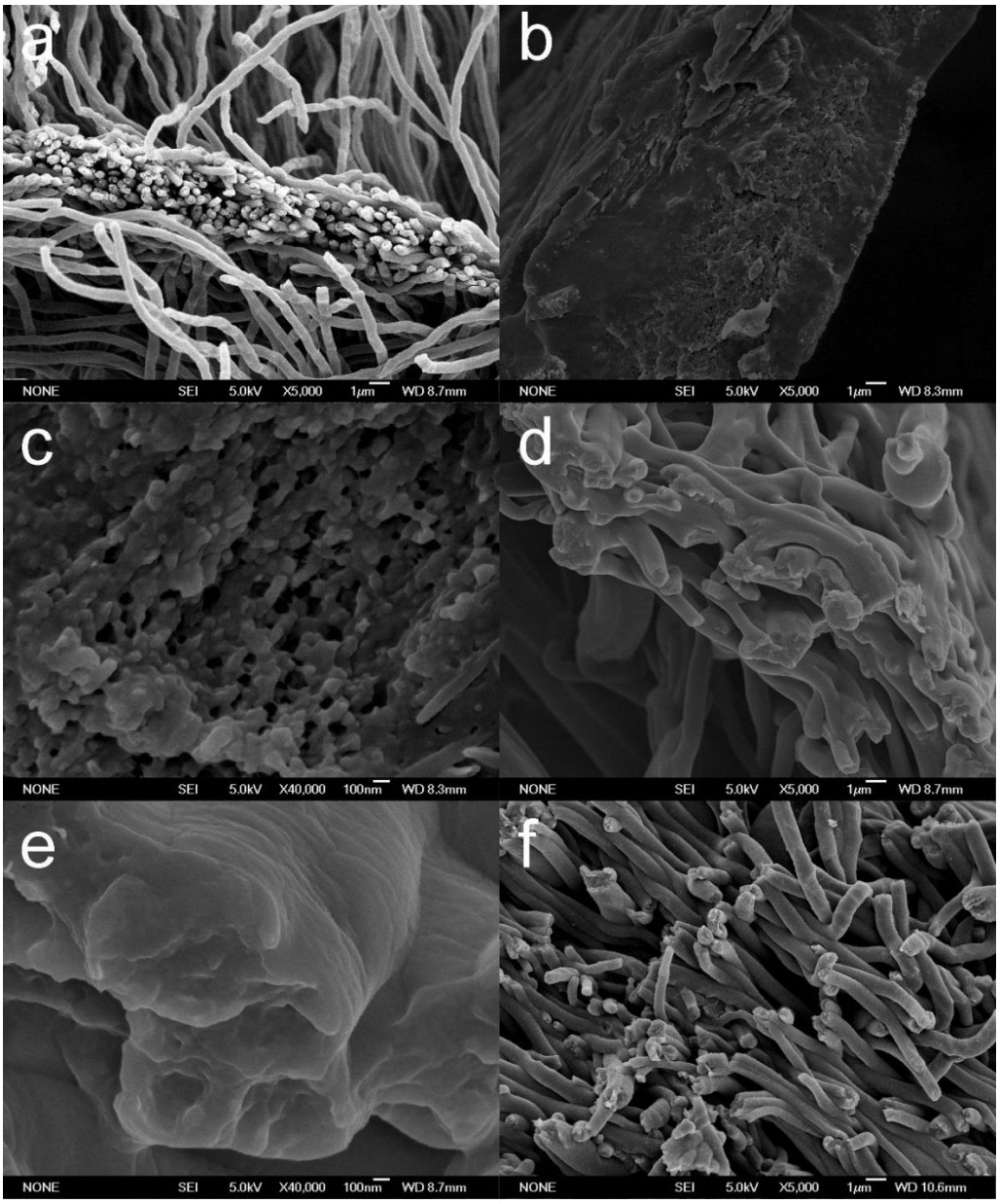

Figure 4.2 Cross-sectional SEM images of electrospun PAN webs: (a) as-electrospun, (b, c) 220-120-H, (d, e) 260-30-H, and (f) 260-120-H.

For the 260-30-H, it remained fibrous structure with swollen fibers connected with each other, forming a layer with larger pores than 220-120-H as shown in Figure 4.2d. Each single fiber had a solid cross-section as seen in the high magnification (× 40,000) image (Figure 4.2e). Since the 260-30-H had higher crosslink density than the 220-120-W, it maintained fiber shape with

limited fusion between adjacent fibers during swelling in hydrolysis treatment. The 260-120-H retained the fiber shape the best among all samples, with slightly increment in fiber diameter as compared to the untreated nanofibers as shown in Figure 4.2f. Because of its high gel fraction and crosslink density, the sample is not damaged by alkaline hydrolysis and its fiber morphology is well preserved. This morphology hints low water absorption ratio (*Q*).

4.3.2 FTIR analysis

FTIR spectra confirmed the structural changes of electrospun PAN webs after alkaline hydrolysis as shown in Figure 4.3. For comparison, all spectra were normalized according to the peak area at 1450 cm^{-1}. The characteristic peak of nitrile (–CN) group stretching at 2242 cm^{-1} appeared in the as-electrospun web and all the heat-treated PAN webs (dash lines). Although the cyclization occurred at the –CN groups during heat treatment, some free –CN groups remained as shown in the spectra of the heat-treated PAN webs. After alkaline hydrolysis, this peak completely disappeared, indicating that the PAN webs were fully hydrolyzed. Meanwhile, new peaks at 1404, 1570, and 1668 cm^{-1} appeared, attributing to the symmetric stretching of carboxylate ($–COO^-$), asymmetric stretching of $–COO^-$ and N–H bending of carboxamide ($–CONH_2$), and C=O stretching of carboxylate ($–COO^-$) and $–CONH_2$ groups, respectively [26, 27].. In addition, a strong and broad peak at 3600–3300 cm^{-1} corresponding to the –OH

group, appeared in the 220-120-H and 260-30-H samples (Figures 4.3b and 4.3c). FTIR spectra support that the remaining –CN groups are fully converted into the solubilizing groups carboxamide, carboxylic acid, and carboxylate groups, which are essential for absorbing and swelling.

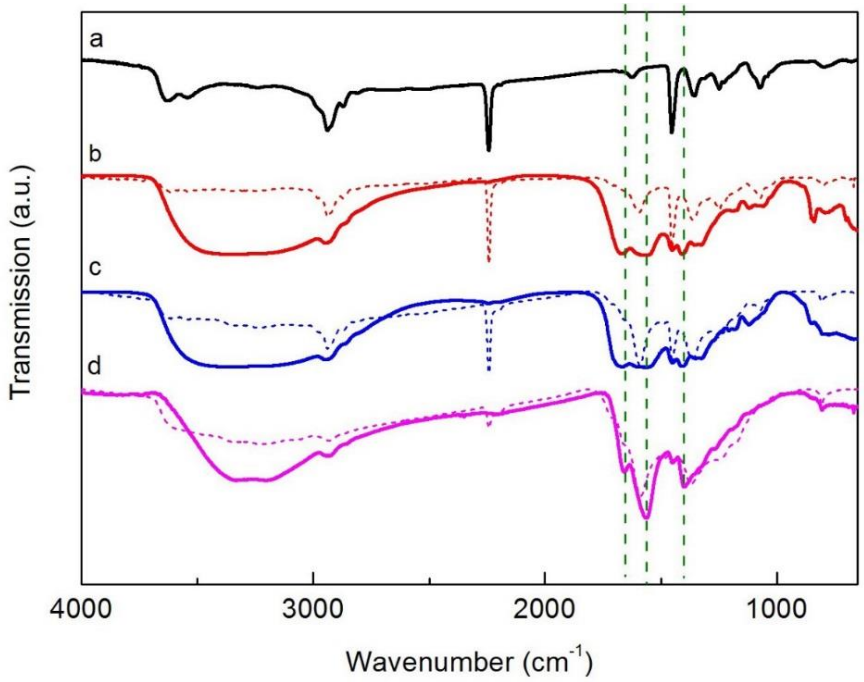

Figure 4.3 FTIR spectra of PAN webs: (a) as-electrospun, (b) 220-120-H, (c) 260-30-H, and (d) 260-120-H, where dash lines represented the heat-treated PAN webs before hydrolysis correspondingly, with all spectra normalized to the peak area at 1450 cm^{-1}.

The FTIR spectrum of 260-120-H showed some differences as compared to that of 220-120-H and 260-30-H. The absorption peaks of two N-H stretching from primary amide ($–CONH_2$) were observed at 3330 and 3200 cm^{-1} as shown in Figure 4.3d. It is due to its high crosslink density so it has less free –CN groups for hydrolysis to produces solubilizing groups. Accordingly, it possibly

has a much lower *Q* value than the above two samples.

4.3.3 Alkaline hydrolysis mechanism

Based on the above analysis of FTIR spectra, the possible reaction mechanism in the PAN nanofibers is demonstrated in Figure 4.4. During the heat treatment, cyclization, dehydrogenation, carbonylation, and crosslinking occur in the PAN nanofibers, and some –CN groups remain along the polymer chains. During alkaline hydrolysis, these free –CN groups are further hydrolyzed into the solubilizing groups –COOH, $–CONH_2$, and $–COO^-$.

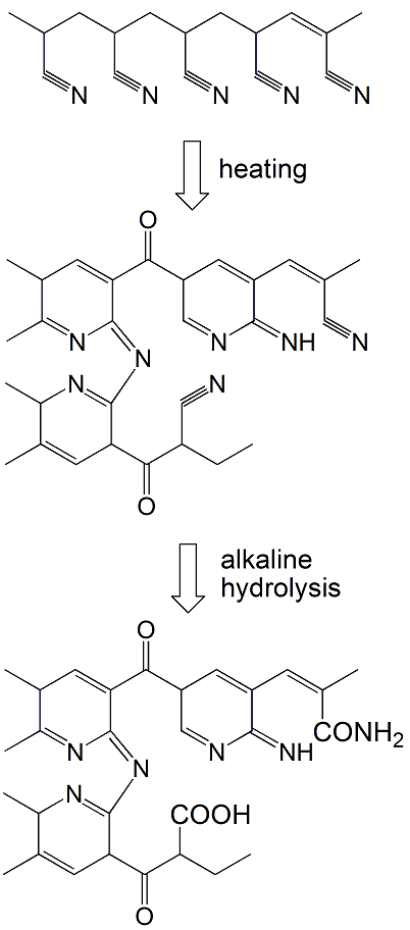

Figure 4.4 Proposed mechanism of reactions in the PAN nanofibers under heating and alkaline hydrolysis.

As illustrated in Figure 4.5, these chemical reactions have led to corresponding morphology changes of the nanofiber webs after heat treatment and alkaline hydrolysis. The low crosslink density results in highly porous structure with small pore size, while the high crosslink density leads to a fibrous structure with large pore size. Figures 4.4 and 4.5 summarize all the above experimental results and indicate the possible variations of properties among the samples.

4.3.4 Water absorption performance

4.3.4.1 Water absorption ratio (*Q*)

The water absorption ability of hydrolyzed electrospun PAN webs was analyzed by measuring their *Q* values over 24 h as shown in Figure 4.6. The as-electrospun PAN web absorbed 20 times of water mainly, owing to the capillary wetting of those interlaced nanofibers. After heat treatment and alkaline hydrolysis, the 220-120-H and 260-30-H gave remarkably high *Q* value of over 100. Though cyclization of –CN side groups occurred during stabilization, the following hydrolysis treatment still produced solubilizing groups –COOH, –$CONH_2$, and $–COO^-$ from the remaining –CN groups, as identified in the FTIR spectra (Figure 4.3). Their highly improved *Q* values showed an agreement with their FTIR results.

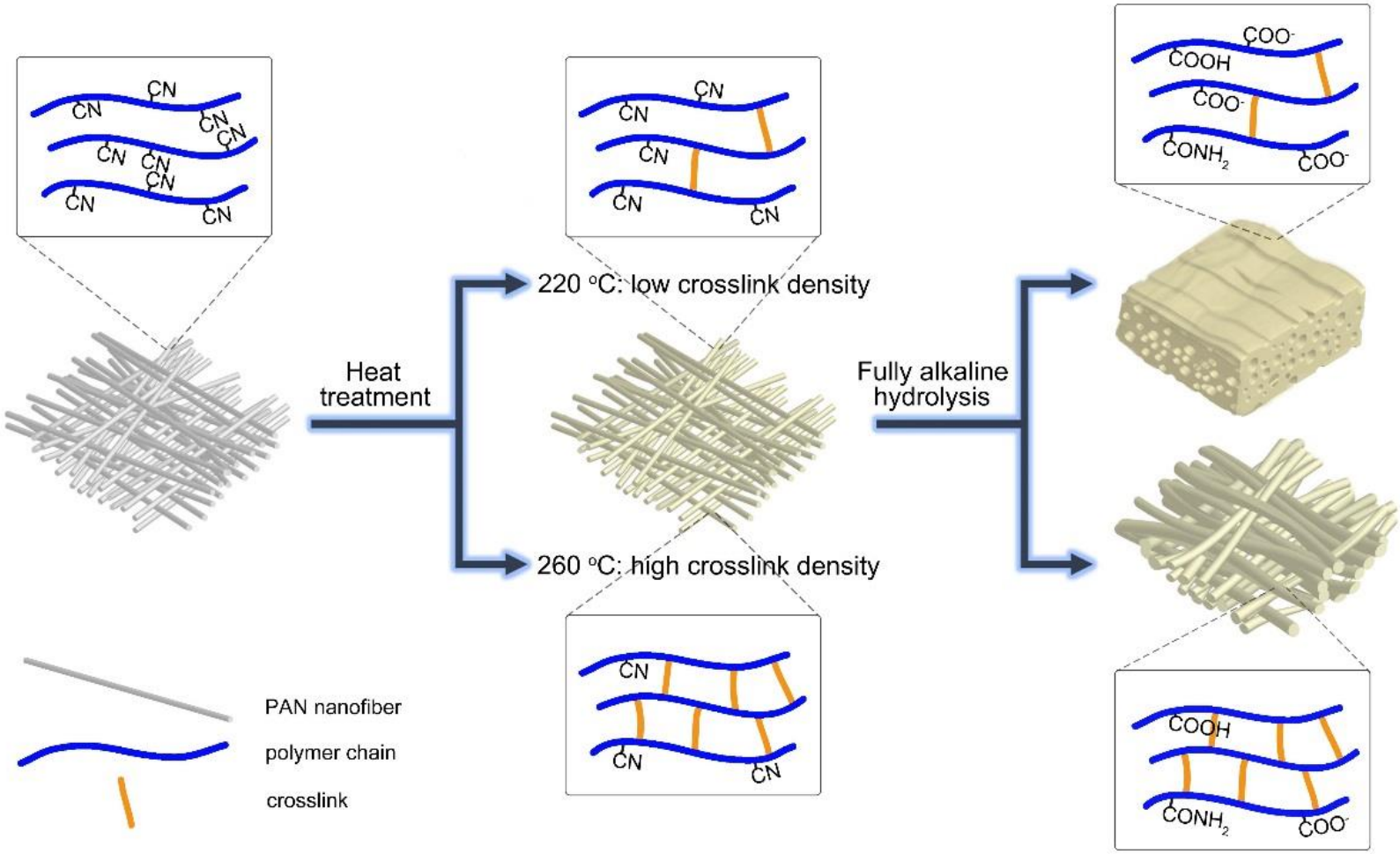

Figure 4.5 Schematic illustration of electrospun PAN webs under heat treatment and alkaline hydrolysis.

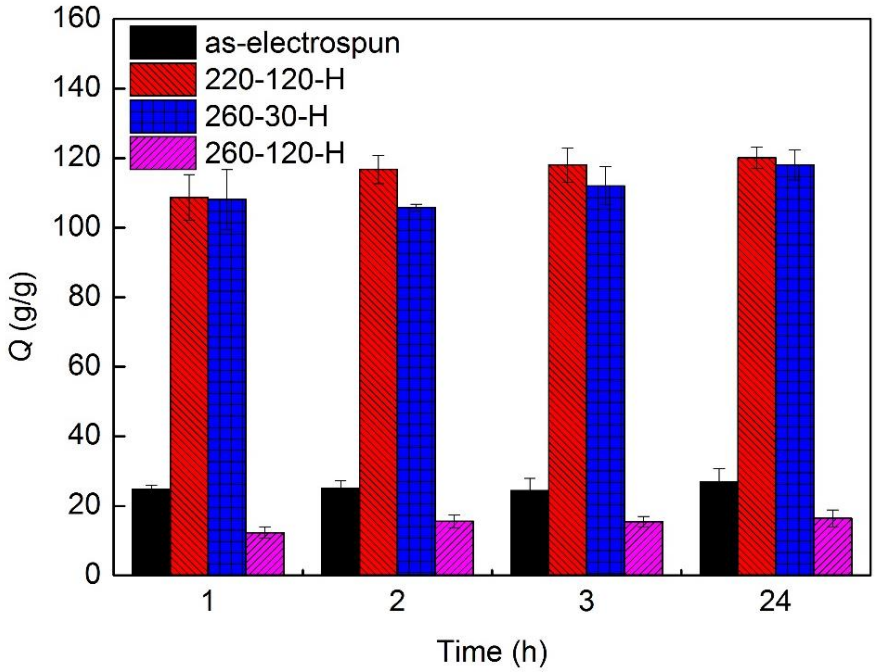

Figure 4.6 The water absorption ratio (*Q*) of as-electrospun PAN web and hydrolyzed samples immersed in DI water for 24 h.

Comparing two samples with high *Q* values, the 220-120-H achieved slightly higher *Q* than 260-30-H because of its lower crosslink density and more solubilizing groups. In contrast, the 260-120-H, being heated at high temperature and long time, absorbed only 15 times of water. It agreed with the previous prediction from SEM and FTIR results that limited swelling and less solubilizing groups were observed. The *Q* value of 260-120-H was even lower than that of as-electrospun PAN web. This reduction in *Q* is mainly caused by the volume shrinkage of web during heating, which results in the partial loss of capillary absorption, and the solubilizing groups produced in hydrolysis do not compensate as much as the loss in capillary absorption. Comparing with previously reported hydrolyzed PAN microfibers [22, 23] and nanofibers [25],

having *Q* values of about 2–50 g/g, our hydrolyzed PAN samples achieved much improved *Q* values. It is because they are in nano-size and fully hydrolyzed.

4.3.4.2 Swelling rate

Apart from swelling capacity, the swelling rate is also important to the practical applications of superabsorbents. The high *Q* value samples—220-120-H and 260-30-H—were compared with as-electrospun PAN web within first 30 min of water absorption as shown in Figure 4.7.

The as-electrospun web absorbed water rapidly and reaches equilibrium *Q* value (~ 22) at the first 15 s. This rapid absorption totally depends on the capillary effect. On the contrary, the 220-120-H and 260-30-H also absorbed water spontaneously in first 15 s and gradually reached the equilibrium ($Q > 100$) within 1 min. This fast absorption is mainly due to their porous structures as shown in the SEM images. The water is drawn in quickly through interconnected pores, and hence their swelling efficiency can be significantly improved. Compared with the as-electrospun PAN web, their fast water absorptions are attributed to both swelling and capillary effect at the first 15 s and then slow diffusion of water into their matrices.

In comparison, the poly (sodium acrylate) particles prepared by Mayoux's group presented a much lower equilibrium *Q* value, which was only half of *Q* value of our sample [28]. Sadeghi's group also reported that their starch-poly

(sodium acrylate-*co*-acrylamide) particles took 9 min to reach 80% of equilibrium *Q* value as measured by a teabag method [29]. In contrast, our samples reach 80% of equilibrium *Q* value within 15 s only. This significant improvement in absorption ratio and rate is mainly attributed to the presence of solubilizing groups of the fully hydrolyzed PAN and assisted by the interconnected pore structure as observed under SEM.

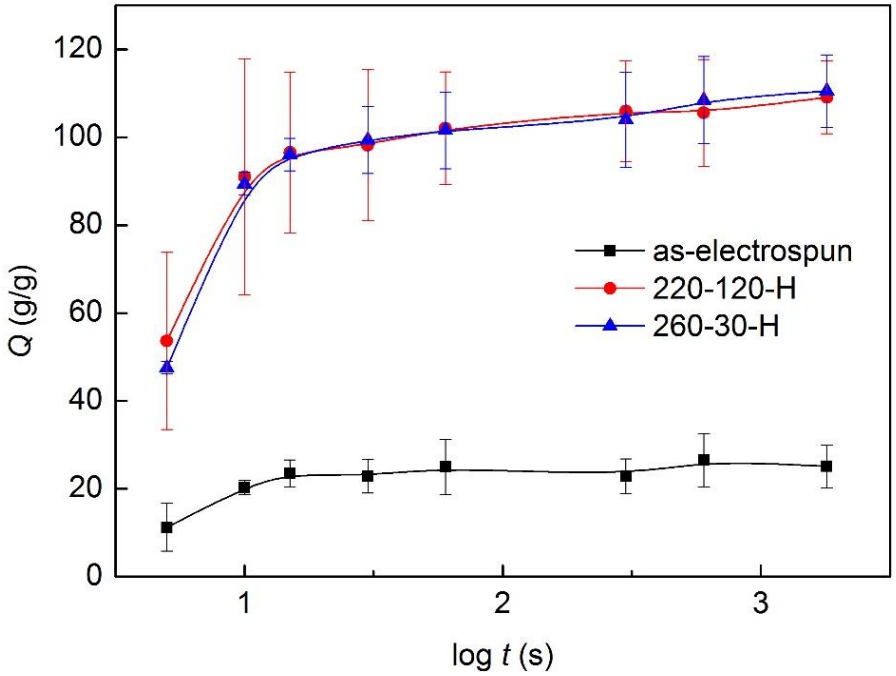

Figure 4.7 The water absorption ratio (*Q*) of as-electropsun PAN web and hydrolyzed samples within 30 min immersion in DI water.

4.3.4.3 Swelling kinetics

In order to quantify the swelling kinetics, the swelling data are analyzed according to the Voigt-based viscoelastic model as the following equation [30]:

$$Q_t = Q_e\left(1 - exp^{-t/\tau}\right) \qquad \text{(Equation 4.2)}$$

where Q_t (g/g) is the degree of swelling at time *t*, Q_e (g/g) is the degree of swelling at equilibrium, t (s) is the time for swelling to Q_t, and τ (s) is the rate parameter that the time required to reach 0.63 of Q_e.

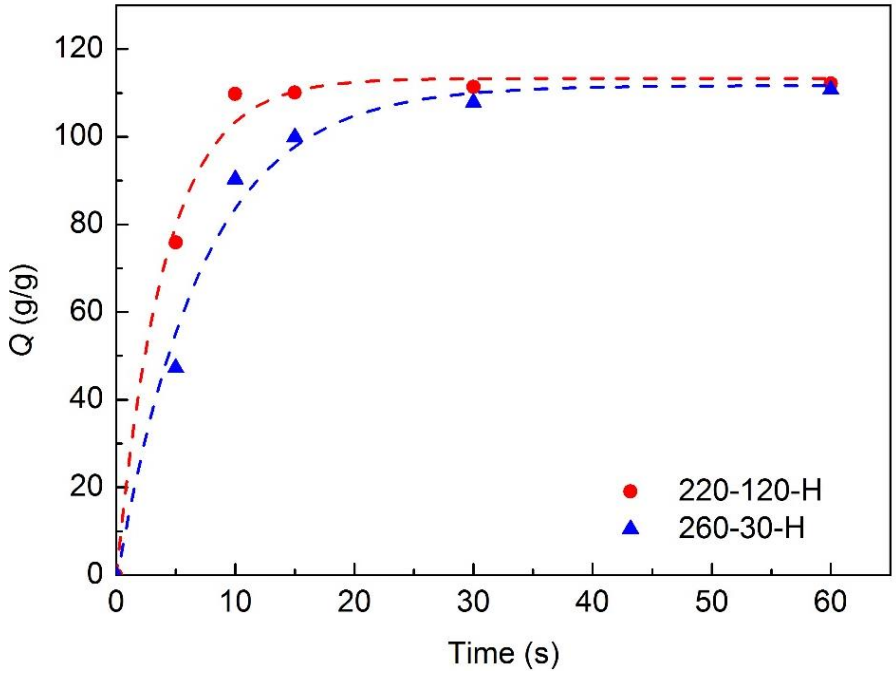

Figure 4.8 Representative curves fitted to the experimental swelling kinetics of 220-120-H and 260-30-H.

As shown in Figure 4.8, the *Q* value increased rapidly at the initial state and then leveled off gradually. The values of Q_e and τ of 220-120-H and 260-30-H were found to be 113.3 g/g and 4.10 s, and 113.7 g/g and 7.15 s, respectively, and their R^2 of curve fitting reached 0.98. According to Omidian [31, 32], the swelling kinetic is greatly affected by the particle size of the superabsorbent. As the particle size is smaller, its swelling rate is higher based on

a lower value of τ. As shown in cross-section SEM images of our samples (Figure 4.2), the fiber or particle diameter of 220-120-H was around 100 nm, which was much smaller than that of 260-30-H having around 1000 nm. Therefore, the swelling kinetic of 220-120-H is faster than that of 260-30-H, showing an agreement with the Voigt model. It has been reported that for starch–poly(sodium acrylate-*co*-acrylamide) superabsorbent particles, τ values of 348, 642, and 696 s were obtained from particles of 100–250, 250–400, and 400–550 μm respectively [29]. Our porous nanofiber webs are also superior to common superabsorbent particles because of their small unit size.

4.3.5 Mechanical properties

The average mechanical properties and typical tensile curves of dry and wet specimens are shown in Table 4.1 and Figure 4.9 respectively. However, the 220-120-H was too weak to be measured after alkaline hydrolysis. As shown in Table 4.1, the as-electropsun PAN obtained the highest apparent breaking stress of 4.2 MPa and the lowest breaking strain of 2.8% among all samples. After equilibrium swelling in DI water, its stress at break decreased greatly to 2.6 MPa while its strain at break increased to 7.5%. The water absorbed in the amorphous structure of PAN highly enhances the flexibility of the polymer chains; however, the water trapped in between PAN nanofibers increases the friction between them so weakens its stiffness.

Table 4.1 Mechanical properties of PAN, 260-30-H and 260-120-H in dry state and wet states. (Values shown are means and ± standard deviation for six specimens)

Samples		Breaking stress MPa	Breaking strain %
PAN	Dry	4.2 ± 1.3	2.8 ± 0.4
	Wet	2.6 ± 1.0	7.5 ± 1.8
260-30-H	Dry	1.3 ± 0.2	32.0 ± 7.1
	Wet	0.03 ± 0.01	21.9 ± 5.3
260-120-H	Dry	2.1 ± 1.1	13.9 ± 3.8
	Wet	0.3 ±0.1	31.7 ± 9.4

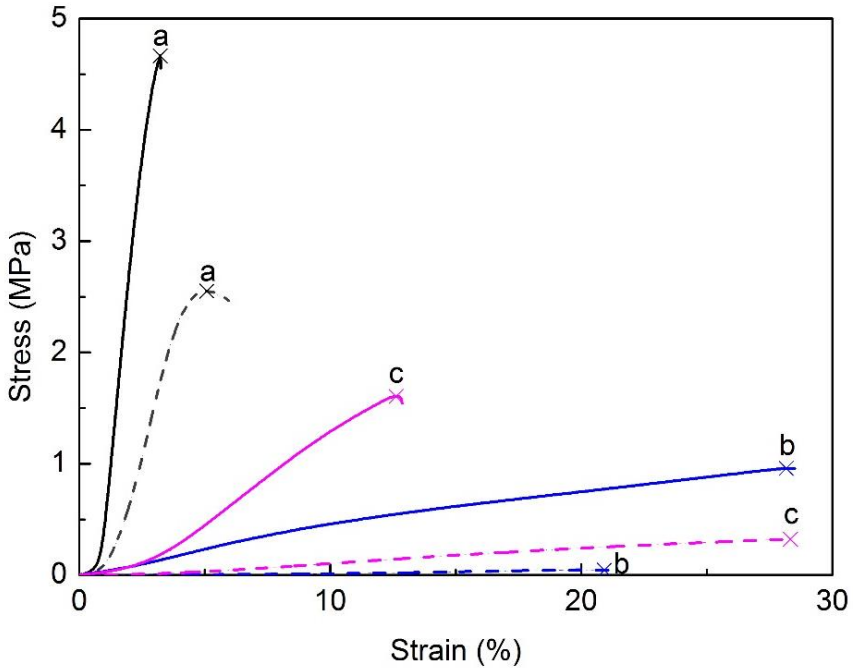

Figure 4.9 Typical tensile curves of as-electropsun PAN web, 260-30-H and 260-120-H, where dash lines represent their swollen states correspondingly.

After the heat-treated samples were hydrolyzed, the apparent breaking stresses of 260-30-H and 260-120-H were greatly decreased to 1.3 and 2.1 MPa,

whereas their breaking strains were increased to 32.0% and 13.9% respectively. This phenomenon is due to the changes in matrix structure resulted from alkaline hydrolysis. The 260-120-H had the highest crosslink density among all samples, so it was able to withstand the harsh alkaline hydrolysis condition and maintain the fiber shape as shown previously in its SEM images (Figures 4.1d and 4.2f). Therefore, it had lower reduction in stress at break. After water absorption, its stress at break significantly decreased to 0.3 MPa but its breaking strain increased to 31.7%. Its high extensibility is possibly due to the mobility of polymer chains in the swollen state.

On the other hand, the wet 260-30-H showed lower stress at break (0.03 MPa) and strain at break (21.9%). It is reasonable to be more brittle and less stretchable after absorbing a large amount of water. As shown in the typical tensile curves in Figure 4.9, it can be seen that the heated and hydrolyzed samples became weaker but they had a higher flexibility than the as-electrospun PAN web. Even though the maximum stresses and strains of our 260-30-H and 260-120-H were lower than those of dry polyacrylate film (~ 2 MPa, ~ 500%) as reported in literature [33], these samples had porous structure that possibly weakened their mechanical properties.

More interestingly, their physiochemical properties provide them stimuli-responsiveness behavior such as pH- and salt-responsiveness reported in literature [34-36]. These properties may support wide applications in artificial

actuators [37] and artificial muscles [38].

4.4 Summary

The electrospun PAN webs were firstly heat stabilized at various temperatures and time to form crosslink and then hydrolyzed to produce hydrogels. The crosslinked PAN webs maintained their integrity against alkaline hydrolysis. Highly interconnected porous structures were observed in the freeze-dried hydrogels under SEM. Their FTIR spectra indicated the conversion of nitrile groups into solubilizing groups of $–CONH_2$, –COOH, and $–COO^-$. Further examining their water absorption performance, high absorption ratio *Q* over 100 within 1 min was achieved with optimized hydrogels. The swelling kinetics of the hydrogels was also quantified according to the Voigt-based viscoelastic model. The hydrogels offered a higher extensibility than the as-electrospun PAN web. These suitable heating and hydrolysis treatments convincingly converted electrospun PAN webs into the fast superabsorbent hydrogels.

References

[1] Gross, J. R. The Evolution of Absorbent Materials. In *Absorbent polymer technology*; Brannon-Peppas, L., Harland, R. S., Eds.; Elsevier: Amsterdam, 1990; Chapter 1, pp. 3-22.

[2] Buchholz, F. L. Absorbency and Superabsorbency. In *Modern superabsorbent polymer technology*; Buchholz, F. L., Graham A. T., Eds.; Wiley-VCH: New York, 1998; Chapter 1, pp. 1-18.

[3] Zohuriaan-Mehr, M. J.; Kabiri, K. Superabsorbent polymer materials: A review. *Iran. Polym. J.* **2008**, 17(6), 451-477.

[4] Islam, M. S.; Rahaman, M. S.; Yeum, J. H. Electrospun novel super-absorbent based on polysaccharide-polyvinyl alcohol-montmorillonite clay nanocomposites. *Carbohydr. Polym.* **2015**, 115, 69-77.

[5] Kosemund, K.; Schlatter, H.; Ochsenhirt, J. L.; Krause, E. L.; Marsman, D. S.; Erasala, G. N. Safety evaluation of superabsorbent baby diapers. *Regul. Toxicol. Pharmacol.* **2009**, 53, 81-89.

[6] Wang, X.; Lu, S.; Gao, C.; Xu, X.; Wei, Y.; Bai, X.; Feng, C.; Gao, N.; Liu, M.; Wu, L. Biomass-based multifunctional fertilizer system featuring controlled-release nutrient, water-retention and amelioration of soil. *RSC Adv.* **2014**, 4(35), 18382-18390.

[7] Samanta, H. S.; Ray, S. K. Synthesis, characterization, swelling and drug release behavior of semi-interpenetrating network hydrogels of sodium alginate and polyacrylamide. *Carbohydr. Polym.* **2014**, 99, 666-678.

[8] Mohamad, N.; Amin, M. C. I. M.; Pandey, M.; Ahmad, N.; Rajab, N. F. Bacterial cellulose/ acrylic acid hydrogel synthesized via electron beam irradiation: Accelerated burn wound healing in an animal model. *Carbohydr. Polym.* **2014**, 114, 312-320.

[9] Chen, J.; Park, H.; Park, K. Synthesis of superporous hydrogels: hydrogels with fast swelling and superabsorbent properties. *J. Biomed. Mater. Res.* **1999**, 44, 53-62.

[10] Chen, J.; Blevins, W. E.; Park, H.; Park, K. Gastric retention properties of superporous hydrogel composites. *J. Control. Release* **2000**, 64, 39-51.

[11] Zhang, X. Z.; Yang, Y. Y.; Chung, T. S.; Ma, K. X. Preparation and characterization of fast response macroporous poly (N-isopropylacrylamide) hydrogels. *Langmuir* **2001**, 17(20), 6094-6099.

[12] Yan, Q.; Hoffman, A. S. Synthesis of macroporous hydrogels with rapid swelling and deswelling properties for delivery of macromolecules. *Polymer* **1995**, 36(4), 887-889.

[13] Nam, Y. S.; Yoon, J. J.; Park, T. G. A novel fabrication method of macroporous biodegradable polymer scaffolds using gas foaming salt as a porogen additive. *J. Biomed. Mater. Res.* **2000**, 53(1), 1-7.

[14] Kabiri, K.; Omidian, H.; Zohuriaan-Mehr, M. Novel approach to highly porous superabsorbent hydrogels: Synergistic effect of porogens on porosity and swelling rate. *Polym. Int.* **2003**, 52(7), 1158-1164.

[15] Van Vlierberghe, S.; Cnudde, V.; Dubruel, P.; Masschaele, B.; Cosijns, A.; De Paepe, I.; Jacobs, P. J. S.; Van Hoorebeke, L.; Remon, J. P.; Schacht, E. Porous gelatin hydrogels: 1. cryogenic formation and structure analysis. *Biomacromolecules* **2007**, 8(2), 331-337.

[16] Fogaca, R.; Catalani, L.; Fogaça, R. PVP hydrogel membranes produced by electrospinning for protein release devices. *Soft Mater*. **2013**, 11(1), 61-68.

[17] Wang, H. J.; Zheng, J.; Peng, M. Ionization-induced ultrarapid response behavior of fibrous and porous electrospun hydrogels containing carboxyl groups. *J. Appl. Polym. Sci.* **2010**, 115, 2485-2492.

[18] Li, L.; Hsieh, Y. L. Ultra-fine polyelectrolyte fibers from electrospinning of poly (acrylic acid). *Polymer* **2005**, 46(14), 5133-5139.

[19] Ji, Y.; Ghosh, K.; Shu, X. Z.; Li, B. Q.; Sokolov, J. C.; Prestwich, G. D.; Clark, R. A. F.; Rafailovich, M. H. Electrospun three-dimensional hyaluronic acid nanofibrous scaffolds. *Biomaterials* **2006**, 27(20), 3782-3792.

[20] Masuda, F. Trends in the Development of Superabsorbent Polymers for Diapers. In *Superabsorbent Polymers: Science and Technology*; Buchholz, F. L., Peppas, N. A., Eds.; ACS symposium series 573; American Chemical Society: Washington, DC, 1994, Chapter 7, pp 88-98.

[21] Bajaj, P.; Surya Kumari, M. Structural investigations on hydrolyzed acrylonitrile terpolymers. *Eur. Polym. J.* **1988**, 24(3), 275-279.

[22] Gupta, M.; Gupta, B.; Oppermann, W.; Hardtmann, G. Surface modification of polyacrylonitrile staple fibers via alkaline hydrolysis for superabsorbent applications. *J. Appl. Polym. Sci*. **2004**, 91(5), 3127-3133.

[23] Hu, X.; Xiao, C. Study on superabsorbent polyacrylonitrile-based fibre. *Indian J. Fibre Text.* **2005**, 30(2), 207-210.

[24] Yang, M.; Tong, J. Loose ultrafiltration of proteins using hydrolyzed polyacrylonitrile hollow fiber. *J. Membr. Sci.* **1997**, 132(1), 63-71.

[25] Liu, H. Q.; Hsieh, Y. L. Preparation of water-absorbing polyacrylonitrile nanofibrous membrane. *Macromol. Rapid Commun.* **2006**, 27(2), 142-145.

[26] Zhang, Y.; Wu, Q.; Zhang, H.; Zhao, J. Intelligent hydrophilic nanoparticles fabricated via alkaline hydrolysis of crosslinked polyacrylonitrile nanoparticles. *J. Nanopart. Res.* **2013**, 15, 1800.

[27] Li, H.; Tripp C. P. Interaction of Sodium Polyacrylate Adsorbed on TiO_2 with Cationic and Anionic Surfactants. *Langmuir* **2004**, 20, 10526-10533.

[28] Mayoux, C.; Dandurand, J.; Ricard, A.; Lacabanne, C. Inverse Suspension Polymerization of Sodium Acrylate: Synthesis and Characterization. *J. Appl. Polym. Sci.* **2000**, 77, 2621-2630.

[29] Sadeghi, M.; Hosseinzadeh, H. Synthesis of starch-poly (sodium acrylate-co-acrylamide) superabsorbent hydrogel with salt and pH-responsiveness properties as a drug delivery system. *J. Bioact. Compat. Polym.* **2008**, 23(4), 381-404.

[30] Omidian, H.; Hashemi, S. A.; Sammes, P. G.; Meldrum, I. A model for the swelling of superabsorbent polymers. *Polymer* **1998**, 39, 6697-6704.

[31] Omidian, H.; Hashemi, S. A.; Sammes, P. G.; Meldrum, I. Modified acrylic-based superabsorbent polymers (dependence on particle size and salinity). *Polymer* **1999**, 40, 1753-1761.

[32] Kabiri, K.; Omidian, H.; Hashemi, S. A.; Zohuriaan-Mehr, M. J. Synthesis of fast-swelling superabsorbent hydrogels: effect of crosslinker type and concentration on porosity and absorption rate. *Eur. Polym. J.* **2003**, 39(7), 1341-1348.

[33] Liu, J. L.; Ma, J. Z.; Wang, J.; Zhu, Z. F.; Tang, H. R.; Zhang, L. M. Nanoparticle morphology and film-forming behavior of polyacrylate/ ZnO nanocomposite. *Compos. Sci. Technol.* **2014**, 98, 64-71.

[34] O' Grady, M. L.; Kuo, P. L.; Parker, K. K. Optimization of electroactive Hydrogel Actuators. *ACS Appl. Mater. Inter.* **2010**, 2(2), 343-346.

[35] Bao, Y.; Ma, J. Z.; Li, N. Synthesis and swelling behaviors of sodium carboxymethyl cellulose-g-poly(AA-co-AM-co-AMPS) / MMT superabsorbent hydrogel. *Carbohydr. Polym.* **2011**, 84(1), 76-82.

[36] Halake, K. S.; Lee, J. Superporous thermo-responsive hydrogels by combination of cellulose fibers and aligned micropores. *Carbohydr. Polym.* **2014**, 105, 184-192.

[37] Choe, K. Y.; Kim, K. J.; Kim, D. Y.; Manford, C.; Heo, S.; Shahinpoor M. Performance Characteristics of electro-chemically Driven Polyacrylonitrile Fiber bundle actuators. *J. Intell. Mater. Syst. Struct.* **2006**, 17, 563-576.

[38] Lee, D. Y.; Kim, Y.; Lee, S. J.; Lee, M. H.; Lee, J. Y.; Kim, B. Y.; Cho, N. I. Characteristics of chemo-mechanically driven polyacrylonitrile fiber gel actuators. *Mater. Sci. Eng. C-Biomim.* **2008**, 28, 294-298.

Chapter 5
Preparation of absorbent silk yarn through in situ polymerization

5.1 Introduction

Silk, being a well-known natural protein fiber produced by silkworm, has been used for thousands of years in textile industry. It is mainly consisted of two proteins—sericin and fibroin. The outer layer is silk sericin that acts like a glue to cement two fibroin fibers together during cocoon formation so as to protect the growing worm [1]. The fiber core is fibroin that is consisted of mainly five types of amino acids: alanine, glycine, serine, tyrosine, and valine, forming an anti-parallel β–sheet structure (silk II) predominantly [2, 3]. Silk has many desirable biological properties; however, silk has several drawbacks like its low water retention, limiting its applications. Therefore, study of modification of silk fiber is necessary to enhance its performance and widen its applications.

Currently, silk fibroin fibers are firstly dissolved into aqueous solution and then processed into hydrogels with various forms like films, sponges, fibers, and microspheres [4]. In order to further enhance the silk fibroin hydrogel gelation process and properties, it has been blended with synthetic polymers like poloxamer 407 [5] and poly(ethylene oxide) [6], as well as with natural polymers like elastin [7] and alginate [8] as reported in literatures. However, these blended

silk fibroin hydrogels have poor swelling properties and weak mechanical properties that hinder their biomedical applications. Even though the formation of semi-interpenetrating network has been introduced to improve mechanical property [5, 9, 10], the preparation of silk fibroin aqueous solution involves a tedious and time-consuming dialysis process.

An alternative approach is surface modification of silk fibroin fibers. It can impart fascinating properties to the silk fibers without damaging fiber interior and deteriorating their fundamental properties [11, 12]. Graft polymerization of vinyl monomers on the silk fiber has been extensively studied. For example, grafting methyl methacrylate on silk improves several properties like mechanical properties and crease recovery [13, 14]. Although numerous polymers have been grafted on silk fibers, these modified silks carry lower water retention value than the raw silk.

As mentioned, silk can be dissolved in various solutions like highly concentrated or mixed salts (e.g., –LiSCN, LiBr, and $CaCl_2$–EtOH–H_2O) and ionic (e.g., 1–butyl–3–methylimidazolium) [15, 16] to prepare the aqueous silk fibroin solutions. Inspired by the above dissolution process, LiBr, which is the common dissolution system [17] and good solubilizing agent for a silk yarn, of lower concentration is used to swell the silk fiber for additional functionalization. In this chapter, the natural silk yarn was modified by in situ free radical polymerization of acrylamide or sodium acrylate by swelling in a low

concentration of LiBr solution. The swelling of silk yarn allowed monomer penetration and further polymerization. These novel modified silk yarns are readily to be woven or knitted into textiles, having potentials of applications in biomedical textiles such as wound dressings and dermal sealants.

5.2 Experimental

5.2.1 Materials

Silk yarn of 20/22D was purchased from Huasheng Industrial Co., Ltd. (Hangzhou, China). It was composed of 14 silk fibroin filaments and had sericin content of 25 wt% as measured by infrared (IR) degumming method. All silk yarns for modification were degummed by IR heating in 1:40 liquor ratio to DI water at 110 ℃ for 60 min. Lithium bromide (LiBr), acrylamide (Am), sodium acrylate (NaA), ammonium persulfate (APS) and *N*,*N'*-methylene bisacrylamide (MBAAm) were purchased from Sigma Aldrich and used without further purification.

5.2.2 Sample preparation

The silk was immersed into 10 wt% monomer solution—acrylamide (Am) or sodium acrylate (NaA) in 4.65 M LiBr for 120 min, with APS and MBAAm as initiator and crosslinker respectively. The control silk yarn was immersed into 4.65 M LiBr only. The swollen silk was then collected from the swelling solution, sealed, and heated at 70 ℃ for 7 h. The resultant yarn was rinsed by DI water to

remove the remaining monomers and LiBr and dried at 70 ℃ until constant weight. The raw silk, control silk, silk treated by acrylamide, and silk treated by sodium acrylate were denoted as RS, CS, S-Am, and S-NaA respectively.

5.2.3 Characterizations

Swelling of silk immersed in 9.3 M and 4.65 M LiBr were observed at room temperature under an optical microscope (Nikon OPTIPHOT-POL) equipped with polarizers. The diameter increment was calculated by

$$\text{Diameter increment} = \frac{D_t - D_i}{D_i} \times 100\% \qquad \text{(Equation 5.1)}$$

where D_i is the fiber diameter before immersion (μm), and D_t the fiber diameter at time *t* (μm), averaged from 5 measurements.

The X-ray diffraction of the samples was obtained by Rigaku SmartLab with Ni-filtered Cu-Kα radiation in the range of 10–40° at 10°/min.

The chemical changes were investigated by attenuated total reflectance Fourier transform infrared (ATR-FTIR) spectroscope (PerkinElmer Spectrum 100) in a spectral region of 4000–650 cm^{-1} with 16 scans at 4 cm^{-1} resolution.

To examine the morphology of silk yarns, they were fully swollen in DI water and freeze-dried (Christ Alpha 1-4 LD), then observed under a field-emission scanning electron microscope (SEM, JEOL JSM-6490) operating at 20 kV after gold sputtering.

To measure the water absorption ratio (*Q*), the dried samples were immersed in DI water for 1, 2, 3, and 24 h sequentially to achieve equilibrium, then centrifuged at 1000 revolutions per minute for 1 min to remove free water. It was calculated by

$$Q\ (\mathrm{g/g}) = \frac{W_f - W_i}{W_i} \qquad \text{(Equation 5.2)}$$

where W_i is the weight of dry sample (g), and W_f is the weight of wet sample (g).

Tensile property was measured by means of the universal material testing machine (Instron 4411, USA) with 2 cm distance between the clamps and 1 cm clamp width, at a strain speed of 10 mm/min. The stress is calculated by Stress (MPa) equals to Force/[π(d/2)^2], where d is the average diameter measured under optical microscope. For dry samples, they were conditioned under standard conditions (T = 25 ℃ and R.H. = 65%) in advance. For wet samples, they were immersed in DI water till equilibrium.

5.2.4 Cytotoxicity study

Human skin keratinocytes (HaCaT) from sterile cell culture flask were trypsinized and neutralized with fetal bovine serum. They were prewashed with phosphate buffered saline, centrifugated, and resuspended in a fresh cell culture medium at a concentration of about 1×10^5 cells/ml counted manually using a haematocytometer under an inverted microscope. The cells were seeded in the 96

-well microtitre plates for 24 h. The sterilized RS, S-NaA, and S-Am were added respectively and incubated for an additional 24 h. The quanitative cell viability was evaluated by sulforhodamine B protein staining methods. The cells were fixed with trichloroacetic acid, washed with DI water, and stained with sulforhodamine B. The cells were washed with acetic acid again and then dissolved a 0.1 ml unbuffered Tris-base. Finally, optical absorptions were measured at 575 nm by a microplate reader (Victor V form Perkin–Elmer, Life Sciences). Each experiment was conducted in triplicate and a mean value was obtained while three independent experiments were performed. Results were shown as mean ± SD from their mean values of these three independent experiments.

5.3 Results and discussion

5.3.1 Swelling behavior of silk in LiBr solution

Swelling of silk yarns in 9.3 M and 4.65 M LiBr was observed under optical microscope equipped with plane-polarized and cross-polarized lights. Figure 5.1 showed the microscopic images of silk swelling in 9.3 M LiBr. Its diameter increased dramatically and became more than double after 120 min. Meanwhile, its crystallinity gradually decreased and was finally lost after 120 min as the brightfield was disappeared under cross-polarized light. It completely dissolved within 180 min since 9.3 M LiBr is an effective dissolution agent for silk fibroin.

By decreasing the concentration of LiBr to 4.65 M, the silk swelled gradually without losing its crystallinity as shown in Figure 5.2.

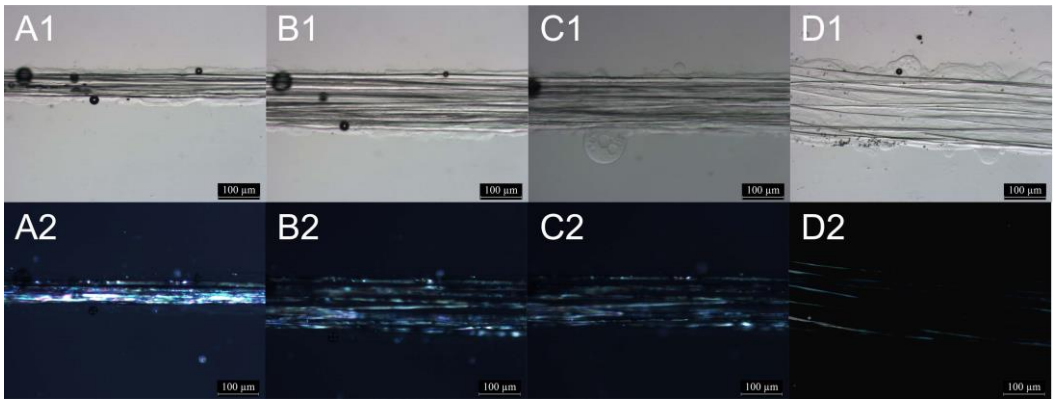

Figure 5.1 Optical microscopic images of silk yarn under (1) plane-polarized light and (2) cross-polarized light in 9.3 M LiBr at (A) 0 min, (B) 30 min, (C) 60 min, and (D) 120 min.

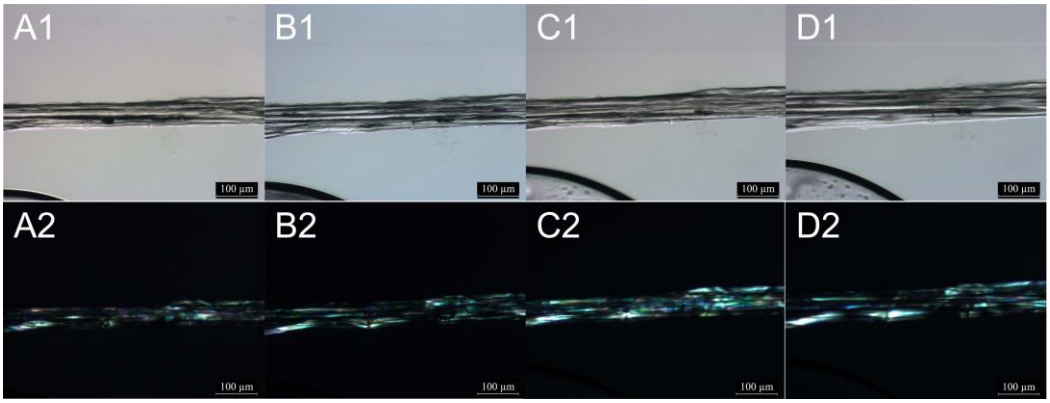

Figure 5.2 Optical microscopic images of silk yarn under (1) plane-polarized light and (2) cross-polarized light in 4.65 M LiBr at (A) 0 min, (B) 30 min, (C) 60 min, and (D) 120 min.

Compared to the completely dissolution of silk in 9.3 M LiBr after 120 min, silk in 4.65 M LiBr had increment in its diameter by 50% and reached equilibrium at 120 min (Figure 5.3). Though swelling of silk in 4.65 M LiBr is less and slower than in 9.3 M LiBr, it provides adequate time for penetration of

monomers into the silk without dissolution. The silk yarn displayed increment in diameter and retained its crystalline strcucture clearly in 4.65M LiBr with 10 wt% acrylamide solution after 120 min immersion as shown in Figure 5.4.

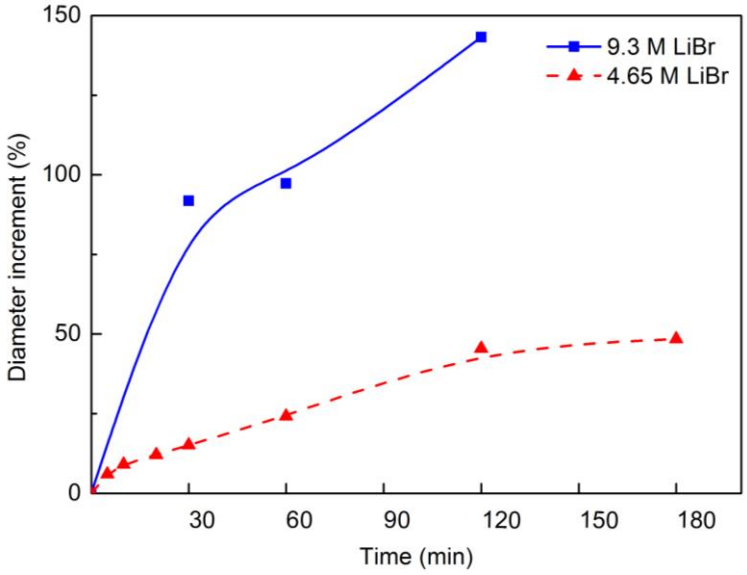

Figure 5.3 Diameter increment percentage of silk yarn in 9.3 M LiBr and 4.65 M LiBr at various time.

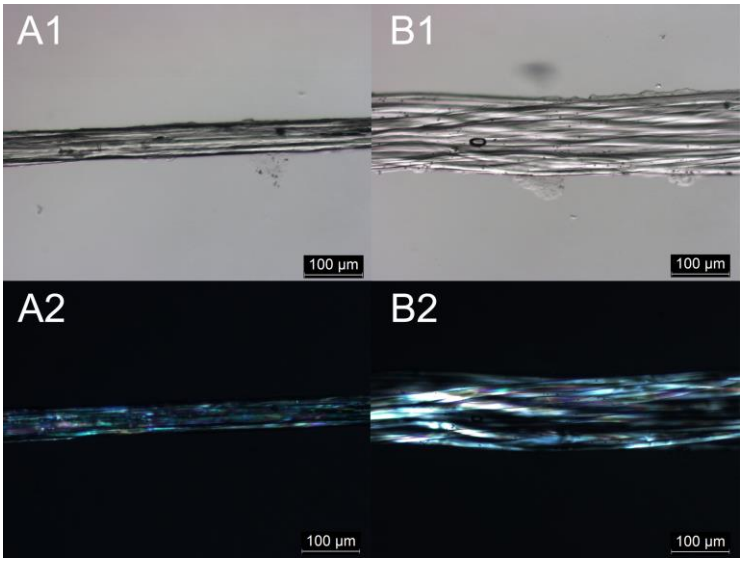

Figure 5.4 Optical microscopic images of silk yarn under (1) plane-polarized light and (2) cross-polarized light in 4.65M LiBr with 10 wt% acrylamide at (A) 0 min and (B) 120 min.

5.3.2 Structural characterization of LiBr treated silk

5.3.2.1 XRD analysis

XRD and FTIR were used to further identify the secondary structural changes in 9.3 M and 4.65 M LiBr after 120 min immersion as shown in Figures 5.5 and 5.6.

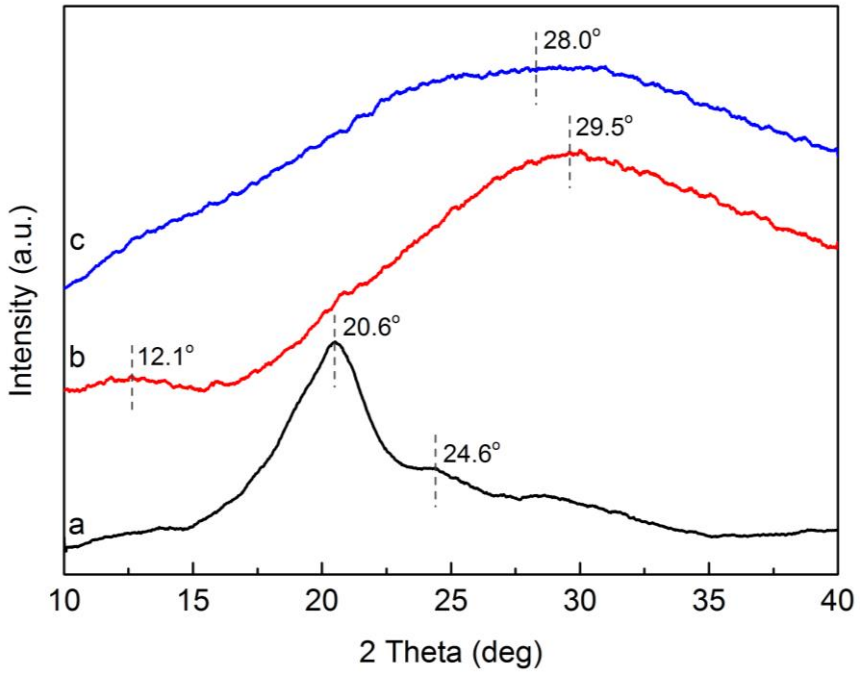

Figure 5.5 X-ray diffractions of (a) RS, (b) silk in 4.65 M LiBr, and (c) silk in 9.3 M LiBr.

The XRD pattern of RS showed the diffraction peaks at 20.6° and 24.6°, indicating the predominant β–sheet crystalline (silk II) structure with spacing of 4.3 and 3.7 Å respectively [18] (Figure 5.5a). As silk yarn was immersed in 4.65 M LiBr, the peak at 29.5° became broad and a new peak at 12.1° appeared, mainly attributing to the α-helix (silk I) conformation [19]. A featureless broad

peak from 10–40° in the XRD pattern of silk immersed in 9.3 M LiBr depicted the amorphous state (random coil structure) [20]. The XRD results demonstrates the conformational changes of silk from β–sheet (silk II) to α-helix (silk I) structure in 4.65 M LiBr, and to amporhous state in 9.3 M LiBr. The conformational state of silk fibroin is highly correlated to the concentration of LiBr solution.

5.3.2.2 FTIR analysis

In addition, the structural changes of silk yarns in 4.65 M and 9.3 M LiBr were further confirmed by FTIR as shown in Figure 5.6.The absorption regions of 1700–1600 cm^{-1}, 1600–1500 cm^{-1}, and 1300–1200 cm^{-1} are assigned to amide I (C=O stretching), amide II (in-plane N-H bending, and C-N bending) and amide III (N-H bending and C-N stretching) of the peptide backbones respectively, which have been used for studying the secondary structure of silk [19].

FTIR spectrum of RS showed the peaks at 1616, 1514, and 1265 (shoulder peak) cm^{-1} indicating the typical silk II structure. When the silk yarn was immersed in 4.65 M LiBr, these peaks gradually shifted to 1644 and 1530 cm^{-1} identifying the presence of silk I conformation. As silk was immersed in 9.3 M LiBr solution, the peaks became broader and shifted to 1660, 1540, and 1235 cm^{-1}, being attributed to the amorphous state. The observed secondary structural changes of silk is due to the presence of strong dissoluting agent LiBr that breaks

the strong hydrogen bondings in silk fibroin [21]. Other literatures also confirmed the relationship between peak shifts and structural changes in silk [22, 23]. The FTIR results are consistent with previous microscopic images (Figure 5.1 and 5.2) and XRD analysis (Figure 5.5). With a combination of these data, the monomers in 4.65 M LiBr are presumably able to penetrate into an individual silk fibroin.

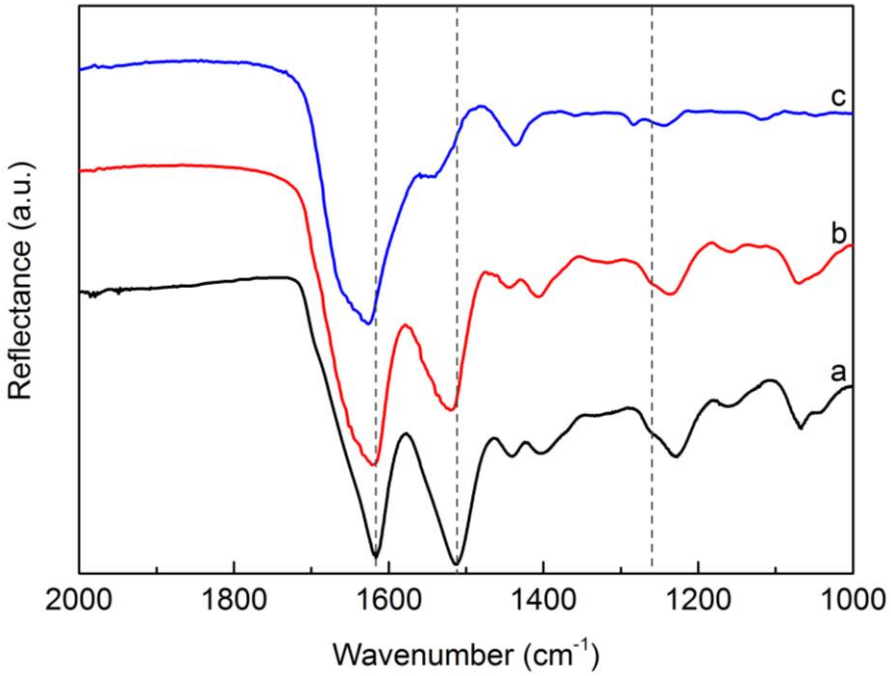

Figure 5.6 FTIR spectra of (a) raw silk, (b) silk in 4.65 M LiBr, and (c) silk in 9.3 M LiBr.

5.3.3 Preparation of in situ polymerization

In Figure 5.7, it illustrates the process of in situ polymerization in silk yarn by swelling in 4.65 M LiBr. During immersion in 4.65 M LiBr, silk yarn is swelled with structural changes so the monomers are able to penetrate into it by diffusion.

The initiator APS decomposes and generates free radicals to initiate the polymerization. Because of the crosslinker MBAm, crosslinking reaction occurs at 70 ℃ and a three-dimensional network is created. The polyacrylamide or poly(sodium acrylate) is physically entangled with the silk fibroin chains to form an interpenetrating network. The silk shrinks during washing, and finally the composite hydrogel structure in the whole silk yarns is formed.

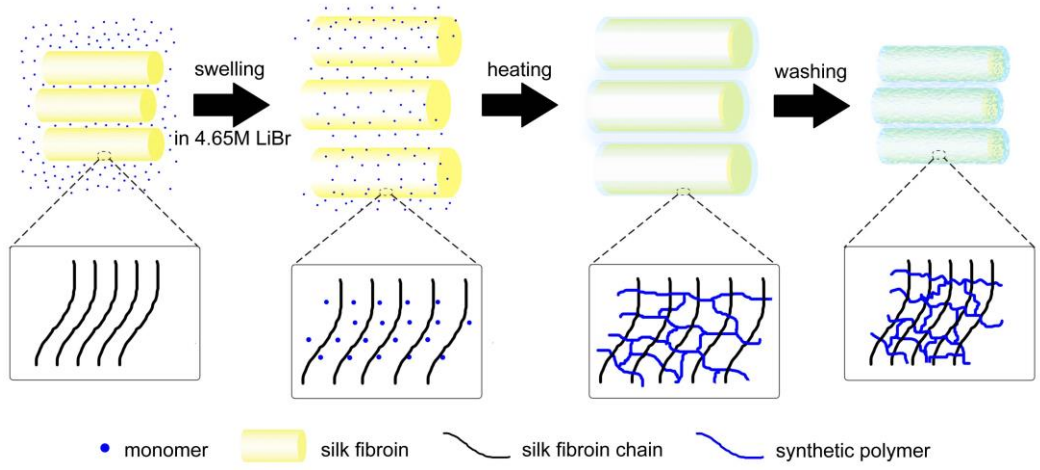

Figure 5.7 Schematic illustration of in situ polymerization in silk yarn.

5.3.4 Dissolution in 9.3 M LiBr

By gravimetric method, the weight uptakes of S-NaA and S-Am were measured to be 14.6% and 18.1% as shown in Table 5.1. Further confirmation was conducted by dissolution in 9.3 M LiBr at 65 ℃. As shown in Figure 5.8, CS nearly dissolved in 9.3 M LiBr after heating for first 30 min, and the solution turned slightly cloudy. On the contrary, both S-NaA and S-Am still retained their fiber shape clearly after heating for further 90 min. It exhibits that the presence of synthetic polymers in individual silk filament prevents them from being

dissolved in the 9.3 M LiBr. The gel fractions of S-NaA and S-Am were calculated to be 66.9% and 80.4% that were much higher than that of CS having negligible 4.0%. Although the value of gel fraction is much higher than weight uptake, they show an agreement that higher weight uptake has higher gel fraction. The high gel fraction is consisted of both synthetic polymer and natural fibroin, revealing the successful formation of interpenetrating network of synthetic polymer in fibroin amorphous region.

Table 5.1 Weight uptake percentage and gel fraction of samples measured by weighing and dissolution in 9.3 M LiBr.

Samples	Gravimetric method	Dissolution in 9.3 M LiBr
	Weight uptake [a] (%)	Gel fraction [b] (%)
CS	-	4.0
S-NaA	14.6	66.9
S-Am	18.1	80.4

[a] Weight uptake (%) after in situ polymerization is calculated by

$$\text{Weight uptake} = \frac{w_f - w_d}{w_d} \times 100\% \qquad \text{(Equation 5.3)}$$

where w_f is the final dry weight of silk after modification (g), and w_d is the dry weight of degummed silk (g).

[b] Samples (≈0.1 g) were firstly soaked in 9.3 M LiBr (weight ratio of sample: 9.3 M LiBr = 1:300) and the solution were then heated at 65 ℃ and observed the changes for every 5 min. After heating for 30 min, CS totally dissolved in the 9.3

M LiBr solution while S-Am and S-NaA still had fibrous residues. The solutions were further heated for another 90 min, then filtered through polytetrafluoroethylene (PTFE) membrane filter and washed thoroughly with DI water. The residues were dried at 100 °C til constant weight. Gel fraction is calculated by

$$\text{Gel fraction of polymer} = \frac{\text{dry weight of residue}}{\text{dry weight of sample}} \times 100\% \qquad \text{(Equation 5.4)}$$

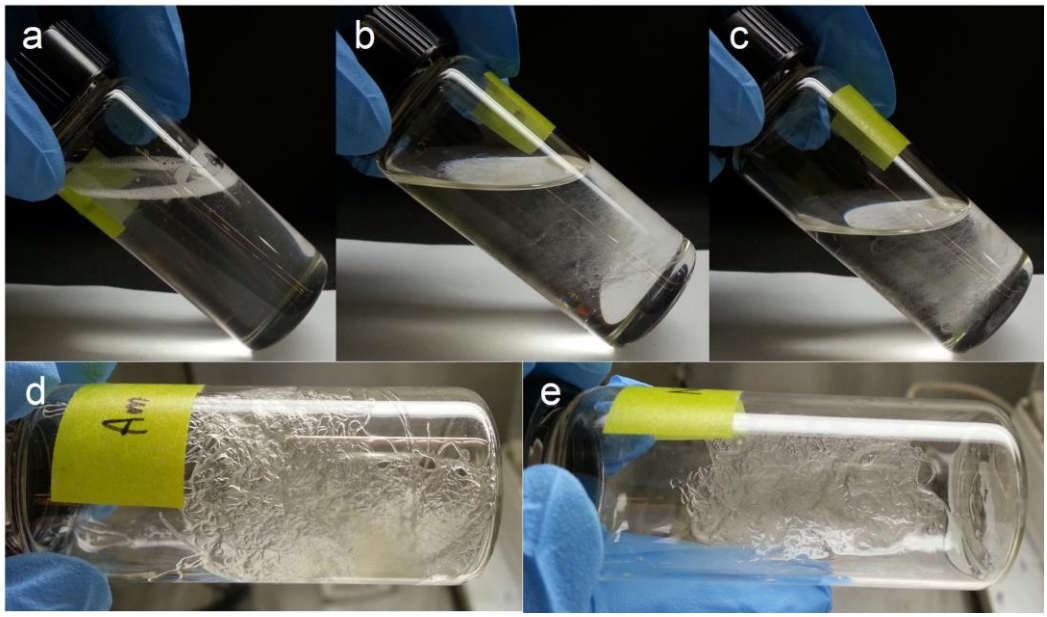

Figure 5.8 Pictures of (a) CS, (b, d) S-Am and (c, e) S-NaA in 9.3 M LiBr solutions after heating at 65 ℃ for 120 min.

5.3.5 Structural characteristics of the modified silk

5.3.5.1 XRD analysis

After in situ polymerization, the crystalline structures of silk samples were re-evaluated by XRD as shown in Figure 5.9. Two diffraction peaks at 20.6° and

24.6°, contributing to the β-sheet crystalline (silk II) structure, appeared in all silk samples RS, CS, S-Am, and S-NaA. Compared to XRD curves of silk yarns swollen in 4.65 M LiBr (Figure 5.5b), it confirms the conformational transition from α-helical structure (silk I) structure to β-sheet (silk II) structure after rinsing and drying. Apart from water-induced crystallization, this kind of transition can also be induced by protein concentration, pH, temperature, ultrasonication, electric field [18, 24-27] etc.

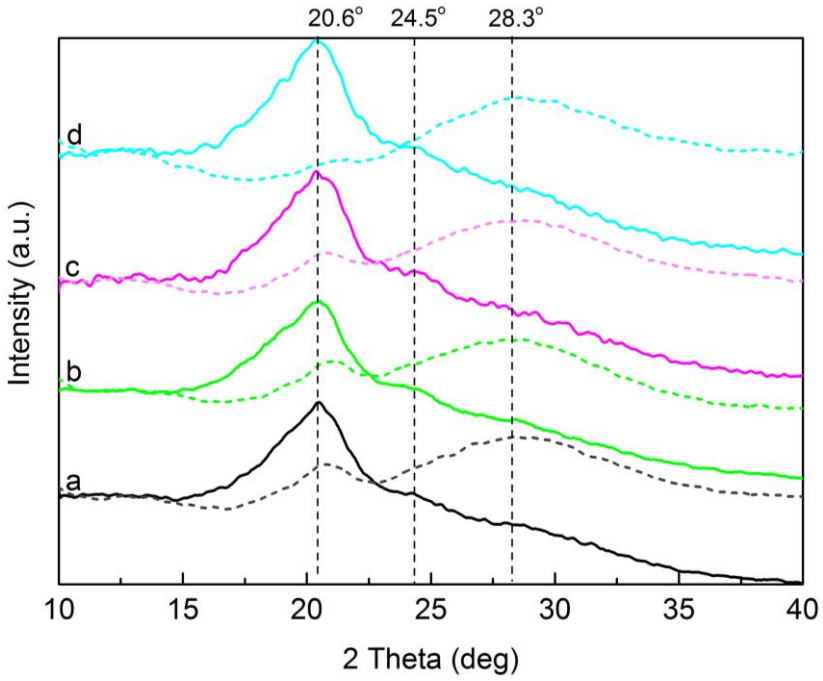

Figure 5.9 X-ray diffractions of (a) RS, (b) CS, (c) S-Am, and (d) S-NaA where the dash lines represent the corresponding samples at equilibrium swelling.

Further experiment on wet samples exhibited some changes in their XRD curves. After swelling the samples in DI water, the intensity at 20.6° decreased, while the intensity at 28.3° increased obviously. It indicates that both of the

β-sheet structure and the amorphous structure exist when swelling in water. Among all samples, S-NaA has less silk II structure since its diffraction peaks at 20.6° nearly disappeared in S-NaA. This highly amorphous structure is closely related to its water absorption performance.

5.3.5.2 FTIR analysis

Furthermore, FTIR spectra in Figure 5.10 provided the information of silk protein secondary structure and also revealed the presence of synthetic polymers after in situ polymerization. The spectra of all silk samples showed the characteristic peaks of typical silk II structure at 1616, 1514, and 1265 cm^{-1}.

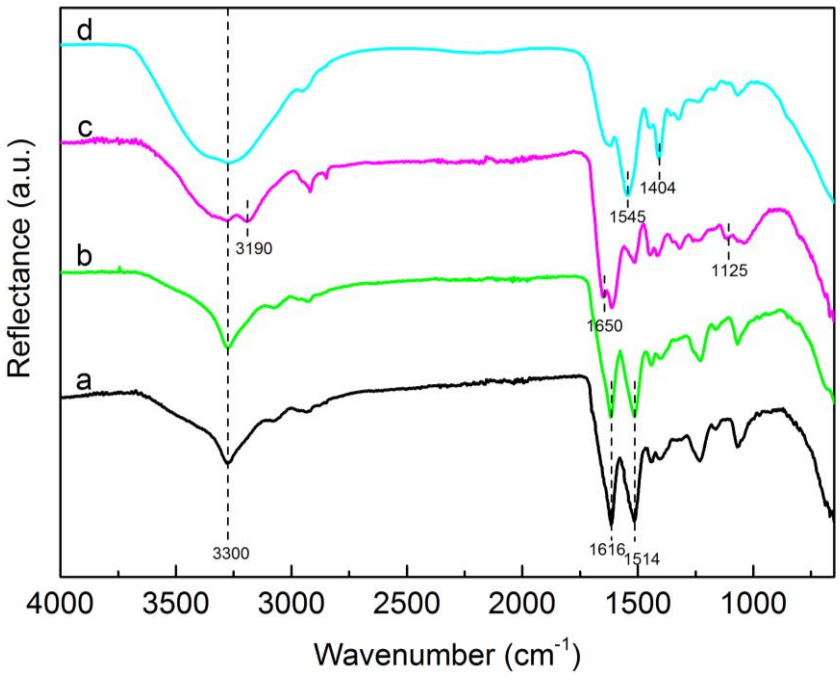

Figure 5.10 FTIR spectra of (a) RS, (b) CS, (c) S-Am, and (d) S-NaA.

In the S-Am, new peaks appeared at 3300, 3190, 1650, and 1125 cm^{-1}, indicating symmetrical and asymmetrical stretching of N-H, stretching of C=O of amide, and out-of-plane bending of NH_2 respectively from polyacrylamide [28, 29]. Likewise, the S-NaA showed two strong absorption peaks at 1545 and 1404 cm^{-1}, corresponding to the asymmetrical and symmetrical stretching of $–COO^-$ group from the poly(sodium acrylate) [30, 21], and a broad peak at 3300 cm^{-1} corresponding to the stretching of –OH group. From both of the XRD and FTIR results, they confirmed the β-sheet and successful incorporation of polyacrylamide and poly(sodium acrylate) into silk yarns.

5.3.6 Morphology of modified silk

The surface and cross-section morphology of silk yarns was examined under SEM after fully swelling and freeze-drying. As seen in Figure 5.11a, the RS was composed of fibroin filaments adhered to each other with a smooth sericin surface. Its cross-section clearly showed a solid cross-section of silk filaments bound tightly by sericin. Compared to the circular shape of silk yarn in RS, CS displayed the individual fibroin filaments clearly, and these silk filaments were easily deformed and loosely packed as seen in its cross-section, owing to the sericin loss as shown in Figure 5.11b.

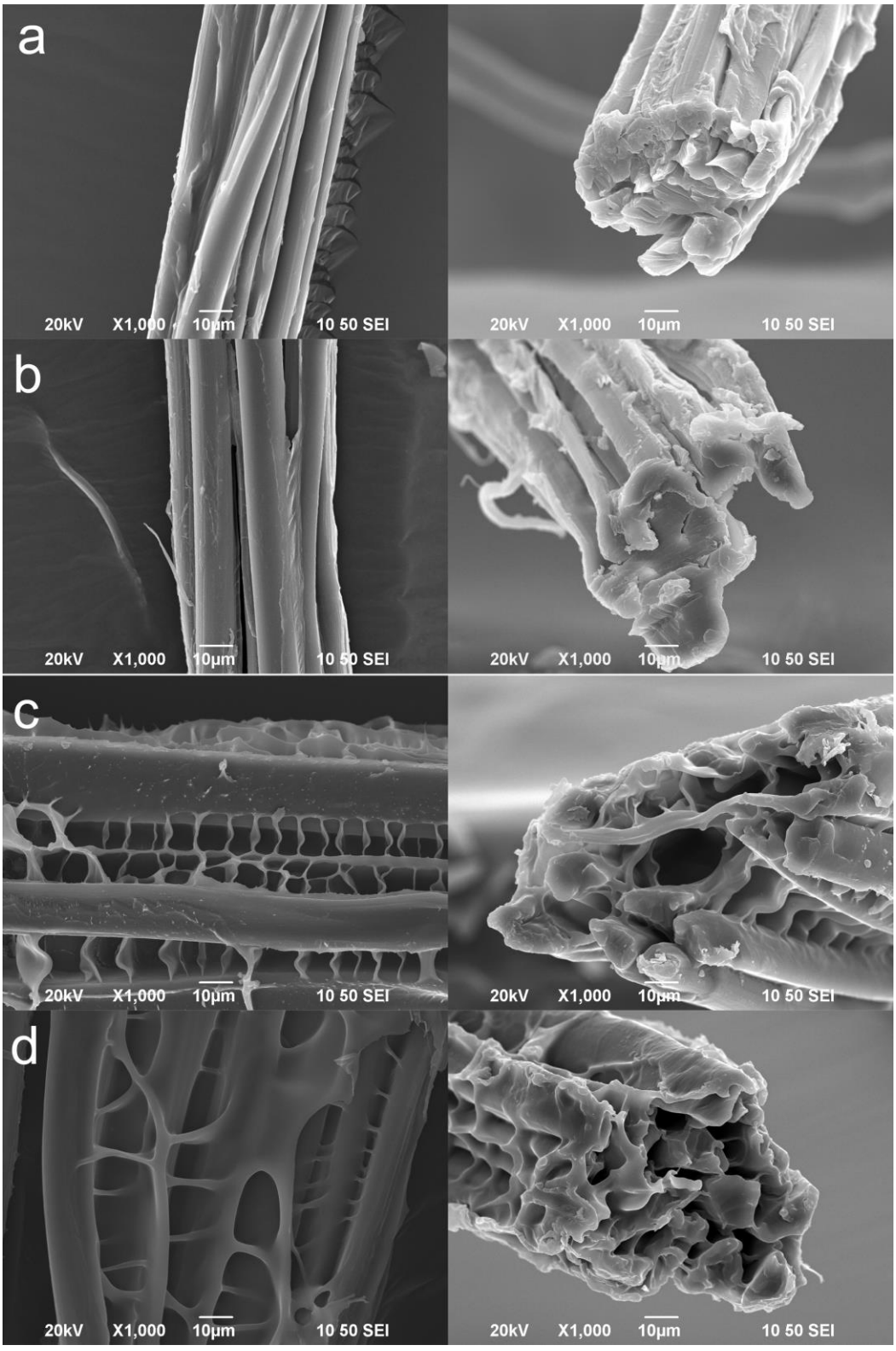

Figure 5.11 SEM images of freeze-dried (a) RS, (b) CS, (c) S-Am and (d) S-NaA, and their corresponding cross-section (right).

After in situ polymerization, ladder structure was observed between the filaments forming porous structure in samples S-Am and S-NaA as shown in Figures 5.11c and 5.11d. The synthetic hydrogel adhered perpendicularly to the filaments. In addition, the diameter of each individual filament also increased by about 40%. This increment is attributed to the crosslinked polyacrylamide or poly(sodium acrylate) gels between and within the silk filaments. In contrast to the solid cross-section of RS and CS, the cross-section views of S-Am and S-NaA showed some pores in between each filaments, while the filaments were held together by the synthetic gels. Both polyacrylamide or poly(sodium acrylate) increased the diameter of silk and created ladder shape composite hydrogel structure along the silk as seen clearly under SEM.

5.3.7 Swelling behavior of modified silk in DI water

Water absorption ratio (*Q*) of modified silk yarns were evaluated as shown in Figure 5.12. The RS and CS absorbed only 0.85 g/g and 1.05 g/g of water. The sericin loss in CS enhanced the capillary effect of the silk yarn so it achieved a higher water absorption than RS. In comparison, S-Am and S-NaA achieved *Q* values of 2.4 g/g and 7.6 g/g of water respectively that were almost 3 and 9 times higher than that of RS.

Das's group prepared the acrylamide grafted silk fibers; however, 73% grafted silk had only 1.9 g/g water rentention value [32]. Our acrylamide

modified silk S-Am achieved a slightly higher *Q* value. It is probably due to the porous hydrogel structure as seen under its SEM images so that it can retain the water in its physical structure. The silk modified by sodium acrylate S-NaA has the highest *Q* value among all the samples, owing to the presence of carboxylate salts in poly(sodium acrylate) and its porous structure. It also agrees with XRD results that the amorphous structure dominates the most in wet S-NaA sample. Therefore, it suggests that the in situ polymerization of acrylamide or sodium acrylate successfully improves the water absorption absorption of silk.

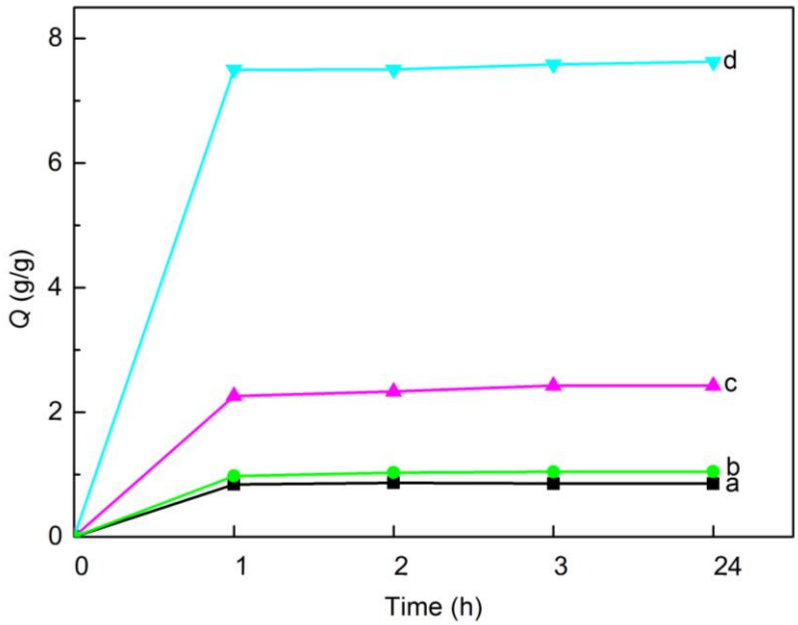

Figure 5.12 Water absorption ratio (*Q*) of (a) RS, (b) CS, (c) S-Am, and (d) S-NaA against time.

5.3.8 Mechanical properties of modified silk

Mechanical properties of silk samples were also measured to evaluate their performance since it is a very important parameter of textiles for practical

application. The average values of breaking stress and breaking strain were shown in Table 5.2. The apparent breaking stress and breaking strain of RS were 282 MPa and 29%. After immersing in 4.65 M LiBr solution only, the breaking stress and breaking strain of CS decreased significantly to 161 MPa and 15% that were lower than that of RS by 43% and 48%.

Table 5.2 Mechanical property of RS, CS, S-Am and S-NaA in dry state and wet states. (Values shown are means and ± standard deviation for six specimens)

Samples		Breaking stress MPa	Breaking strain %
RS	Dry	282 ± 17	29 ± 3
CS	Dry	161 ± 6	15 ± 3
S-Am	Dry	318 ± 17	30 ± 4
	Wet	313 ± 33	31 ± 5
S-NaA	Dry	331 ± 36	31 ± 2
	Wet	20938	36 ± 3

In contrast to the poor mechanical property of CS, notable tensile improvement was observed for modified silk samples S-Am and S-NaA as shown in the typical tensile curves (Figure 5.13). The breaking stress and breaking strain of S-Am increased to 318 MPa and 30%, which were 98% and 100% higher than that of CS, respectively. When this yarn was fully wetted, its strength decreased while its extension increased slightly. Moreover, the S-NaA showed even better mechanical improvement than S-Am, having 331 MPa in stress at break and 31% in strain at break. In its wet state, though its breaking

stress decreased, its breaking strain increased obviously to 36%. It is probably due to the conformational changes from β-sheet (silk II) structure to amorphous structure in a larger extent as shown in previous XRD result.

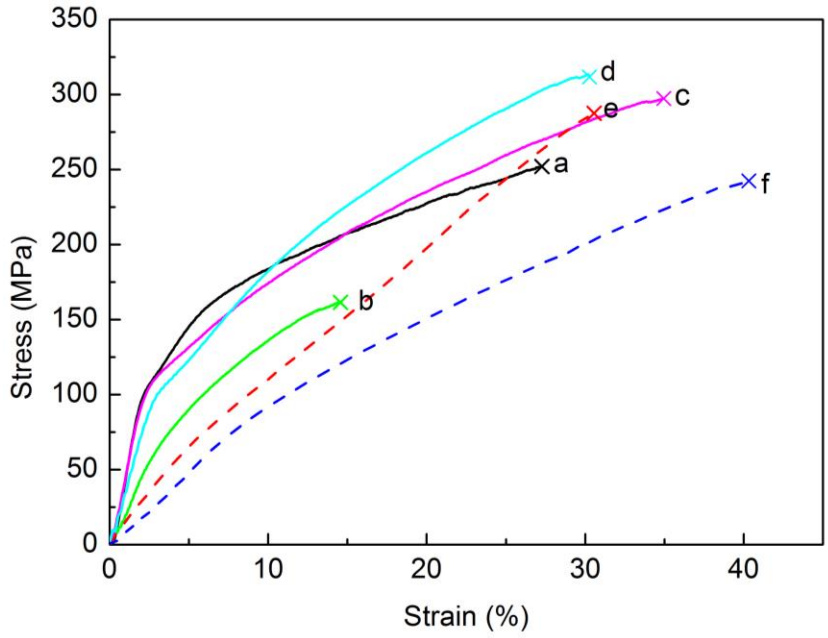

Figure 5.13 Typical tensile curves of (a) dry RS, (b) dry CS, (c, d) S-Am in dry and wet states, and (e, f) S-NaA in dry and wet states.

For those silk fibers modified by graft polymerization reported in literatures, their mechanical properties were only slightly improved. For example, the silk fibers modified by gelatin had its breaking stress increased by 15% but had its breaking strain decreased by 24% [33]. However, our modified silks S-Am and S-NaA showed significant improvement in mechanical properties in both dry and wet states after polymerization. It suggests that the interpenetrating network structure in individual fibroin filament is created in the swollen state and the composite hydrogel structure along the silk is formed after washing. As a

result, the modified silks with enhanced mechanical properties are still suitable for textile applications.

5.3.9 Cytotoxicity study

The preliminary cytotoxcity was studied by the viability of human skin keratinocytes (HaCaT). The optical images of RS and S-NaA showed relatively higher integrities of cellular structures than that of S-Am, having certain degree of cellular shrinkage and nuclear condensation as shown in Figure 5.14a. The cell viability of RS and S-NaA had more than 80%, while that of S-Am had only 56% (Figure 5.14b). Therefore, these results reveal that RS and S-NaA have no cytotoxic effects towards skin keratinocytes.

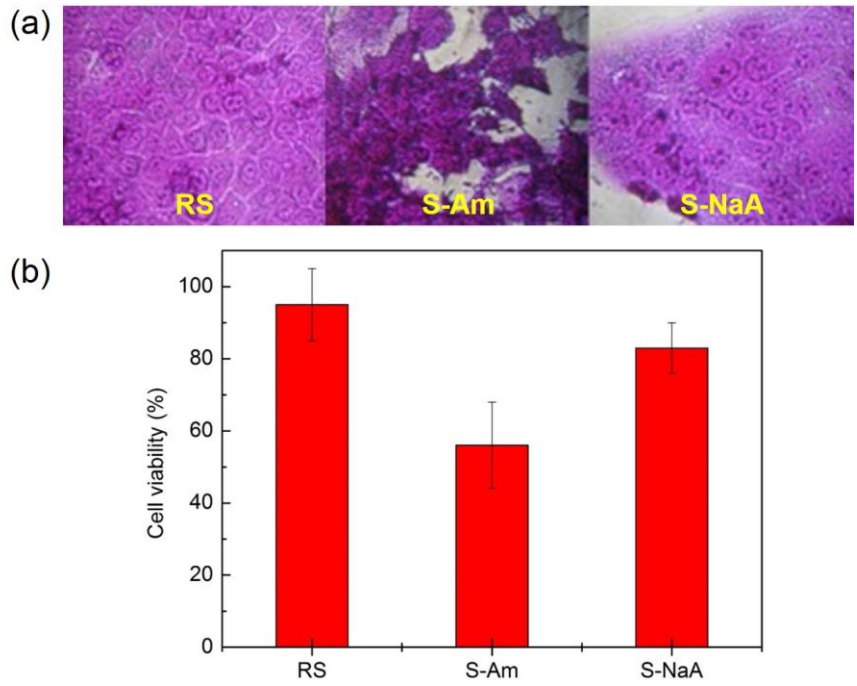

Figure 5.14 (a) Optical images showing the viability of skin keratinocytes; and (b) Cell viability percentage of RS, S-Am, and S-NaA.

5.4 Summary

The silk yarns have been potently modified through in situ acrylamide and sodium acrylate polymerization. The optical microscopic images confirmed the swelling of silk yarns in 4.65 M LiBr without destroying their fiber integrity. XRD and FTIR suggested that the conformational changes in 4.65 M LiBr allowed the penetration of monomers into the silk. Dissolution and FTIR spectra indicated the formation of interpenetrating network of polyacrylamide and poly(sodium acrylate) in the silk. These synthetic hydrogels appeared as ladder structure in between adjacent filaments after being freeze-dried as shown under SEM. These silk yarns presnted significant improvement in water absorption performance and mechanical properties. Therefore, those modified silk yarns, especially S-NaA, are promising for biomedical textiles applications.

References

[1] Altman, G. H.; Diaz, F.; Jakuba, C.; Calabro, T.; Horan, R. L.; Chen, J.; Lu, H.; Richmond, J.; Kaplan, D. L. Silk-based biomaterials. *Biomaterials* **2003**, 24(3), 401-416.

[2] Oyama, F.; Mizuno, S.; Shimura, K. Studies on immunological properties of fibroin heavy and light chains. *J. Biochem.* **1984**, 96(6), 1689-1694.

[3] Zhou, C. Z.; Confalonieir, F.; Medina, N.; Zivanovic, Y.; Esnault, C.; Yang, T.; Jacquet, M.; Janin, J.; Duguet, M.; Perasso, R.; Li, Z. G. Fine organization of Bombyx mori fibroin heavy chain gene. *Nucleic Acids Res.* **2000**, 28(12), 2413-2419.

[4] Rockwood, D. N.; Preda, R. C.; Yucel, T.; Wang, X. Q.; Lovett, M. L.; Kaplan, D. L. Materials fabrication from Bombyx mori silk fibroin. *Nat. Protoc.* **2011**, 6, 1612-1631.

[5] Yoo, M. K.; Kweon, H. Y.; Lee, K. G.; Cho, C. S. Preparation of semi-interpenetrating polymer networks composed of silk fibroin and poloxamer macromer. *Int. J. Biol. Macromol.* **2004**, 34, 263–270.

[6] Jin, H. J.; Fridrikh, S. V.; Rutledge, G. C.; Kaplan, D. L. Electrospinning Bombyx mori silk with Poly(ethylene oxide). *Biomacromolecules* **2002**, 3 (6), 1233-1239.

[7] Vasconcelos, A.; Gomes, A. C.; Cavaco-Paulo, A. Novel silk fibroin-elastin wound dressings. *Acta Biomater.* **2012**, 8, 3049-3060.

[8] Roh, D. H.; Kang, S. Y.; Kim, J. Y.; Kwon, Y. B.; Kweon, H. Y.; Lee, K. G.; Park, Y. H.; Baek, R. M.; Heo, C. Y.; Choe, J.; Lee, J. H. Wound healing effect of silk fibroin/ alginate-blended sponge in full thickness skin defect of rat. *J. Mater. Sci. Mater. Med.* **2006**, 17(6), 547-552.

[9] Mandal, B. B.; Kapoor, S.; Kundu, S. C. Silk fibroin/ polyacrylamide semi-interpenetrating network hydrogels for controlled drug release. *Biomaterials* **2009**, 30, 2826-2836.

[10] Kundu, B.; Kundu, S. C. Silk sericin/ polyacrylamide *in situ* forming hydrogels for dermal reconstruction. *Biomaterials* **2012**, 33, 7456-7467.

[11] Das, A. M.; Chowdhury, P. K.; Saikia, C. N.; Rao, P. G. Some Physical Properties and Structure Determination of Vinyl Monomer-Grafted Antheraea assama Silk Fiber. *Ind. Eng. Chem. Res.* **2009**, 48(20), 9338-9345.

[12] Li, G. H.; Liu, H.; Li, T. D.; Wang, J. Y. Surface modification and functionalization of silk fibroin fibers-fabric toward high performance applications. *Mat. Sci. Eng. C-Biomim.* **2012**, 32(4), 627-636.

[13] Maji, T. K.; Basu, D.; Datta, C.; Banerjee, A. Studies of mechanical and moisture regain properties of methyl methacrylate grafted silk fibers. *J. Appl. Polym. Sci.* **2002**, 84(5), 969-974.

[14] Prachayawarakorn, J.; Boonsawat, K. Physical, chemical, and dyeing properties of *Bombyx mori* silks grafted by 2-hydroxyethyl methacrylate and methyl methacrylate. *J. Appl. Polym. Sci.* **2007**, 106(3), 1526-1534.

[15] Ajisawa, A. Dissolution of silk by calcium-chloride/ ethanol aqueous solution. *J. Seric. Sci. Jpn.* **1998**, 67(2), 91-94.

[16] Phillips, D. M.; Drummy, L. F.; Conrady, D. G.; Fox, D. M.; Naik, R. R.; Stone, M. O.; Trulove, P. C.; De Long, H. C.; Mantz, R. A. Dissolution and Regeneration of Bombyx mori Silk Fibroin Using Ionic Liquids. *J. Am. Chem. Soc.* **2004**, 126, 14350-14351.

[17] Wang, H. Y.; Zhang, Y. Q. Effect of regeneration of liquid silk fibroin on its structure and characterization. *Soft Matter* **2013**, 9, 138-145.

[18] Kim, U. J.; Park, J.; Li, C. M.; Jin, H. J.; Valluzzi, R.; Kaplan, D. L. Structure and properties of silk hydrogels. *Biomacromolecules* **2004**, 5, 786-792.

[19] Ming, J.; Pan, F. K.; Zuo, B. Q. Influence factors analysis on the formation of silk I structure. *Int. J. Biol. Macromol.* **2015**, 75, 398-401.

[20] Pei, Y. Z.; Liu, X.; Liu, S. S.; Lu, Q.; Liu, J.; Kaplan, D. L.; Zhu, H. S. A mild process to design silk scaffolds with reduced β-sheet structure and various topographies at the nanometer scale. *Acta Biomater.* **2015**, 13, 168-176.

[21] Monti, P.; Freddi, G.; Bertoluzza, A.; Kasai, N.; Tsukada, M. Raman spectroscopic studies of silk fibroin from *Bombyx mori*. *J. Raman Spectrosc.* **1998**, 29(4), 297-304.

[22] Jin, H. J.; Park, J.; Karageorgiou, V.; Kim, U. J.; Valluzzi, R.; Kaplan, D. L. Water-stable silk films with reduced beta-sheet content. *Adv. Funct. Mater.* **2005**, 15(8), 1241-1247.

[23] Lu, Q.; Hu, X.; Wang, X. Q.; Kluge, J. A.; Lu, S. Z.; Cebe, P.; Kaplan, D. L. Water-insoluble silk films with silk I structure. *Acta Biomater.* **2010**, 6(4), 1380-1387.

[24] Nagarkar, S.; Nicolai, T.; Chassenieux, C.; Lele, A. Structure and gelation mechanism of silk hydrogels. *Phys. Chem. Chem. Phys.* **2010**, 12, 3834-3844.

[25] Matsumoto, A.; Chen, J.; Collette, A. L.; Kim, U. J.; Altman, G. H.; Cebe, P.; Kaplan, D. L. Mechanisms of silk fibroin sol-gel transitions. *J. Phys. Chem. B* **2006**, 110, 21630-21638.

[26] Hu, X.; Lu Q.; Sun, L.; Cebe, P.; Wang, X.; Zhang, X.; Kaplan, D. L. Biomaterials from Ultrasonication-Induced Silk Fibroin−Hyaluronic Acid Hydrogels. *Biomacromolecules* **2010**, 11, 3178-3188.

[27] Kojic, N.; Panzer, M. J.; Leisk, G. G.; Raja, W. K.; Kojic, M.; Kaplan, D. L. Ion electrodiffusion governs silk electrogelation. *Soft Matter* **2012**, 8, 6897-6905.

[28] Zhang, J. The surface characterization of mulberry silk grafted with acrylamide by plasma copolymerization. *J. Appl. Polym. Sci.* **1996**, 64, 1713-1717.

[29] Kirwan, L. J.; Fawell, P. D.; van Bronswijk, W. In Situ FTIR-ATR Examination of Poly(acrylic acid) Adsorbed onto Hematite at Low pH. *Langmuir* **2003**, 19, 5802-5807.

[30] Samanta, H. S.; Ray, S. K. Synthesis, characterization, swelling and drug release behavior of semi-interpenetrating network hydrogels of sodium alginate and polyacrylamide. *Carbohydr. Polym.* **2014**, 99, 666-678.

[31] Li, H.; Tripp, C. P. Interaction of Sodium Polyacrylate Adsorbed on TiO2 with Cationic and Anionic Surfactants. *Langmuir* **2004**, 20, 10526-10533.

[32] Das, A. M.; Chowdhury, P. K.; Saikia, C. N.; Rao, P. G. Silk fibre modification through graft copolymerization using vinyl monomer. *Indian J. Fibre Text.* **2010**, 35, 107-114.

[33] Wang, H. Y.; Zhang, Y. Q. Effect of regeneration of liquid silk fibroin on its structure and characterization. *Soft Matter* **2013**, 9, 138-145.

Chapter 6

Photo-induced crosslinking of silk fibers

6.1 Introduction

Silk fiber is a natural silk protein mainly composed of glycine (Gly, G), alanine (Ala, A), serine (Ser, S), tyrosine (Tyr, Y), and valine (Val, V) [1]. The characteristic repeating sequences of silk fibroin are known as GAGAGS in the crystalline region, GAGAGY and/ or GAGAGVGY in semi crystalline regions. In this study, the amino acid we focus on is Tyr that presents in both crystalline and amorphous regions [2].

Both physical and chemical methods have been widely studied to crosslink the protein chains. For physical gelation, induction of β-sheet crystalline structure (silk II) is the main cause. It can be induced by several factors such as temperature, pH, ultrasonication, and electricity [3–6]. For chemical crosslinking, synthetic crosslinkers, such as gluteraldehyde [7], have been reported but their toxicity limits the applications in biomedical fields [8]. Some natural crosslinkers like genipin [9, 10] and enzymatic reaction by tyrosinase [11] have also been applied; however, these crosslinking reactions required a long time for around 20 h that was time-consuming and not efficient in textile industry.

Nowadays, photochemistry has drawn back the attention since Ciamician reported the visible light photo-redox catalysis nearly a century ago [12–14].

Abundant and renewable light sources can perform “green chemical reactions” under mild and environmental friendly conditions [15, 16]. Commercial household light bulb can be an irradiation light source without any specialized equipment like high-energy ultraviolet (UV) light. A photocatalyst such as organometallic ruthenium(II) polypyridine complexes (i.e., $Ru(bpy)_3^{2+}$) has been extensively studied because of their chemical stability at room temperature and long lifetime of excited state (τ = 1100 ns) [17]. Among these complexes, tris(2,2′-bipyridyl)dichlororuthenium(II) ($Ru(bpy)_3Cl_2$) is commercially available and has been widely used as a photocatalyst.

Photo-induced crosslinking of protein by using $Ru(bpy)_3Cl_2$ was proposed by Fancy and co-workers [18, 19]. A few studies on photo-induced protein crosslinking have been conducted such as rec1-resilin protein [20], recombinant spider silk protein [21], and silk fibroin protein [22]. $Ru(bpy)_3^{2+}$ acts as a photosensitizer and a photocatalyst, while ammonium persulfate (APS) acts as the electron acceptor. By irradiating the $Ru(bpy)_3^{2+}$ with visible light (λ_{max} = 452 nm), it is promoted to the excited state via metal-to-ligand charge transfer to $*Ru(bpy)_3^{2+}$ (Scheme 6.1(1)) [17]. The persulfate anion ($S_2O_8^{2-}$) is an effective oxidative quenchers of $*Ru(bpy)_3^{2+}$ since it is a strong oxidizing agent and can be decomposed into two ions by photo-reduction [23, 24]. Therefore, $*Ru(bpy)_3^{2+}$ is rapidly quenched by $S_2O_8^{2-}$ to produce $Ru(bpy)_3^{3+}$, $SO_4^{-\bullet}$, and SO_4^{2-} through both static and dynamic processes (Scheme 6.1(2)) [25]. The

resultant $Ru(bpy)_3^{3+}$ and $SO_4^{-\bullet}$ are both strong oxidants [23, 26], while SO_4^{2-} is inactive species [27]. These two photo-generated oxidants have high potential in oxidizing primarily aromatic residues, such as tyrosine (Tyr, Y), tryptophan (Trp, W), and cysteine (Cys, C) residues [28-31]. Since silk fibroin contains 4.98 mol% of Tyr [2], $Ru(bpy)_3^{3+}$ and $SO_4^{-\bullet}$ species react with the Tyr residues to form the side-chain tyrosyl radicals (Schemes 6.1(3) and 6.1(4)). The reactive $Ru(bpy)_3^{3+}$ returns to its ground state $Ru(bpy)_3^{2+}$ after being reacted with Tyr residues, allowing its re-activation by light absorption. As a result, a di-tyrosine is formed from two tyrosyl radicals of different protein chains bridging via –C–C– bonds (Scheme 6.1(5)). The overall proposed reaction mechanism of photo-induced tyrosine crosslinking is illustrated in Scheme 6.1.

$Ru(bpy)_3^{2+}$ mediates rapid and efficient di-tyrosine crosslinking of SF. This facile metal mediated reaction is not cytotoxic and can crosslink through a photodynamic approach at room temperature with commercially available light [32]. In this chapter, the change of $Ru(bpy)_3^{2+}$ and APS system was monitored by UV-vis spectrophotometer. The photo-induced crosslinking of silk fibers under $Ru(bpy)_3^{2+}$/APS system was observed by dissolution in 9.3 M LiBr under optical microscope and analyzed by FTIR spectroscopy.

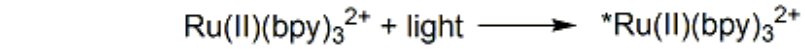

(1)

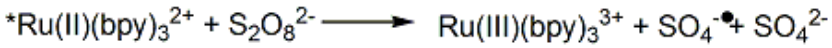

(2)

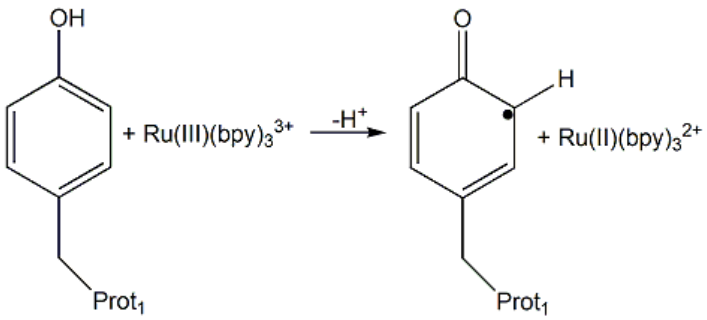

(3)

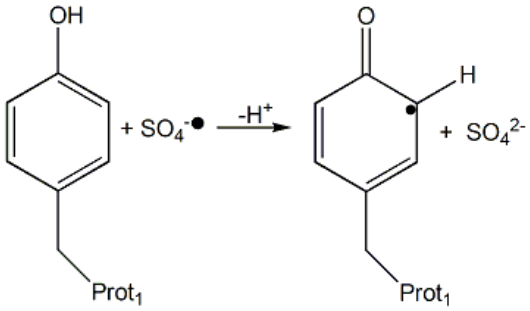

(4)

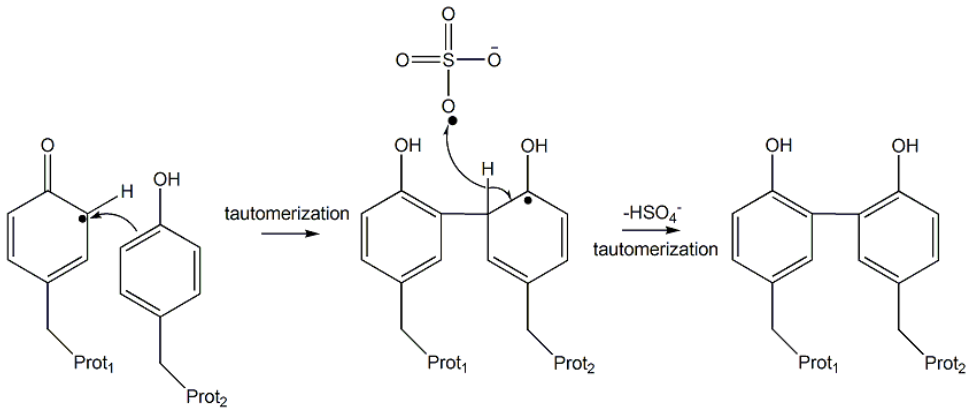

(5)

Scheme 6.1 Proposed reaction mechanism of photo-induced tyrosine crosslinking.

6.2 Experimental

6.2.1 Materials

Bombyx Mori silk cocoon was purchased from Aurora Silk (USA). Sodium acrylate (NaA), *N,N'*-methylene bisacrylamide (MBAAm), tris(2,2′-bipyridyl)dichlororuthenium(II) hexahydrate ($Ru(bpy)_3^{2+}$), and ammonium persulfate (APS) were all purchased from Sigma-Aldrich Co. and used without further purification.

6.2.2 Photochemical crosslinking of silk fiber

Raw silk fiber was denoted as RS. Control silk fiber was treated in DI water throughout the whole process and denoted as CS. Silk fibers were immersed in the solution of $Ru(bpy)_3^{2+}$ and APS in DI water for 60 min at room temperature, whilst preventing exposure to light. The mole ratio of $Ru(bpy)_3^{2+}$ to APS was fixed at 1:20. The solution was exposed to a 2200 Lux fluorescent light tube (Maxlite, 25W High Lumen, T8, 5000K) with diffuser, and the irradiation distance between them was fixed at 57.0 cm. The light source was measured by Spectroradiometer CS-2000 (Konica Minolta). The combination of concentration and irradiation time was listed in Table 6.1. The resulted silk fibers were rinsed by DI water thoroughly to remove the residues and dried at 65 ℃ in the oven till constant weight.

Table 6.1 Initial selection of $Ru(bpy)_3^{2+}$ concentration and irradiation time.

$Ru(bpy)_3^{2+}$ (mM)	APS (mM)	Irradiation time (min)	Sample notation
0.50	20	90	TrialS
0.10	2	15, 30, 60, 90	Ru10-[Time]
0.25	5	15, 30, 60, 90	Ru25-[Time]
0.50	10	15, 30, 60, 90	Ru50-[Time]

6.2.3 Photochemical crosslinking of sodium acrylate

Sodium acrylate of 10 wt% was dissolved in various combination of $Ru(bpy)_3^{2+}$, APS and MBAAm. The solution was then exposed to the fluorescent light to observe its changes.

6.2.4 Dissolution of silk fiber in 9.3 M LiBr

Samples were sandwiched between cover slide and glass slide. LiBr solution of 9.3 M was added to the samples for 60 min at room temperature and then heated in the oven for 60 min at 65 ℃. The samples were observed under optical microscope (OM, Nikon OPTIPHOT-POL) equipped with polarizers. The fiber diameter change (μm/μm) was calculated by

$$\text{Diameter change (μm/μm)} = \frac{\text{Fiber diameter after immersion/heating (μm)}}{\text{Fiber diameter before immersion (μm)}}$$

averaged from 5 measurements.

6.2.5 Characterizations

UV-vis absorbance spectrum was obtained by means of Cary 8454 UV-vis spectrophotometer (Aligent Technologies), using a quartz cuvette with a path length of 10 mm. Solution of 50 μM $Ru(bpy)_3^{2+}$ and 1000 μM APS in DI water was prepared for measurement.

FTIR spectrum was collected by attenuated total reflection Fourier transform infrared (ATR-FTIR) spectroscope (PerkinElmer Spectrum 100) in a spectral region of 4000–650 cm^{-1} with 16 scans at of 4 cm^{-1} resolution.

Mechanical property was measured by the universal material testing machine (Instron 5566, USA) with 2 cm distance between the clamps and 1 cm clamp width, at a strain speed of 10 mm/min. The stress is calculated by Stress (MPa) = Force/$[\pi(d/2)^2]$, where d is the average fiber diameter measured under optical microscope. The samples were conditioned under standard conditions (T = 25 ℃ and R.H. = 65%).

6.3 Results and discussion

6.3.1 $Ru(bpy)_3^{2+}$/APS system

The light intensity against wavelength for the 2200 Lux fluorescent light tube was shown in Figure 6.1. It showed the typical spectral graph of the fluorescent lamp, emitting the radiation over several narrow regions such as 435, 545, and 612 nm. The visible light photo-redox catalysis can be carried out under this

common light source, which is advantageous in the industrial process.

As $Ru(bpy)_3^{2+}$ and $Ru(bpy)_3^{3+}$ exhibit different UV-vis spectra, formation of $Ru(bpy)_3^{3+}$ can be observed. As shown in Figure 6.2, the broad absorption peak at 452 nm (log ε = 4.16) is assigned as the low-energy metal-to-ligand (*d* - π^*) charge transfer (MLCT), while the strong absorption peak at 286 nm (log ε = 4.94) is ascribed to the high-energy ligand-centered π - π^* transition. In addition, two weak shoulders at 354 nm (log ε = 3.81) and 245 nm (log ε = 4.47) are due to the metal-centered *d* - *d* transitions [33, 34].

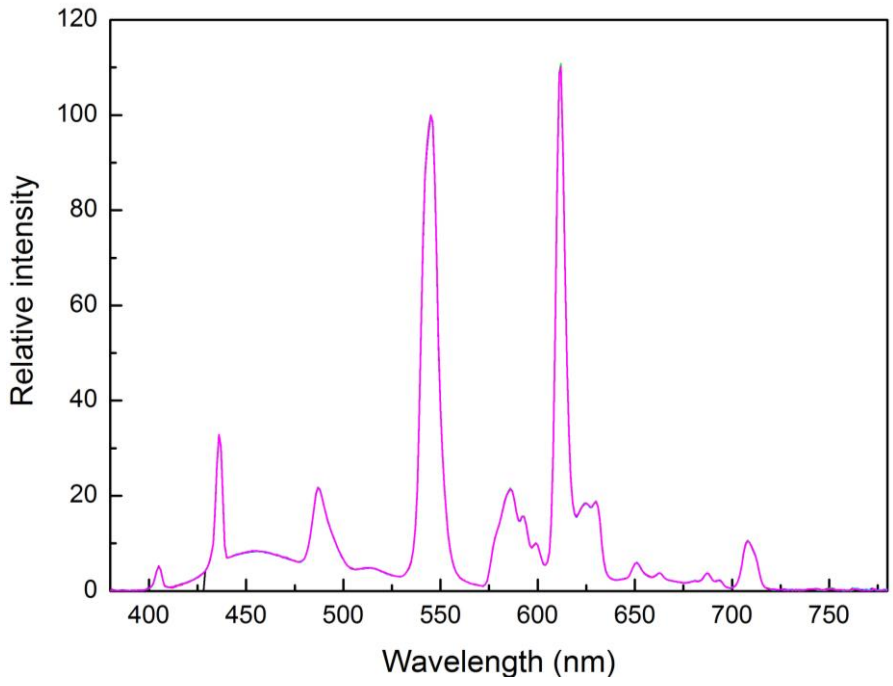

Figure 6.1 Spectral graph of the 2200 Lux fluorescent light tube, normalized at 545 nm.

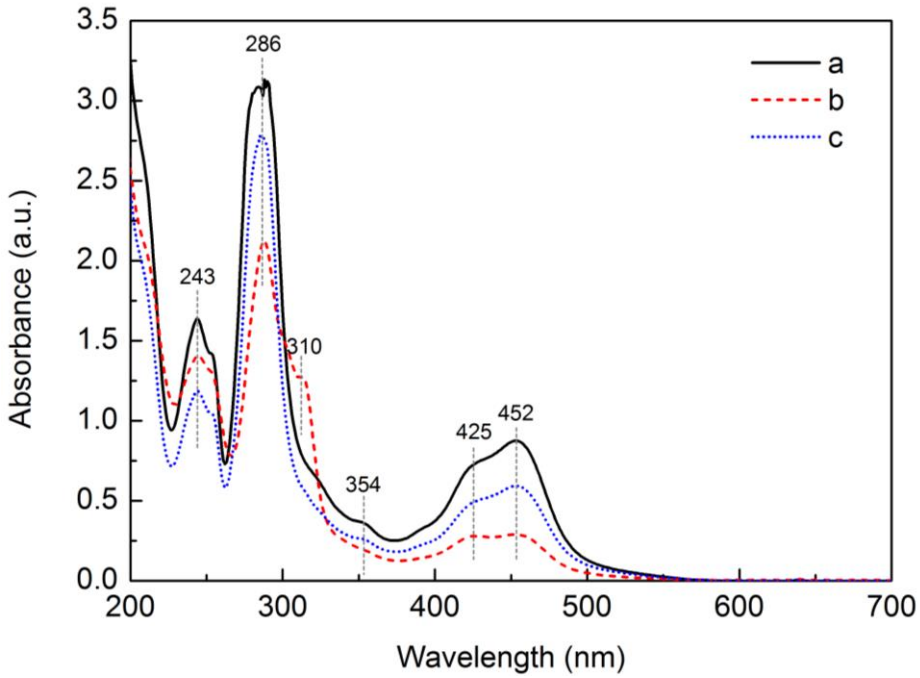

Figure 6.2 UV-vis spectra of $Ru(bpy)_3^{2+}$/APS solutions (a) freshly prepared without irradiation, (b) after 2 h irradiation, and (c) placed in the darkness for 24 h after 2 h irradiation.

As shown in Figure 6.3a, no change was observed in the UV-vis spectrum of pure $Ru(bpy)_3^{2+}$ solution without the electron acceptor APS after irradiation for 2 h. In contrast, when APS was added to $Ru(bpy)_3^{2+}$ solution, the intensity of absorption peak at 452 nm obviously decreased and the intensity of absorption peak at 425 nm increased after irradiation for 2 h as shown in Figure 6.3b. A peak with low extinction coefficient at around 310 nm was also observed. It is due to the spontaneously excitation of $Ru(bpy)_3^{2+}$ to $*Ru(bpy)_3^{2+}$, followed by oxidation of $*Ru(bpy)_3^{2+}$ to $Ru(bpy)_3^{3+}$ by $S_2O_8^{2-}$ (Schemes 6.1(1) and 6.1(2)) [34, 35]. From UV-vis spectra, these changes identify the formation of $Ru(bpy)_3^{3+}$ after irradiation. As shown in Figure 6.2, after placing the irradiated

solution back in the darkness for 24 h, disappearance of peak at 310 nm, lower intensity of peak at 425 nm, and higher intensity of peak at 452 nm were observed. Even though some changes are observed after 2 h irradiation, the UV-vis spectrum of the solution placed in the darkness is similar to that of freshly prepared solution before irradiation, indicating the recovery of $Ru(bpy)_3^{2+}$ (Figures 6.2a and 6.2c). It is due to the consumption of sacrificial electron acceptor $S_2O_8^{2-}$. Therefore, the UV-vis spectra suggested that this photocatalyst can be regenerated by placing it in the darkness.

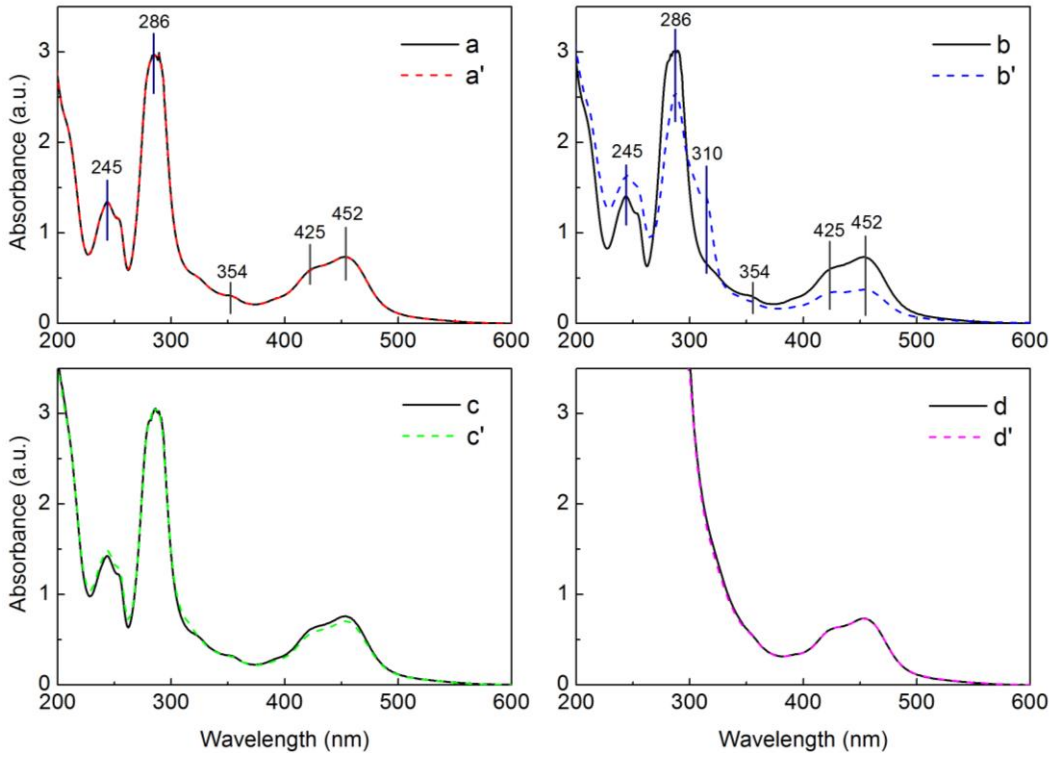

Figure 6.3 UV-vis spectra of solutions of (a) 50 μM $Ru(bpy)_3^{2+}$, (b) 50 μM $Ru(bpy)_3^{2+}$/1000 μM APS, (c) 50 μM $Ru(bpy)_3^{2+}$/1000 μM APS/silk, and (d) 50 μM $Ru(bpy)_3^{2+}$/1000 μM APS/10 wt% NaA, where dash lines (---) and apostrophe (') indicated irradiation of solutions for 2 h.

After the silk fibers or NaA was added to the $Ru(bpy)_3^{2+}$/APS solution, no obvious change was observed in their UV-vis spectra as shown in Figures 6.3c and 6.3d. When the UV-vis spectrum of $Ru(bpy)_3^{2+}$/APS solution with silk fiber was observed carefully, the intensity of the characteristic absorption peak of $Ru(bpy)_3^{2+}$ at 452 nm slightly lowered. It is due to the reactive $Ru(bpy)_3^{3+}$ rapidly reacts with Tyr residue of silk fiber and returns to its ground state $Ru(bpy)_3^{2+}$. Since only small amount of silk fibers were immersed in the solution, slightly degeneration of $Ru(bpy)_3^{2+}$ occurred. Moreover, after 10 wt% NaA was added into $Ru(bpy)_3^{2+}$/APS solution, two strong oxidants $Ru(bpy)_3^{3+}$ and $SO^{4-}\bullet$ resulted from irradiation oxidize the vinyl NaA monomers to form free radicals. $Ru(bpy)_3^{3+}$ returns to its ground state $Ru(bpy)_3^{2+}$ spontaneously so its UV-vis spectrum shows no change.

6.3.2 Photo-induced sodium acrylate polymerization

In order to observe the effect of NaA in the $Ru(bpy)_3^{2+}$/APS system, various solutions were prepared as shown in Table 6.2. Solution A contained both initiator and crosslinker for polymerization. However, heat is required for generating the free radicals to initiate the polymerization so the solution A remained as liquid at room temperature as shown in Figure 6.4A. Solution B contained $Ru(bpy)_3^{2+}$ and APS. As shown in Figure 6.4B, an obvious color change from orange-red color to greenish-yellow color was observed after

irradiation. The color change is due to the transition from $Ru(bpy)_3^{2+}$ to $Ru(bpy)_3^{3+}$ after photo-reduction by electron donor $S_2O_8^{2-}$, showing an agreement with the shift of the UV-vis spectrum of $Ru(bpy)_3^{2+}$/APS solution after irradiation as shown in Figure 6.3b.

Table 6.2 Compositions of various solutions.

Solutions	$Ru(bpy)_3^{2+}$	APS	NaA	MBAAm
A	-	10 mM	10 wt%	2 wt% of NaA
B	0.5 mM	10 mM	-	-
C	0.5 mM	10 mM	10 wt%	-
D	0.5 mM	10 mM	10 wt%	2 wt% of NaA

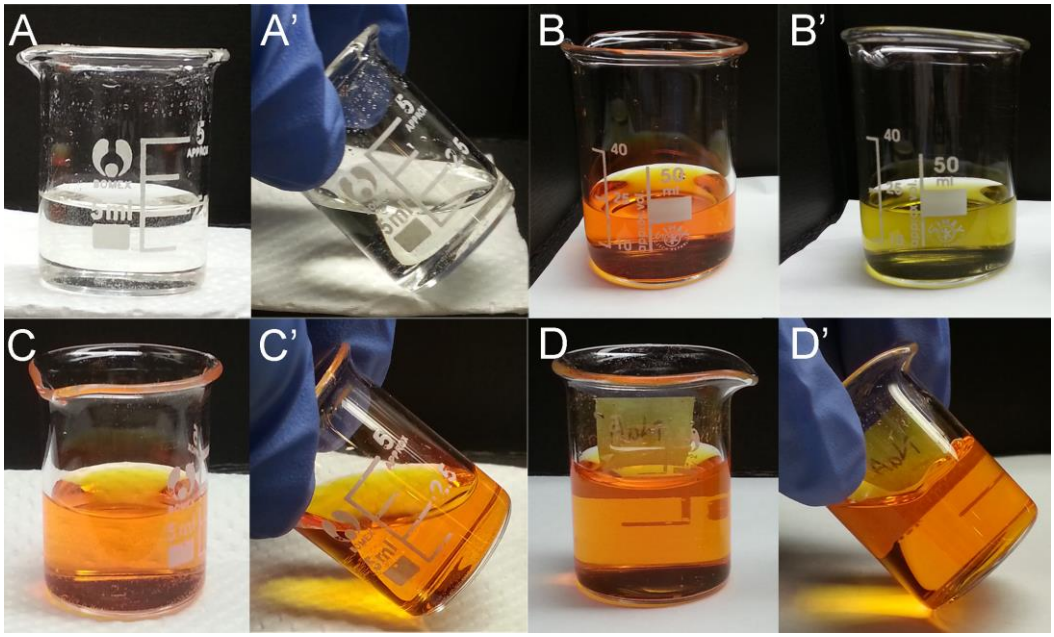

Figure 6.4 Photos of solutions A, B, C, and D, where apostrophe (') indicated that the solution was irradiated for 60 min.

In contrast, when NaA was added to the solutions C and D, they had no color change after irradiation as shown in Figures 6.4C and 6.4D. However, only

solution D with crosslinker MBAAm gelled after irradiation. In the presence of crosslinker, two strong oxidants $Ru(bpy)_3^{3+}$ and $SO_4^{-\bullet}$ generated by irradiation initiate the polymerization to form a solid. Therefore, taking the advantage of photocatalyst, the polymerization can be carried out at room temperature so it can highly save the energy consumption.

6.3.3 Photo-induced crosslinking of silk fibers

The swelling behavior of CS and TrialS in 9.3 M LiBr solution was observed under optical microscope as shown in Figure 6.5. When 9.3 M LiBr was just added to CS, the outer surface of CS swelled immediately in a large extent with irregular shape. Its diameter increased with diameter change of 1.3 (Table 6.3) after immersion for 60 min. After heating, two silk fibroin of CS was softened and merged with each other, and its boundary was hardly seen (Figure 6.5-a3). Since a single silk fiber was mounted and sandwiched in between glass slide and cover lid without shaking, it was kept in position so it did not dissolve totally. Therefore, the residue of CS was still barely observed after heating.

On the other hand, TrialS had no obvious swelling when it was initially immersed in 9.3 M LiBr. Its outer surface gradually swelled with diameter change of 1.7 (Table 6.2) in a confined manner, which can be measured as fiber diameter, after immersion for 60 min. Two silk fibroins were fully swollen and clearly seen even after heating (Figure 6.4-b3). Its fiber shape with defined

boundary was maintained. Under $Ru(bpy)_3^{2+}$/APS system, the two tyrosyl groups of silk are crosslinked preventing it from dissolution in 9.3 M LiBr solution under heating.

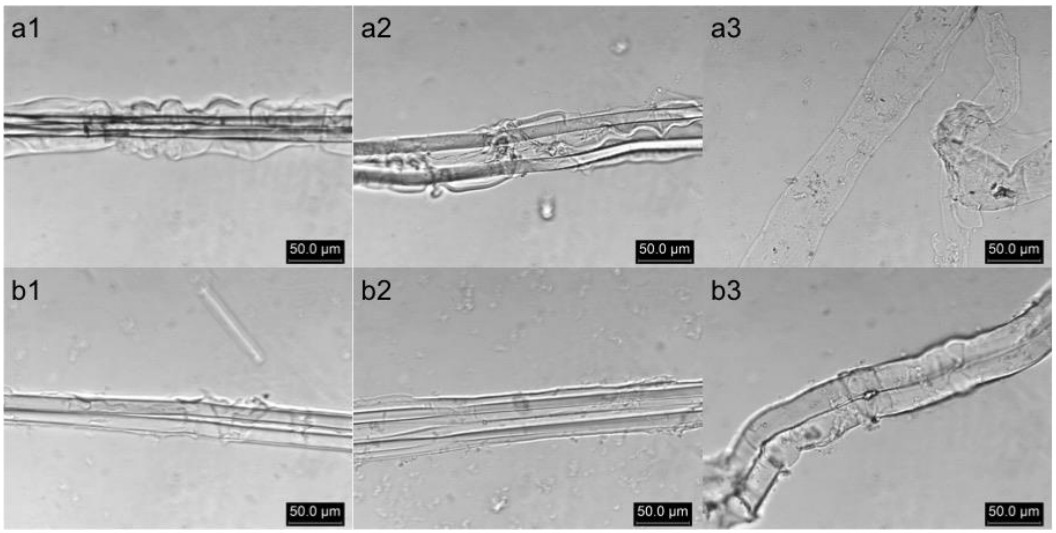

Figure 6.5 Optical microscope images of dissolution in 9.3 M LiBr of (a) CS and (b) TrialS under (1) immersion, (2) after immersion for 60 min, and (3) after heating for 60 min at 65 ℃.

Table 6.3 Diameter change of silk fiber during dissolution in 9.3M LiBr.

Samples	Immersion	After Immersion		After heating	
	Bright [a]	Diameter change (μm/μm)	Bright [a]	Diameter change (μm/μm)	Bright [a]
CS	Yes	1.3	Yes	-	-
TrialS	Yes	1.7	Yes	1.9	No

[a] Bright under polarized light, indicating the molecular orientation and crystallization.

6.3.2.1 Effect of concentration and irradiation time on photo-induced cross-linking

Effect of $Ru(bpy)_3^{2+}$ concentration and irradiation time was investigated by dissolution in 9.3 M LiBr. In order to examine the preliminary strength of silk fiber, the silk sample with 9.3 M LiBr solution was firstly heated at 65 ℃ for 60 min, then immersed in fresh 9.3 M LiBr solution and finally observed under optical microscope as shown in Figure 6.6.

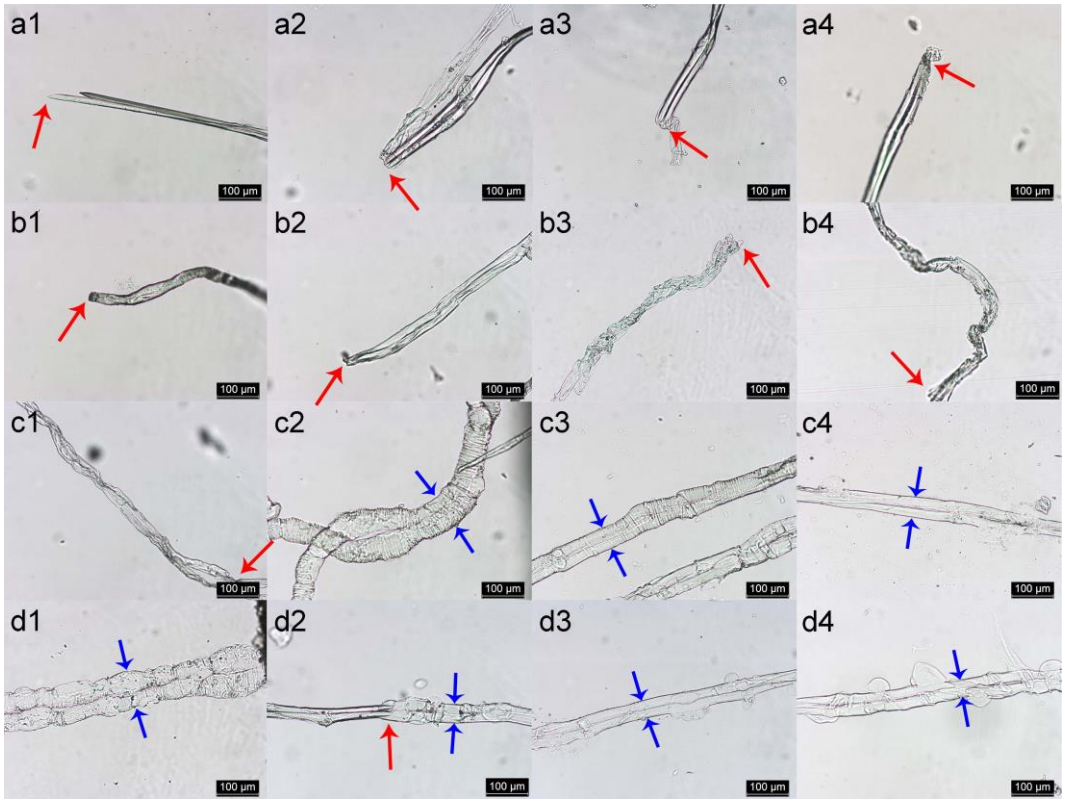

Figure 6.6 Optical microscope images of (a) CS, (b) Ru10, (c) Ru25, and (d) Ru50 under (1) 15 min, (2) 30 min, (3) 60 min, and (4) 90 min irradiation time, where red arrows and blue arrows indicated blue arrows indicated the boundary of dry and wet section, and the silk fiber diameter respectively.

For CS, the wetted part in 9.3 M LiBr dissolved in fresh 9.3 M LiBr and showed a broken end as shown in Figure 6.6a under various irradiation times. It is reasonable that a sharp broken interface between dry and wet section is observed since no crosslinking is formed in the silk fibroin. For the low concentration of 0.10 mM $Ru(bpy)_3^{2+}$, Ru10 also broke in fresh 9.3 M LiBr under various irradiation time. However, its broken end occurred along the swollen fiber with distorted fiber shape as shown in Figure 6.6b. It reveals that the low $Ru(bpy)_3^{2+}$ concentration still show certain degree of crosslinking effect on silk fiber.

As the $Ru(bpy)_3^{2+}$ concentration increased to 0.25 and 0.50 mM, the crosslinking effect become more significant. Ru25 and Ru50 maintained their fiber shape, except the Ru25-15 that was irradiated for 15 min, two silk fibroins were swelled with clear fiber shape as shown in Figures 6.6c and 6.6d. As the irradiation time is longer, the swollen fiber had a relatively smooth fiber surface and smaller fiber diameter. For an example, compared to the smooth and straight fiber shape of Ru25-90, Ru25-30 had more wrinkle and curly fiber shape. The dry and wet sections remained connected even after immersion in fresh 9.3 M LiBr as observed clearly in Figure 6.6-d2. Therefore, microscopic images of silk samples in 9.3 M LiBr solution support the photo-induced crosslinking of silk fibers.

The relationship between the diameter change, and $Ru(bpy)_3^{2+}$ concentration and irradiation time is summarized in Figure 6.7. The diameter change (μm/μm) is calculated by dividing fiber diameter after heating by fiber diameter before immersion. Higher the $Ru(bpy)_3^{2+}$ concentration or longer the irradiation time, the diameter change becomes smaller, owing to the crosslinking density. Since high $Ru(bpy)_3^{2+}$ concentration shortened the irradiation time, 0.5 mM $Ru(bpy)_3^{2+}$ was chosen in the following experiment.

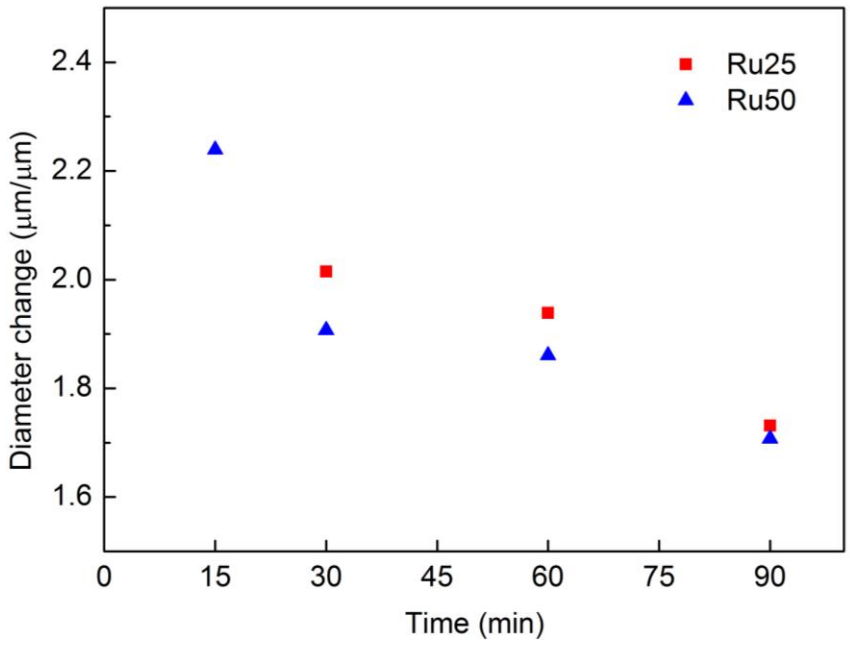

Figure 6.7 Fiber diameter changes of Ru25 and Ru50 at various irradiation times.

6.3.2.2 FTIR analysis

In order to have a deep insight into the crosslinked proteins, CS and Ru50-60 (around 0.005 g) was immersed into 20 g of 9.3 M LiBr solution separately, the solutions were then heated at 65 ℃ and observed their changes for every 5 min. After 30 min, CS totally dissolved in 9.3 M LiBr, while Ru50-60 had some

residue left. The residue of Ru50-60 remained even further heating for 30 min. Finally, it was collected by filtration using polytetrafluoroethylene (PTFE) membrane filter, rinsed thoroughly by DI water and dried at 65 ℃ in the oven till constant weight. The gel fraction of Ru50-60 residue was 51.8%. It was calculated by the following equation:

$$\text{gel fraction} = \frac{\text{dry weight of residue}}{\text{dry weight of original sample}} \times 100\% \qquad \text{(Equation 6.1)}$$

Structural changes of the crosslinked silk fibers were further analyzed by FTIR spectroscope. As shown in Figure 6.8, the FTIR spectra of CS and Ru50-60 were similar, so it was difficult to observe any change after photo-induced crosslinking of silk fiber. However, by dissolution in 9.3 M LiBr, the Ru50-60 residue displayed some noticeable changes in its FTIR spectrum (Figure 6.8c). The absorption regions of 1700–1600 cm^{-1}, 1600–1500 cm^{-1} and 1300–1200 cm^{-1} are assigned to amide I (C=O stretching), amide II (in-plane N-H bending and C-N bending) and amide III (N-H bending and C-N stretching) of the peptide backbones respectively, which have been used for studying the secondary structure of silk [36, 37]. For their secondary structures, CS and Ru50-60 showed the characteristic absorption peaks at 1621 (with shoulder peak at 1698 cm^{-1}), 1513, and 1262 (shoulder peak) cm^{-1} indicating the typical β-sheet (Silk II) structure. In the FTIR spectrum of Ru50-60 residue, these peaks shifted to 1637, 1532, and 1231 cm^{-1}, indicating its α-helix (silk I) structure. Monti and

co-workers reported that other characteristic bands of silk I at about 1410, 1382, and 1334 cm^{-1}, corresponding to δ ($C_\alpha H_2$ in $(AG)_n$), δ (CH_3) and δ_s (CH_3) respectively, were used to discriminate between silk I and random structure [38].

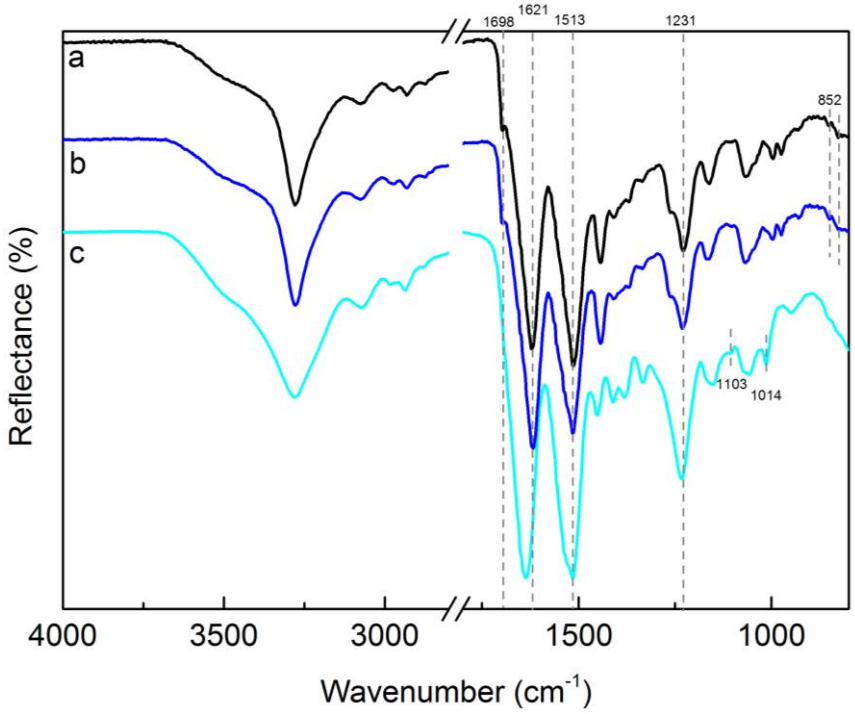

Figure 6.8 FTIR spectra of (a) CS, (b) Ru50-60, and (c) Ru50-60 residue.

By this dissolution technique, the changes in their primary structures can be noticed obviously. The peaks at 852 and 826 cm^{-1} ascribing to benzene ring bending of Tyr disappeared in FTIR spectrum of Ru50-60 residue [39]. It is probably due to the formation of di-tyrosine linkage that inhibits the bending of two phenol groups [22] and hence the absorption peak disappears. After dissolution in 9.3 M LiBr, some uncrosslinked proteins dissolved and crosslinked proteins remained. Therefore, their characteristic absorption peaks were noticeable, especially Tyr. The characteristic peaks of Tyr at 1014 and 1103

cm^{-1}, corresponding to r (CH_2) and δ ($C_{ring}H$) of Tyr [40, 41], became more intense. To conclude, dissolution test and FTIR spectrum of Ru50-60 residue support the formation of di-tyrosine linkage in silk fiber via light irradiation of the $Ru(bpy)_3^{2+}$/APS solution.

6.3.2.3 Mechanical properties of crosslinked silk fibers

The mechanical properties of various silk fibers were measured as shown in Figure 6.9. The breaking strain of Ru10 increased by 28% and 22% after irradiation for 15 min and 30 min respectively. After irradiation for a longer time 90 min, its breaking stress increased by 16%. In general, low concentration of $Ru(bpy)_3^{2+}$ slightly affects the mechanical properties of silk fiber. As the concentration of $Ru(bpy)_3^{2+}$ increased to 0.25 mM, the breaking stress and strain of Ru25 improved slightly after irradiated for 15 min by 11% and 8% respectively. As irradiation time increased to 90 min, its break and strain gradually decreased by 29% and 46% than that of CS. Silk fiber becomes tougher and less extensible after irradiation for a long time. It is probably due to the di-tyrosine linkage lowers the flexibility of silk fibroin protein chains. When the concentration of $Ru(bpy)_3^{2+}$ increased even higher to 0.50 mM, the effect of di-tyrosine linkage on mechanical properties was remarkable. The breaking stress and strain of Ru50 increased slightly by 22% and 8% respectively after 15 min irradiation. However, when the irradiation time increased to 60 and 90 min,

its strain at break dramatically decreased by 23% and 36%, but its strain at break increased by 13% and 25% respectively. Higher concentration and longer irradiation time lead to higher stiffness and lower extensibility, owing to the crosslinking of silk fibers. Hence, it limits the immobility of protein chains when being stretched.

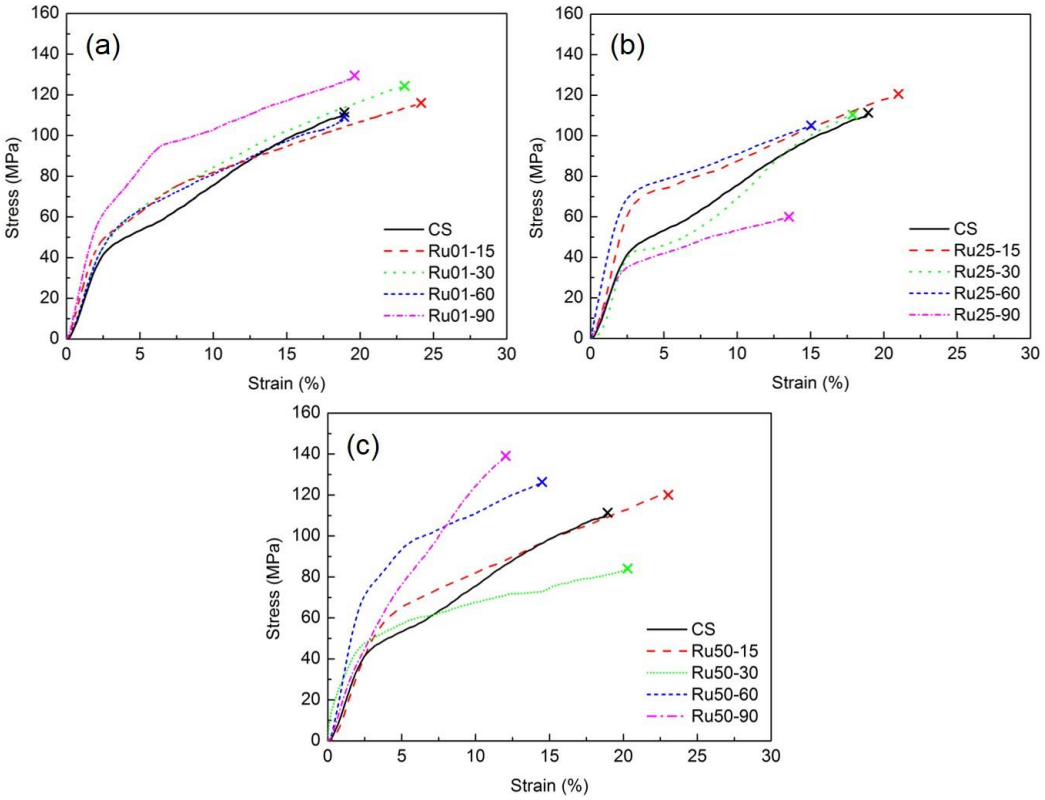

Figure 6.9 Typical stress-strain curves of (a) Ru10, (b) Ru25, and (c) Ru50 under various irradiation times.

6.4 Summary

In this chapter, the $Ru(bpy)_3^{2+}$/APS system was investigated and monitored by the UV-vis spectroscopy. It also revealed the possibility of regenerating the photocatalyst $Ru(bpy)_3^{2+}$. This $Ru(bpy)_3^{2+}$/APS photo-induced system was able

to crosslink the silk fiber and initiate the NaA polymerization. The crosslinked silk fiber maintained their fiber shape in 9.3 M LiBr as observed clearly under optical microscope. The defined fiber shape was optically measured in 0.25 mM and 0.50 mM $Ru(bpy)_3^{2+}$ solution with long enough irradiation time. The residue of the crosslinked silk fiber from dissolution in 9.3 M LiBr was analyzed by FTIR spectroscope that further confirmed the existence of di-tyrosine linkage. The mechanical property of crosslinked silk was also influenced by the $Ru(bpy)_3^{2+}$ concentration and irradiation time. This environmental friendly $Ru(bpy)_3^{2+}$/APS photocatalyst system promisingly initiated the photo-induced crosslink of silk fibers as well as initiated the polymerization of NaA.

References

[1] Kaplan, D. L. Silk. In *Encyclopedia of polymer science and technology*, 4th ed.; Chichester: Wiley-Blackwell, 2014.

[2] Asakura, T.; Sugino R.; Yao J.; Takashima, H.; Kishore, R. Comparative Structure Analysis of Tyrosine and Valine Residues in Unprocessed Silk Fibroin (Silk I) and in the Processed Silk Fiber (Silk II) from *Bombyx mori* using Solid-State ^{13}C,^{15}N, and ^{2}H NMR. *Biochemistry* **2002**, 41, 4415-4424.

[3] Ayub, Z. H.; Arai, M.; Hirabayashi, K. Mechanism of the gelation of fibroin solution. *Biosci. Biotech. Biochem.* **1993**, 57, 1910-1912.

[4] Hu, X.; Lu, Q.; Sun, L.; Cebe, P.; Wang, X.; Zhang, X.; Kaplan, D. L. Biomaterials from Ultrasonication-Induced Silk Fibroin−Hyaluronic Acid Hydrogels. *Biomacromolecules* **2010**, 11, 3718-3188.

[5] Kojic, N.; Panzer, M. J.; Leisk, G. G.; Raja, W. K.; Kojic, M.; Kaplan, D. L. Ion electrodiffusion governs silk electrogelation. *Soft Matter* **2012**, 8, 6897-6905.

[6] Matsumoto, A.; Chen, J.; Collette, A. L.; Kim, U. J.; Altman, G. H.; Cebe, P.; Kaplan, D. L. Mechanisms of silk fibroin sol-gel transitions. *J. Phys. Chem. B* **2006**, 110, 21630-21638.

[7] Chen, X.; Li, W.; Zhong, W.; Lu, Y.; Yu, T. pH sensitivity and ion sensitivity of hydrogels based on complex-forming chitosan-silk fibroin interpenetrating polymer network. *J. Appl. Polym. Sci.* **1997**, 65, 2257-2262.

[8] Kang, G. D.; Lee, K. H.; Ki, C. S.; Nahm, J. H.; Park, Y. H. Silk Fibroin/Chitosan Conjugate Crosslinked by Tyrosinase. *Macromol. Res.* **2004**, 12, 534-539.

[9] Vasconcelos, A.; Gomes, A. C.; Cavaco-Paulo, A. Novel silk fibroin/elastin wound dressings. *Acta Biomater.* **2012**, 8, 3049-3060.

[10] Silva, S. S.; Maniglio, D.; Motta, A.; Mano, J. F.; Reis, R. L.; Migliaresi, C. Genipin-modified silk-fibroin nanometric nets. *Macromol. Biosci.* **2008**, 8, 766-774.

[11] Kang, G. D.; Lee, K. H.; Ki, C. S.; Park, Y. H. Crosslinking Reaction of Phenolic Side Chains in Silk Fibroin by Tyrosinase. *Fibers Polym.* **2004**, 204, 5, 234-238.

[12] Ciamician, G. The Photochemistry of the Future. *Science* **1912**, 36, 385-394.

[13] Hoffmann, N. Photochemical reactions as key steps in organic synthesis. *Chem. Rev.* **2008**, 108, 1052-1103.

[14] Xuan, J.; Xiao, W. J. Visible-Light Photoredox Catalysis. *Angew. Chem. Int. Ed.* **2012**, 51, 6828-6838.

[15] Prier, C. K.; Rankic, D. A.; MacMillan, D. W. C. Visible Light Photoredox Catalysis with Transition Metal Complexes: Applications in Organic Synthesis. *Chem. Rev.* **2013**, 113, 5322-5363.

[16] Schultz, D. M.; Yoon, T. P. Solar Synthesis: Prospects in Visible Light Photocatalysis. *Science* **2014**, 343,985-993.

[17] Narayanam, J. M. R.; Stephenson, C. R. J. Visible light photoredox catalysis- applications in organic synthesis. *Chem. Soc. Rev.* **2011**, 40, 102-113.

[18] Fancy, D. A.; Kodadek, T. Chemistry for the analysis of protein-protein interactions- rapid and efficient cross-linking triggered by long wavelength light. *Proc. Natl. Acad. Sci. USA* **1999**, 96, 6020-6024.

[19] Fancy, D. A; Denison, C.; Kim, Y.; Xie, Y.; Holdeman, T.; Amini, F.; Kodadek, T. Scope, limitations and mechanistic aspects of the photo-induced cross-linking of proteins by water-soluble metal complexes. *Chem. Biol.* **2000**, 7, 697-708.

[20] Truong, M. Y.; Dutta, N. K.; Choudhury, N. R.; Kim, M.; Elvin, C. M.; Nairn, K. M.; Hill, A. J. The effect of hydration on molecular chain mobility and the viscoelastic behavior of resilin-mimetic protein-based hydrogels. *Biomaterials* **2011**, 32, 8462-8473.

[21] Schacht, K.; Scheibel, T. Controlled Hydrogel Formation of a Recombinant Spider Silk Protein. *Biomacromolecules* **2011**, 12, 2488-2495.

[22] Whittaker, J. L.; Choudhury, N. R., Dutta, N. K.; Zannettino, A. Facile and rapid ruthenium mediated photo-crosslinking of *Bombyx mori* silk fibroin. *J. Mater. Chem. B* **2014**, 2, 6259-6270.

[23] Minisci, F.; Citterio, A. Electron-transfer processes: peroxydisulfate, a useful and versatile reagent in organic chemistry. *Acc. Chem. Res.* **1983**, 16, 27-32.

[24] White, H. S.; Bard, A. J. Electrogenerated chemiluminescence 41 Electrogenerated chemiluminescence and chemiluminescence of the Ru(2,21- bpy)$_3^{2+}$-$S_2O_8^{2-}$system. *J. Am. Chem. Soc.* **1982**, 104, 6891-6895.

[25] Nishida, S.; Kimura, M. Light-induced electron-transfer reactions. 5. Kinetics of the oxidation of ethylenediaminetetraacetatocobaltate(II) complexes by peroxodisulfate ion, induced by irradiation with visible light of aqueous solutions containing Tri(2, 2'-bipyridine)ruthenium(II) ion. *Bull. Chem. Soc. Jpn.* **1987**, 60, 2367-2372.

[26] Bolletta, F.; Ciano, M.; Balzani, V.; Serpone, N. Polypyridine transition metal complexes as light emission sensitizers in the electrochemical reduction of the persulfate ion. *Inorg. Chim. Acta* **1982**, 62, 207-213.

[27] Nickel, U.; Chen, Y. H.; Schneider, S.; Silva, M. I.; Burrows, H. D.; Formosonho, J. Mechanism and Kinetics of the Photocatalyzed Oxidation of p-Phenylenediamines by Peroxydisulfate in the Presence of Tri-2,2'-bipyridylylruthenium(II). *J. Phys. Chem.* **1994**, 98, 2883-2888.

[28] Bosio, G.; Criado, s.; Massad, W.; Nieto, F. J. R.; Gonzalez, M. C.; García, N. A.; Mártire, D. O. Kinetics of the interaction of sulfate and hydrogen phosphate radicals with small peptides of glycine, alanine, tyrosine and tryptophan. *Photochem. Photobiol. Sci.* **2005**, 4, 840-846.

[29] Gau, B. C.; Chen, H.; Zhang, Y.; Gross, M. L. Sulfate Radical Anion as a New Reagent for Fast Photochemical Oxidation of Proteins. *Anal. Chem.* **2010**, 82, 7821-7827.

[30] Herman, L.; Ghosh, S.; Defrancq, E.; Mesmaeker, A. K. D. Ru(II) complexes and light: molecular tools for biomolecules. *J. Phys. Org. Chem.* **2008**, 21, 670-681.

[31] Pattison, D. I.; Rahmanto, A. S.; Davies, M. J. Photo-oxidation of proteins. *Photochem. Photobiol. Sci.* **2012**, 11, 38-53.

[32] Elvin, C. M.; Vuocolo, T.; Brownlee, A. G.; Sando, L.; Huson, M. G.; Liyou, N. E.; Stockwell, P. R.; Lyons, R. E.; Kim, M.; Edwards, G. A.; Johnson G.; McFarland, G. A.; Ramshae, J. A. M.; Werkmeister, J. A. A highly elastic tissue sealant based on photopolymerised gelatin. *Biomaterials* **2010**, 31, 8323-8331.

[33] Lee, K. W.; Slinker, J. D.; Gorodetsky, A. A.; Flores-Torres, S.; Abruña, H. D.; Houston, P. L., Malliaras, G. G. Photophysical properties of tris(bipyridyl)ruthenium(II) thin films and devices. *Phys. Chem. Chem. Phys.* **2003**, 5, 2706-2709.

[34] Kalyanasundaram, K. Photophysics, photochemistry and solar energy conversion with tris(bipyridyl)ruthenium(II) and its analogues. *Coord. Chem. Rev.* **1982**, 159-244.

[35] Al Lawati, H. A. J.; Al Dahmani, Z. M.; Varma, G. B.; Suliman, F. O. Photoinduced oxidation of a tris(2,2'-bipyridyl)ruthenium(II)–peroxodisulfate chemiluminescence system for the analysis of mebeverine HCL pharmaceutical formulations and biological fluids using a two-chip device. *Luminescence* **2014**, 29, 275-283.

[36] Koperska, M. A.; Pawcenis, D.; Bagniuk, J.; Zaitz, M. M.; Missori, M., Łojewski, T.; Łojewski, T. Degradation markers of fibroin in silk through infrared spectroscopy. *Polym. Degrad. Stabil.* **2014**, 105, 185-196.

[37] Mandal, B. B.; Kapoor, S.; Kundu, S. C. Silk fibroin/polyacrylamide semi-interpenetrating network hydrogels for controlled drug release. *Biomaterials* **2009**, 30, 2826-2836.

[38] Monti, P.; Taddei, P.; Freddi, G.; Ohgo, K.; Asakura, T. Vibrational ^{13}C-cross-polarization-magic angle spinning NMR spectroscopic and thermal characterization of poly(alanine-glycine) as model for silk I *Bombyx mori* fibroin. *Biopolymers (Biospectroscopy)* **2003**, 72, 329-338.

[39] Sampaio, S.; Taddei, P.; Monti, P.; Buchert, J.; Freddi, G. Enzymatic grafting of chitosan onto Bombyx mori silk fibroin- kinetic and IR vibrational studies. *J. Biotechnol.* **2005**, 116, 21-33.

[40] Boulet-Audet M.; Lefèvre, T.; Buffeteau, T.; Pézolet. M. Attenuated total reflection infrared spectroscopy-an efficient technique to quantitatively determine the orientation and conformation of proteins in single silk fibers. *Appl. Spectrosc.* **2008**, 62, 956-962.

[41] Wolpert, M.; Hellwig, P. Infrared spectra and molar absorption coefficients of the 20 alpha amino acids in aqueous solutions in the spectral range from 1800 to 500 cm^{-1}. *Spectrochim. Acta A* **2006**, 64, 987-1001.

Chapter 7
Photo-induced crosslinking and sodium acrylate polymerization on silk fiber

7.1 Introduction

Modification of silk fiber by graft polymerization is a common method to improve the performance of silk. Many vinyl monomers like acrylamide [1], vinyltrimethoxysilane [2], phosphoamide [3], methylmethacrylate [4], and acrylonitrile [5] have been extensively studied to be grafted onto the silk fiber so as to improve its properties such as thermal stability, crease recovery, and resistance to bacteria. However, the water absorption performance of silk after modification remains poor. For example, graft polymerization of methyl methacrylate on silk fiber diminished its water retention value from 3.8 g/g (ungrafted) to 1.82 g/g (grafted) [6]. In order to enhance the water absorption performance of silk fiber, sodium acrylate monomer, which is well-known as the main component in superabsorbent polymers, is used in this study. Improvement in water absorbency of silk fiber or fabric can widen its applications in biomedical textiles, such as wound dressings and sutures. For example, high absorbency can prevent the accumulation of exudates at the wound area and keep the wound at optimal microenvironment for cell proliferation, migration, and differentiation.

In previous chapter, the $Ru(bpy)_3^{2+}$/APS system successfully induces the crosslinking of silk fiber as well as initiates the polymerization of NaA under mild and environmentally friendly conditions. An abundant and renewable light source is required to trigger those reactions at room temperature. In this chapter, various methods were applied to crosslink the silk fiber and incorporate the sodium acrylate onto its surface simultaneously. Dissolution of silk samples in 9.3 M LiBr and swelling of samples in DI water were observed under optical microscope. The silk samples were characterized by Fourier transform infrared (FTIR) spectroscope and thermogravimetric analyzer (TGA). Their surface morphology was observed under scanning electron microscope (SEM). The water absorption performance was measured by gravimetric method (bulk absorption) and thermogravimetric analyzer (single fiber absorption).

7.2 Experimental

7.2.1 Materials

Bombyx Mori silk cocoon was purchased from Aurora Silk (USA). Sodium acrylate (NaA), *N,N'*-methylene bisacrylamide (MBAAm), tris(2,2′-bipyridyl)dichlororuthenium(II) hexahydrate ($Ru(bpy)_3^{2+}$), ammonium persulfate (APS), and formic acid were all purchased from Sigma-Aldrich Co. and used without further purification.

7.2.2 Crosslinking and polymerization on silk fibers

7.2.2.1 One-step method

Control silk fiber (denoted as CS) was treated in DI water throughout the whole process. Silk fiber was immersed in the solution of 10 wt% NaA, 0.5 mM $Ru(bpy)_3^{2+}$ as catalyst and 10 mM APS as electron acceptor in DI water, and irradiated directly to a 2200 Lux fluorescent light tube (Maxlite, 25W High Lumen, T8, 5000K) with diffuser for 60 min at a fixed distance of 57.0 cm. The resulted silk fiber was then rinsed by DI water to remove residues and dried at 65 ℃ in the oven till constant weight. This sample was denoted as S-1.

7.2.2.2 Drying method

Silk fibers were immersed in 0.5 mM $Ru(bpy)_3^{2+}$ and 10 mM APS in DI water for 60 min preventing exposure to light. Treated silk fibers were used as macro-initiators. For method A, the excess solution on silk was removed by tissue paper. The silk fiber was then immersed in 10 wt% NaA and 2 wt% (of NaA) MBAAm in DI water under irradiation for 60 min. For method B, the excess solution on silk was air-dried in the darkness for 24 h. The silk fiber was then immersed in 10 wt% NaA and 2 wt% (of NaA) MBAAm in DI water under irradiation for 60 min. Finally, the resulted silk fibers were rinsed by DI water to remove residues and dried at 65 ℃ in the oven till constant weight. The samples prepared by method A and B was denoted as S-A and S-B respectively.

7.2.2.3 Swelling method

Silk fiber was swelled during immersion. Silk fiber was immersed in 0.5 mM $Ru(bpy)_3^{2+}$, 10 mM APS, 10 wt% NaA, and 2 wt% (of NaA) MBAAm in DI water or formic acid (pH 1.9) for 60 min in the darkness at room temperature. The wet samples were taken out and irradiated under light for 60 min at room temperature. Then, the resulted silk fibers were rinsed by DI water to remove residues and dried at 65 ℃ in the oven till constant weight. The samples prepared in DI water and formic acid were denoted as S-DI and S-FA respectively.

7.2.3 Dissolution of silk fiber in 9.3 M LiBr

Samples were sandwiched between cover slide and glass slide. LiBr solution of 9.3 M was added to the samples for 60 min at room temperature and then heated in the oven for 60 min at 65 ℃. The sample was observed under optical microscope (OM, Nikon OPTIPHOT-POL) equipped with polarizers. The fiber diameter change (μm/μm) was calculated by

$$\text{Diameter change (μm/μm)} = \frac{\text{Fiber diameter after immersion/heating (μm)}}{\text{Fiber diameter before immersion (μm)}}$$

averaged from 5 measurements.

7.2.4 Characterizations

FTIR spectra of silk samples were collected by attenuated total reflection Fourier

transform infrared (ATR-FTIR) spectroscope (PerkinElmer Spectrum 100) in reflectance mode in a spectral region of 4000–650 cm^{-1} with 16 scans at of 4 cm^{-1} resolution.

Thermal behaviors of samples were measured by thermogravimetric analyzer (TGA, Mettler Toledo TGA 1). The sample mass was maintained at around 5 mg. The temperature range was from 30–700 ℃ at a heating rate of 10 ℃/min under static air atmosphere (50 ml/min).

To examine the surface morphology of samples, they were fully swollen in DI water, freeze-dried (Christ Alpha 1-4LD), and then observed under a field emission scanning electron microscope (FE-SEM, JEOL JSM-6490) operating at 20 kV after gold sputtering.

7.2.5 Water absorption

To observe the swelling of silk samples in DI water, optical microscope (OM, Nikon OPTIPHOT-POL) equipped with polarizers was used. The optical microscopic images were taken at dry state, 15, 30, 30, and 60 s after adding DI water. The fiber diameter change (μm/μm) was calculated by

$$\text{Diameter change } (\mu m/\mu m) = \frac{\text{Fiber diameter of swollen sample } (\mu m)}{\text{Fiber diameter of dry sample } (\mu m)}$$

averaged from 5 measurements.

To measure the water absorption in bulk, the samples were immersed in DI water until equilibrium weight was achieved. The swollen silk fibers were then

centrifuged at 1000 revolutions per min for 1 min to remove free water in between each single fiber. The water absorption ratio (Q) was calculated by

$$Q\,(\mathrm{g/g}) = \frac{W_d - W_w}{W_w} \qquad \text{(Equation 7.1)}$$

where W_d is the weight of dry sample (g), and W_w is the weight of wet sample (g).

To measure the water absorption of single fiber, the samples were immersed in DI water for 24 h. The swollen silk fibers were centrifuged at 500 revolutions per min for 1 min to remove free water. Each single silk fiber was taken out one by one to further eliminate the water trapped between adjacent fibers. The swollen silk samples (around 5 mg) was measured by thermogravimetric analyzer (TGA, Mettler Toledo TGA 1) with temperature range of 30–120 ℃ at 10 ℃/min and then hold at 120 ℃ for 30 min under air atmosphere with flow rate of 50 ml/min.

7.3 Results and discussion

7.3.1 One-step method

In this one-step method, the silk fiber denoted as S-1 was immersed in the NaA/$Ru(bpy)_3^{2+}$/APS solution and then underwent direct irradiation. Its dissolution behavior in 9.3 M LiBr solution was observed under optical microscope as shown in Figure 7.1. Comparing to the CS and TrialS, S-1 showed

different dissolution behavior. TrialS was the silk fibers treated by $Ru(bpy)_3^{2+}$/APS solution and swelled regularly in 9.3 M LiBr. On the contrary, CS swelled irregularly in a large extent. S-1 swelled like the combination of CS and TrialS. After heating, the two silk fibroin of S-A were clearly seen. Referring to Table 7.1, the fiber surface of S-1 swelled dramatically with fiber diameter change of 2.1, which was higher than that of CS and TrialS. It retained crystalline structure after immersion but totally lost its crystallinity after heating as indicated by the brightness under polarized light. Therefore, it can be seen that the photo-induced crosslinking of silk fibers is not strongly affected by NaA monomers.

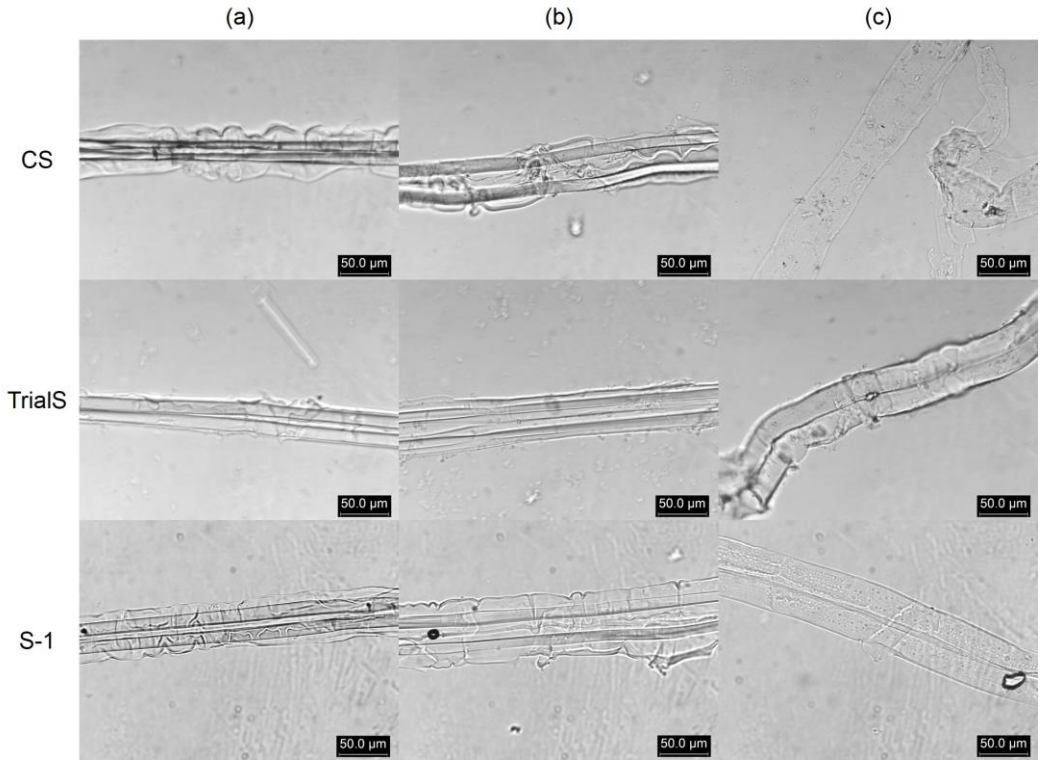

Figure 7.1 Optical images of dissolution in 9.3 M LiBr of silk samples under (a) immersion, (b) after immersion for 60 min, and (c) after heating for 60 min at 65 ℃.

Table 7.1 Fiber diameter change of dissolution of silk fiber in 9.3 M LiBr.

Samples	Immersion		After Immersion		After heating
	Brightness [a]	Diameter change	Brightness [a]	Diameter change	Brightness [a]
CS	Yes	1.3	Yes		-
TrialS	Yes	1.7	Yes	1.9	No
S-1	Yes	2.1	Yes	2.1	No

[a] Brightness under polarized light, indicating the molecular orientation and crystallization.

In order to further observe the swelling property of a single silk fiber in DI water, it was sandwiched in between coverlid and glass slide. The microscopic images were taken at fixed intervals after a few drop of DI water was added. As shown in Figure 7.2, when water was added to CS, no obvious swelling was observed with diameter change of 1.0 after immersion for 60 s as shown in Table 7.2. In contrast, the fiber diameter of S-1 showed noticeable increment as shown in Figure 7.3. Its diameter change after swelling for 60 s was 1.2 (Table 7.2). However, no crosslinker was added in this sample so the synthetic NaA polymer in the silk fiber might be soluble in water.

Table 7.2 Diameter changes of CS and S-1 after swelling in DI water for 60 s.

Samples	Dry (μm)	After 60 s (μm)	Diameter change (μm/μm)
CS	12.8 ± 1.6	13.0 ± 1.0	1.0
S-1	16.4 ± 0.9	19.9 ± 0.6	1.2

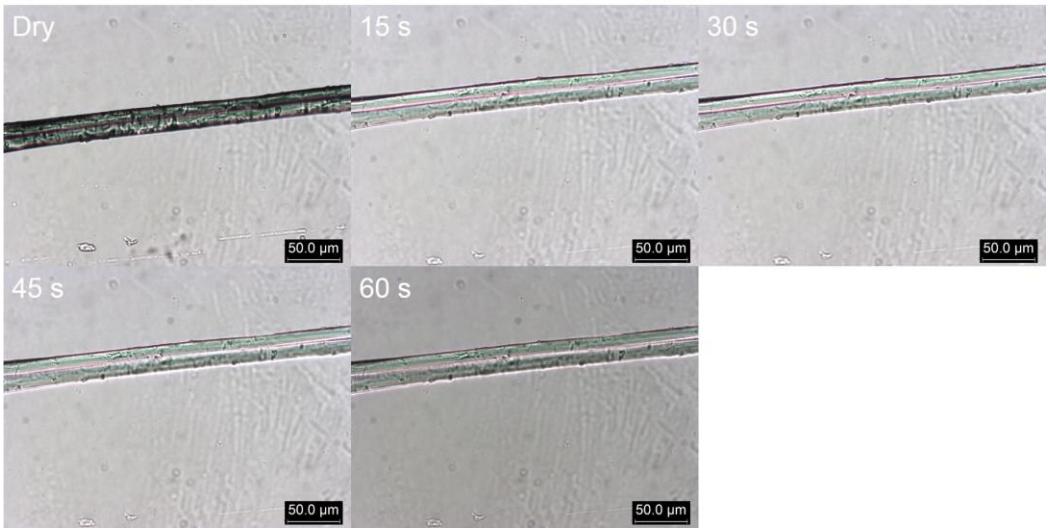

Figure 7.2 Optical images of CS swelling in DI water at various times.

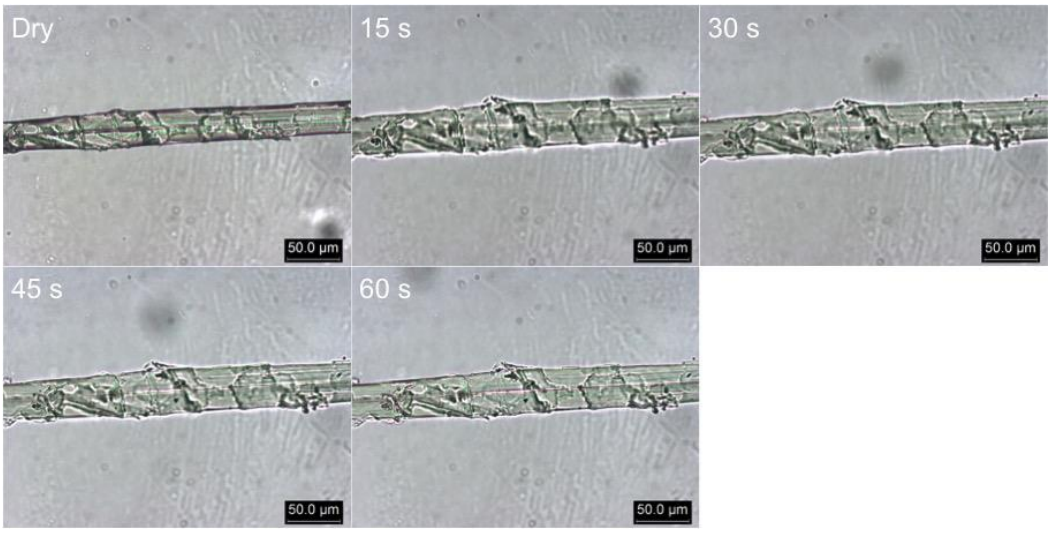

Figure 7.3 Optical images of S-1 swelling in DI water at various times.

7.3.2 Drying method

In this drying method, the silk fiber was immersed in $Ru(bpy)_3^{2+}$/APS solution to activate its surface as the macro-initiator for further photo-induced crosslinking and polymerization. Dissolution of silk samples S-A and S-B in 9.3 M LiBr was observed under optical microscope as seen in Figure 7.4. When the 9.3 M LiBr was added, these samples swelled in a similar behavior as TrialS that swelled

slightly with smooth surface. Both of them swelled with defined boundary after immersion for 60 min and their two silk fibroins were clearly seen after heating. Some creases were observed in the sample S-B. By dissolution in 9.3 M LiBr, the microscopic images support the crosslinking of silk fibers prepared by drying method.

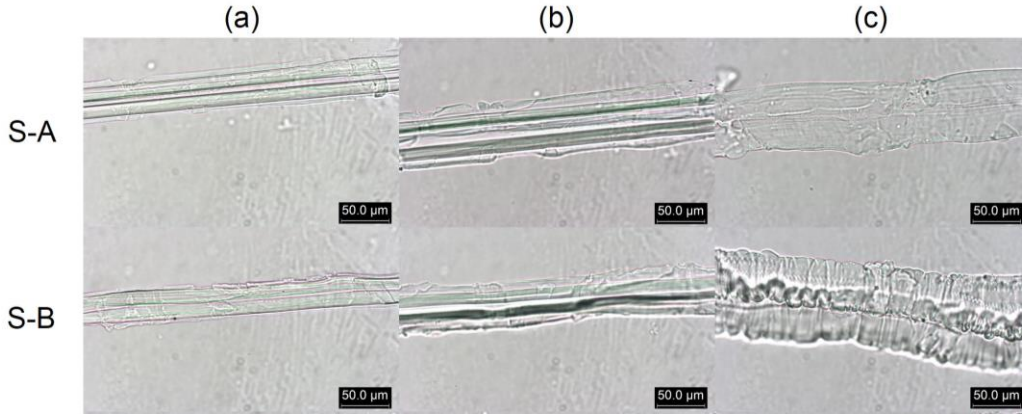

Figure 7.4 Optical images of dissolution in 9.3 M LiBr of S-A and S-B, at (a) immersion, (b) after immersion for 60 min, and (c) after heating for 60 min at 65 ℃.

Furthermore, when S-A and S-B were immersed in DI water, their diameter changes were more obvious than S-1 as shown in Figures 7.5 and 7.6. When the water was added to the S-A and S-B, their fiber diameters increased spontaneously at the first 15 s and remained similar afterward. As shown in Table 7.3, the diameter changes of S-A and S-B were 1.4 and 1.6 that were higher than that of S-1.

Table 7.3 Diameter changes of S-A and S-B swelling in DI water for 60s.

Samples	Dry (μm)	After 60 s (μm)	Diameter change (μm/μm)
S-A	15.6 ± 0.5	21.0 ± 0.5	1.4
S-B	12.9 ± 1.3	21.2 ± 0.6	1.6

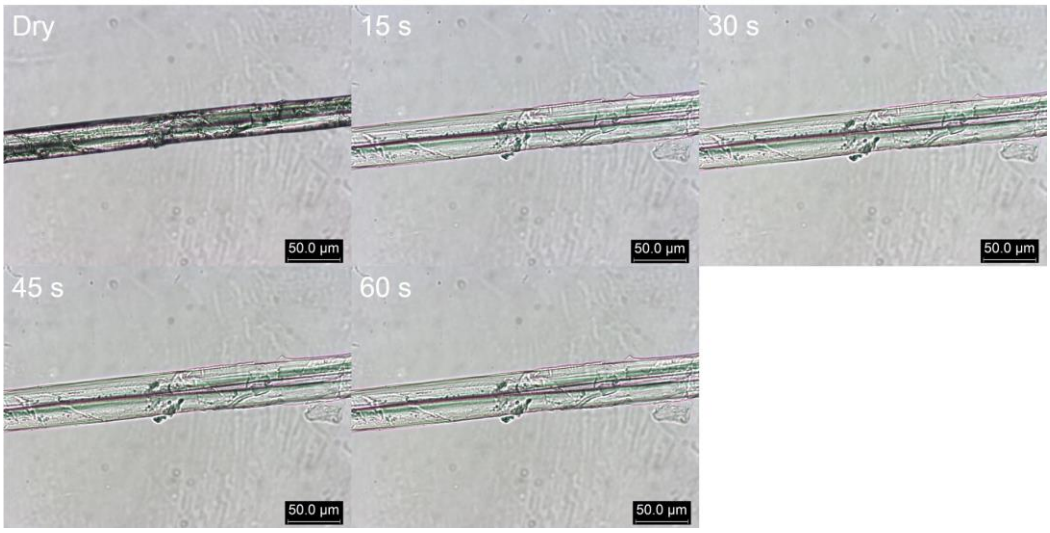

Figure 7.5 Optical images of S-A swelling in DI water at various times.

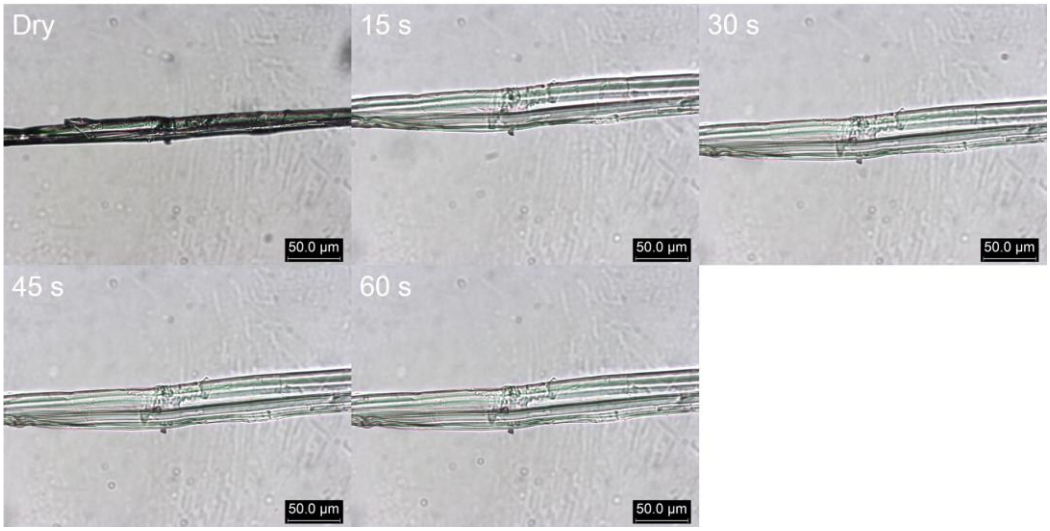

Figure 7.6 Optical images of S-B swelling in DI water at various times.

7.3.3 Swelling method

In this swelling method, the silk fiber was firstly swelled in DI water or formic

acid solution (pH 1.9) and then irradiated for 60 min. When the swollen sample was irradiated, the photo-induced crosslinking and polymerization occurred simultaneously. The dissolution of S-DI and S-FA in 9.3 M LiBr was observed under optical microscope as shown in Figure 7.7. When 9.3 M LiBr was added, both of them swelled slightly with irregular shape. They gradually swelled in a confined fiber shape and two distinct silk fibroins were seen after heating. However, S-FA showed some fragments along the fiber, owing to the degradation of silk protein in the highly acidic formic acid solution during immersion [7].

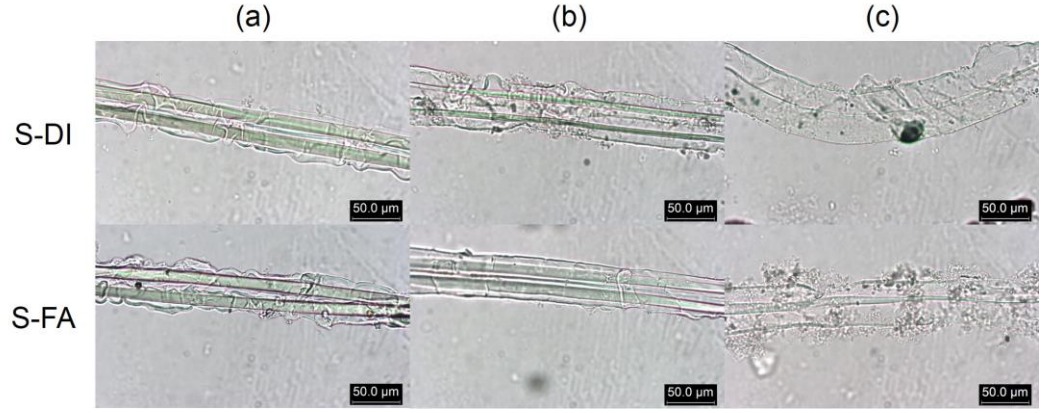

Figure 7.7 Optical images of dissolution in 9.3 M LiBr of S-DI and S-FA, at (a) immersion, (b) after immersion for 60 min, and (c) after heating for 60 min at 65 ℃.

In addition, when S-DI and S-FA were immersed in DI water, their diameter changes were less obvious than S-A and S-B as shown in Figures 7.8 and 7.9. When the water was added to the samples, their fiber diameters increased spontaneously at the first 15 s and remained similar afterward. As

shown in Table 7.4, the diameter changes of S-DI and S-FA were 1.4 and 1.3 respectively, which were lower than that of S-A and S-B.

Table 7.4 Diameter changes of S-A and S-B swelling in DI water for 60s.

Samples	Dry (μm)	After 60 s (μm)	Diameter change (μm/μm)
S-DI	12.4 ± 0.4	17.8 ± 0.5	1.4
S-FA	14.4 ± 1.1	18.0 ± 1.4	1.3

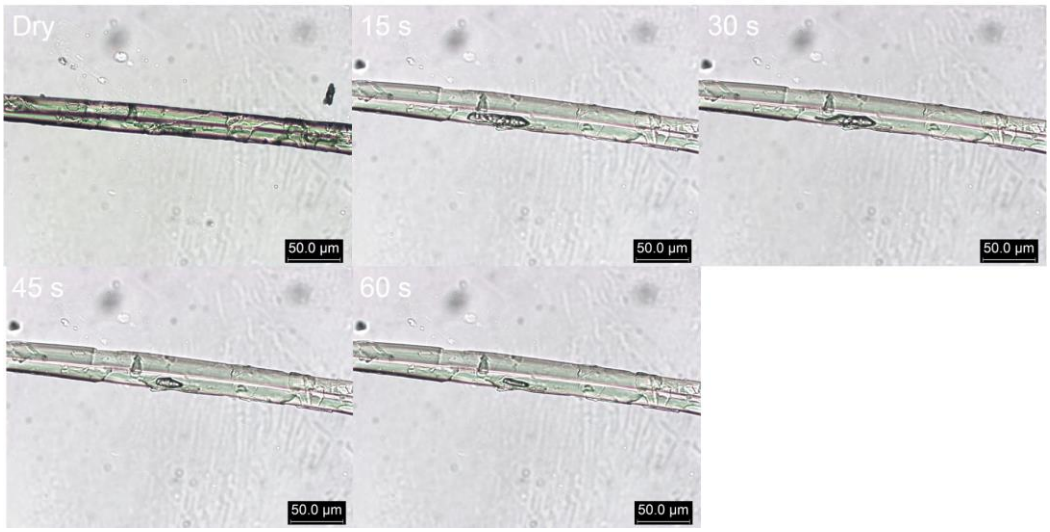

Figure 7.8 Optical images of S-DI swelling in DI water at various times.

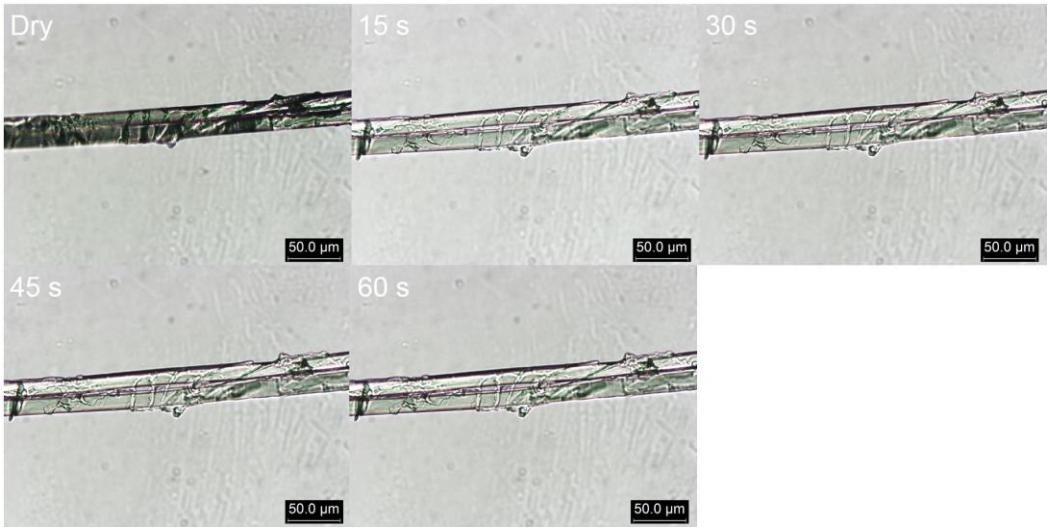

Figure 7.9 Optical images of S-FA swelling in DI water at various times.

7.3.4 Characterizations

7.3.4.1 FTIR analysis

Figure 7.10 showed the FTIR spectra of various silk fiber samples. For comparison, all FTIR spectra were normalized at 3275 cm^{-1}. The characteristic absorption peaks of poly(sodium acrylate) are at 1554, 1404, and 1453 cm^{-1}, corresponding to asymmetric and symmetric stretching of carboxylate ion (COO^-), and bending of CH_2 respectively [8, 9]. These peaks overlapped with the characteristic absorption peak of silk at 1515, 1440, and 1410 cm^{-1}, ascribing to N-H deformation and C-N stretching, CH_2 bending, and $C_\alpha H_2$ wagging of silk protein polymer chains respectively [10, 11]. However, by normalizing the spectra at 3275 cm^{-1} peak, the increment in peak intensity at 1404 cm^{-1} was clearly observed in the silk samples, especially S-A, S-B, and S-DI. This peak also slightly shifted from 1410 to 1404 cm^{-1}. Their relative peak intensity of 1440 cm^{-1} to 1404 cm^{-1} became closer, especially the S-A, S-B, and S-DI. This FTIR results are consistent with the fiber diameter change by swelling in DI water. Among all samples, S-FA showed the least swelling degree in DI water as observed under optical microscope. Therefore, these FTIR spectra suggest the presence of poly(sodium acrylate) on the silk fiber surface.

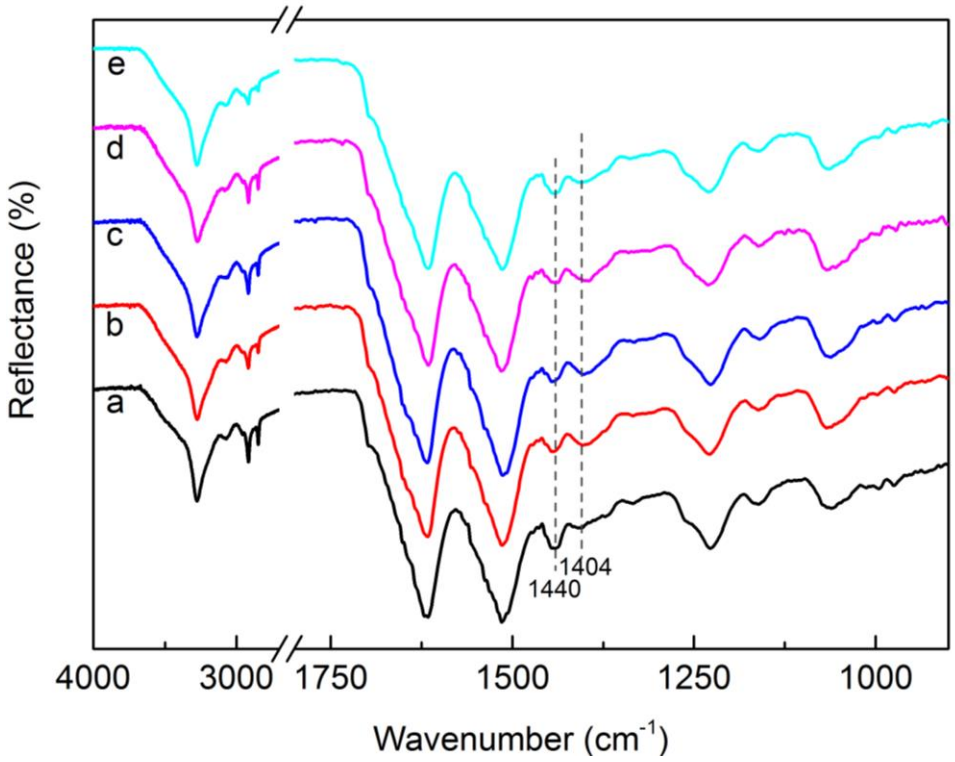

Figure 7.10 FTIR spectra of silk fibers samples (a) CS, (b) S-A, (c) S-B, (d) S-DI and (e) S-FA, where all curves were normalized at 3275 cm^{-1}.

7.3.4.2 TG analysis

Thermal behavior of silk samples was analyzed by TGA and their corresponding DTG curves as shown in Figure 7.11. From TG curve, 3 main degradation steps took place in CS including initiation, propagation, and carbonization [12]. The initial mass loss is attributed to the absorbed water in the air. The second decomposition temperature was at 316 ℃ and the final decomposition occurred at 555 ℃. These values were in agreement with other literatures [6, 13]. Moreover, the decomposition temperature of poly(sodium acrylate) prepared by the $Ru(bpy)_3^{2+}$/APS system was at a lower temperature of 442 ℃. From DTG curves, the second decomposition temperature of all S-A, S-B, S-DI and S-FA

samples was the same as CS at 316 ℃. However, the third decomposition temperatures of S-A and S-B samples were lowered slightly to 520 and 513 ℃, while that of S-DI and S-FA decreased significantly to 488 and 504 ℃. It is because of the low decomposition temperature of poly(sodium acrylate). Therefore, TG results support that the polymerization occurred on the silk fibers and hence their thermal stability at third decomposition stage was affected.

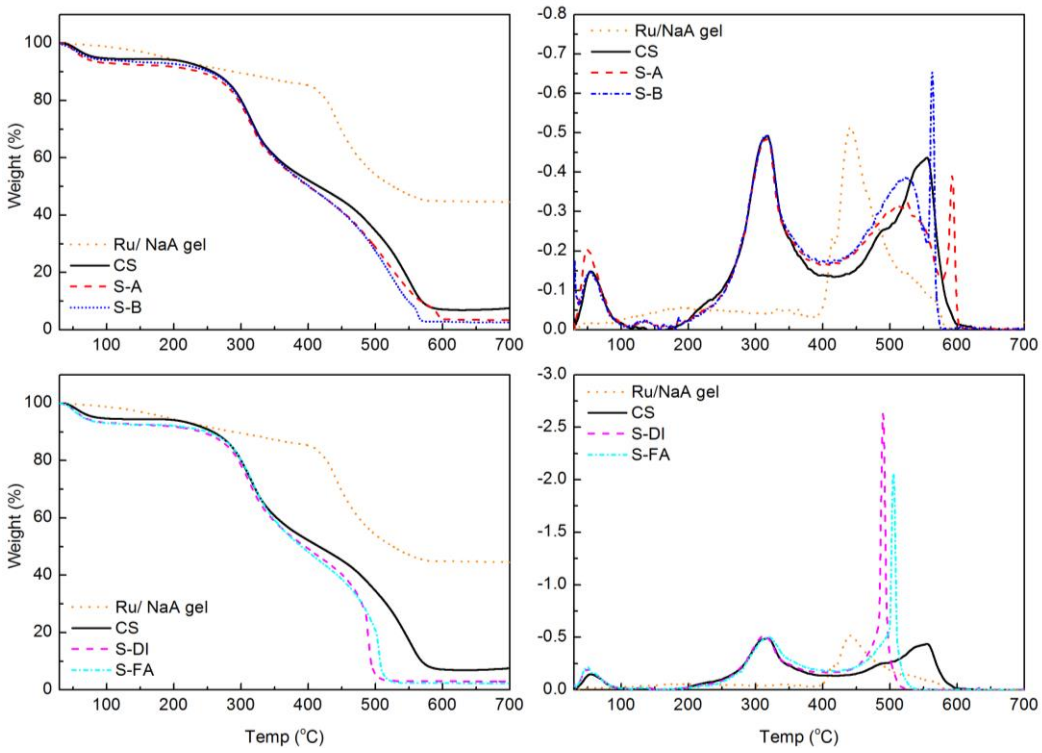

Figure 7.11 TG curves (left) and corresponding DTG curves (right) of the samples: CS, NaA gel prepared from $Ru(bpy)_3^{2+}$/APS system (Ru/NaA gel), S-A, S-B, S-DI, and S-FA.

7.3.4.3 Surface morphology

Surface morphology of the freeze-dried silk samples was observed by SEM as seen in Figure 7.12. The surface of the raw silk fiber was smooth, and its two silk

fibroins could be seen clearly. Its fiber diameter is about 11.5 µm. CS was treated with pure DI water only. Its surface became smoother than that of raw silk and separated silk fibroin was observed. Its fiber diameter was smaller than that of raw silk, probably because of sericin lost.

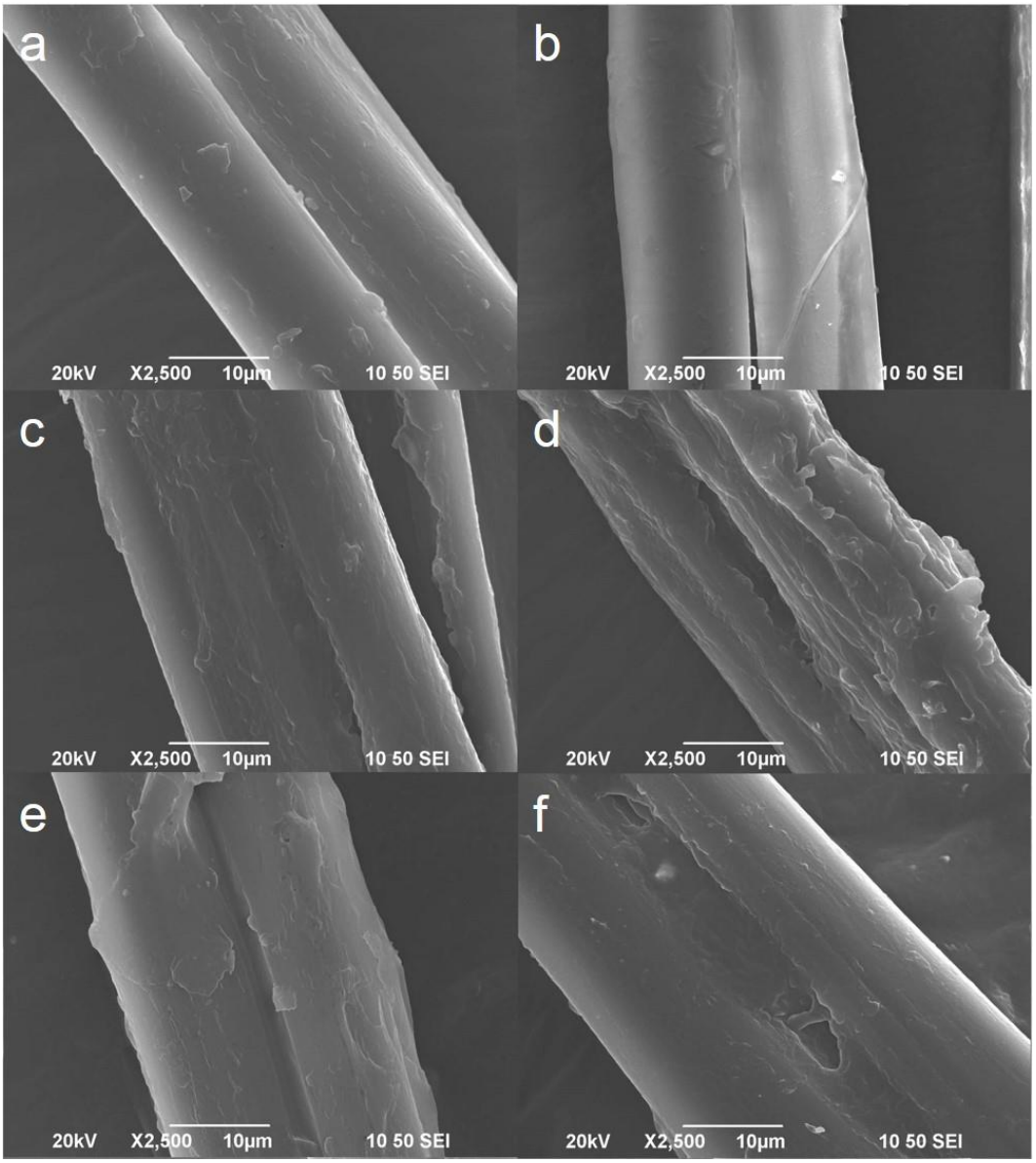

Figure 7.12 SEM images of freeze-dried (a) Raw silk, (b) CS, (c) S-A, (d) S-B, (e) S-DI, and (f) S-FA.

After polymerization, the surface of all silk samples appeared differently. Compared to the smooth surface of raw silk, S-A and S-B had a very rough surface, while S-DI and S-FA also showed some unevenness on their surfaces. It be clearly seen that two silk fibroins of S-A, S-B, S-DI, and S-FA were adhered together, while the two fibroins of CS separated with each other. Due to the silk fibers are obtained from natural silk cocoons directly, their fiber diameters may vary slightly for each sample.

7.3.4.4 Water absorption performance

Two methods were used to test their water absorption for a bundle of silk fibers and a single silk fiber. By using the gravitational method, water absorption ratio of a bundle of silk fibers were measured by weighing the change after immersion in DI water. As shown in Table 7.5, the water absorption ratio of CS was only 1.8 g/g, while that of silk samples was over 8.0 g/g. Though no trend was observed among these modified silk fibers bundle, all of them achieved at least 4 times higher water absorption ratio than that of CS. It indicates that the polymerization of sodium acrylate successfully enhanced the water absorption ability of the silk fibers using the $Ru(bpy)_3^{2+}$/APS system.

Moreover, the water absorption of individual fibers was measured by using TGA. In order to minimize the water trapped in between the silk fibers, the silk fibers were fully swelled in DI water and taken out one by one. TG curves

obtained from the fully swollen silk fiber samples were shown in Figure 7.13. The weight loss percentage of CS was around 40% only, while the modified silk samples lost more than 60% of their wet weight. Their water contents were calculated from the TG curves as shown in Table 7.6. The water content of CS was 0.7 g/g that was much lower than that of the modified silk samples. The water content of these modified silk fibers was two to five times higher than that of CS.

Comparing with the bulk water absorption measurement, the water content for single fiber was low. It is because the water trapped in between the silk fibers is minimized. However, the water content shows consistency with the diameter change of a single fiber swelling in DI water. Among the silk samples, S-B shows the largest diameter change and achieves the highest water content value, while CS shows the smallest diameter change and obtains the lowest water content value. Therefore, both water absorption results of fiber bundles and single fiber confirm the improvement of water absorption ability of silk fibers via polymerization of sodium acrylate on silk fiber using $Ru(bpy)_3^{2+}$/APS system.

Table 7.5 Bulk water absorption ratio of samples at equilibrium absorption.

Samples	Water absorption ratio (g/g)
CS	1.8
S-A	8.7
S-B	8.0
S-DI	8.9

S-FA	8.6

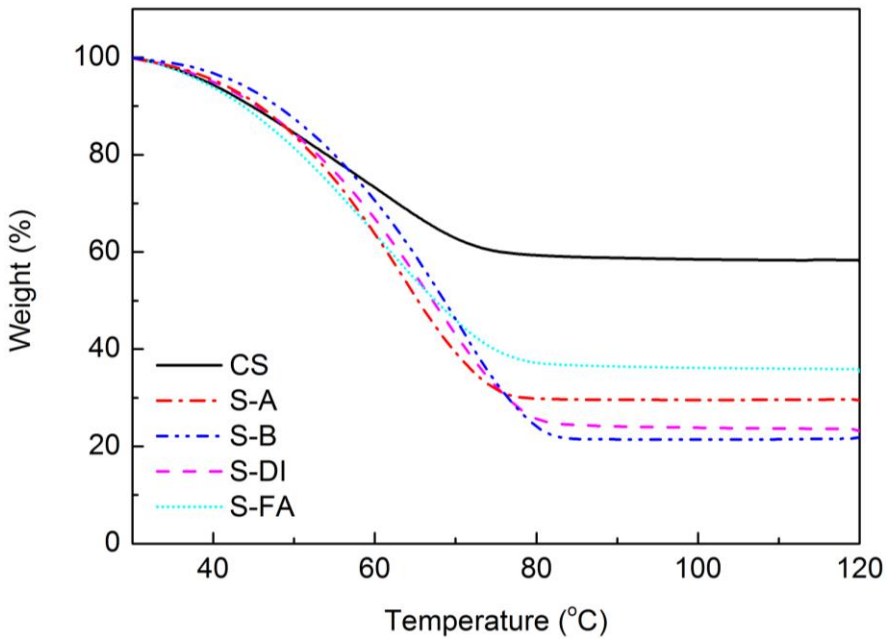

Figure 7.13 TG curves of weight % of wet samples at equilibrium water absorption against temperature.

Table 7.6 Single silk fiber water content of samples calculated from TG curves.

Samples	Water content [a] (g/g)	Diameter change (μm/μm)
CS	0.7	1.0
S-A	2.4	1.4
S-B	3.7	1.6
S-DI	3.3	1.4
S-FA	1.8	1.3

[a] Water content (g/g) is calculated by

$$\text{Water content} = \frac{W_w - W_d}{W_d} \qquad \text{(Equation 7.4)}$$

where W_w is the total weight of single wet silk fibers at equilibrium absorption (g), and W_d is the total weight of single dry silk fibers (g).

7.4 Summary

Silk fibers were further modified by NaA polymerization using the $Ru(bpy)_3^{2+}$/APS system. Using the one-step method, it clearly showed that the photo-induced crosslinking of silk fibers was not strongly affected by NaA. Therefore, the silk fibers were modified via two approaches—drying method and swelling method. These modified silk fibers were crosslinked and able to maintain its fiber shape as observed under optical microscope by dissolution in 9.3 M LiBr. FTIR and TGA results confirmed the structural changes owing to the polymerization of sodium acrylate. The water absorption performance of silk fibers was significantly improved after modification. Since the silk fibers were crosslinked and deposited with poly(sodium acrylate) on surface, these successfully modified silk fibers will be favorable in biomedical textiles applications.

References

[1] Das, A. M.; Chowdhury, P. K.; Saikia, C. N.; Rao, P. G. Silk fibre modification through graft copolymerization using vinyl monomer. *Indian J. Fibre Text.* **2010**, 35, 107-114.

[2] Tsukada, M; Arai, T.; Winkler, S.; Freddi, G. Physical properties of silk fibers grafted with vinyltrimethoxysilane. *J. Appl. Polym. Sci.* **2001**, 79(10), 1764-1770.

[3] Guan, J.; Chen, G. Performance of flame retardancy silk modified with water-soluble vinyl phosphoamide. *J. Appl. Polym. Sci.* **2013**, 129, 2335-2341.

[4] Maji, T. K.; Basu, D.; Datta, C.; Banerjee, A. Studies of mechanical and moisture regain properties of methyl methacrylate grafted silk fibers. *J. Appl. Polym. Sci.* **2002**, 84(5), 969-974.

[5] Bajpai, S. K.; Chand, N.; Mary G. Preparation of poly(acrylonitrile)-grafted silk fibers with antibacterial properties. *Fiber. Polym.* **2010**, 11(3), 338-345.

[6] Das, A.; Saikia, C. N.; Hussain, S. Grafting of methyl methacrylate (MMA) onto Antheraea assama silk fiber. *J. Appl. Polym. Sci.* **2001**, 81(11), 2633-2641.

[7] Zhang, F.; Lu, Q.; Ming, J.; Dou, H.; Liu, Z.; Zuo, B.; Qin, M.; Li, F.; Kaplan, D. L.; Zhang, X. Silk dissolution and regeneration at the nanofibril scale. *J. Mater. B.* **2014**, 2, 3879-3885.

[8] Kirwan, L. J.; Fawell, P. D.; van Bronswijk, W. In Situ FTIR-ATR Examination of Poly(acrylic acid) Adsorbed onto Hematite at Low pH. *Langmuir* **2003**, 19, 5802-5807.

[9] Li, H.; Tripp, C. P. Interaction of Sodium Polyacrylate Adsorbed on TiO2 with Cationic and Anionic Surfactants. *Langmuir* **2004**, 20, 10526-10533.

[10] Boulet-Audet M.; Lefèvre, T.; Buffeteau, T.; Pézolet. M. Attenuated total reflection infrared spectroscopy-an efficient technique to quantitatively determine the orientation and conformation of proteins in single silk fibers. *Appl. Spectrosc.* **2008**, 62, 956-962.

[11] Koperska, M. A.; Pawcenis, D.; Bagniuk, J.; Zaitz, M. M.; Missori, M., Łojewski, T.; Łojewski, T. Degradation markers of fibroin in silk through infrared spectroscopy. *Polym. Degrad. Stabil.* **2014**, 105, 185-196.

[12] Mishra, M.; Nayak, P. K.; Sahu, G. Graft copolymerization of methyl methacrylate (MMA) onto silk using potassium peroxydiphosphate–cysteine (PP–Cys) redox system. *J. Appl. Polym. Sci.* **1982**, 27, 2403-2408.

[13] Ojah, R.; Dolui, S. K. Graft copolymerization of vinyl monomers onto silk fibers initiated by a semiconductor-based photocatalyst. *J. Appl. Polym. Sci.* **2007**, 105, 2164-2175.

Chapter 8

Conclusion and suggestions for future work

8.1 Conclusion

Polyacrylonitrile (PAN) is the main component for producing acrylic fiber. An important feature of PAN is that it can be stabilized by the oxidative stabilization, being pivotal for the success in post-treatment. Its fiber diameter can be lowered from micro- to nano-scale via a simple and versatile method, that is, electrospinning. This oxidative stabilization kinetics involves three main reactions including cyclization, dehydrogenation, and carbonylation. Fourier transform infrared (FTIR) spectroscopy was employed to monitor the relative reaction rates. After heating the as-electrospun PAN nanofibers under different temperatures and durations, some representative peaks appeared in FTIR spectra. These peaks, which were normalized to the nitrile group at 2242 cm^{-1}, were evaluated to compare the relative reaction rates. It was found that the relative rates follow the order of cyclization > dehydrogenation > carbonylation in PAN nanofibers during stabilization. Because of more effective oxygen diffusion, difference in stabilization kinetic rates was revealed between the microfibers and nanofibers. By extraction in dimethylformamide, the gel content was found to increase with heating temperature and duration of stabilization process. Furthermore, the fiber integrity against the alkaline hydrolysis was observed

under scanning electron microscope (SEM). Therefore, it is confirmed that PAN is stabilized and crosslinked during oxidative stabilization. Through proper controls of heat treatment, the crosslinked PAN nanofiber is suitable for preparing the hydrogels.

Heat-treated PAN nanofibers further underwent alkaline hydrolysis to produce hydrogels. These hydrolyzed PAN webs maintained their integrity and showed highly interconnected pore structures in the freeze-dried hydrogels under SEM. Their FTIR spectra indicated the presence of solubilizing groups including $–CONH_2$, –COOH, and $–COO^-$ in the hydrolyzed PAN. Their highly interconnected pore structure greatly enhanced their swelling rate, while their solubilizing groups significantly improved their swelling ability. As a result, the optimized hydrogels achieved very high absorption ratio (Q) of over 100 g/g within 1 min. By considering both suitable heating and alkaline hydrolysis treatments, electrospun PAN webs have been successfully converted into the fast superabsorbent hydrogels.

Another common textile material silk has been used for thousands of years in textile industry. Two approaches have been applied to modify the water absorption behavior of silk. Firstly, because of its high swelling degree without dissolution in low LiBr concentration, the silk yarns were modified through in situ acrylamide and sodium acrylate polymerization in 4.65 M LiBr solution. The swelling of silk yarns in 4.65 M LiBr without losing their fiber integrity were

clearly discovered under optical microscope. The in situ polymerization of acrylamide and sodium acrylate in the silk yarn was identified by FTIR spectroscopy. An interesting ladder structures were obtained in between adjacent filaments of the modified silk yarns via SEM images. Our modified silk yarns achieved a significant improvement in water absorption ratio and also mechanical property. These fascinating improvements were due to the interpenetrating network structure in individual fibroin filament and the composite hydrogel structure along the silk. Thus, our modified silk yarns have been successfully imparted with some favorable properties without destroying their fundamental properties.

Secondly, in order to utilize the chemical structure of silk proteins, the tyrosyl groups on the silk proteins are crosslinked using the photocatalyst tris(2,2′-bipyridyl)dichlororuthenium(II) hexahydrate ($Ru(bpy)_3^{2+}$) and electron acceptor ammonium persulfate (APS). The crosslinking effect on silk fiber was determined under optical microscope by dissolution in 9.3 M LiBr. The existence of crosslinking was further demonstrated by analyzing the resultant residue of the crosslinked silk fiber using FTIR. This environmentally friendly $Ru(bpy)_3^{2+}$/APS system was also proven to be useful in inducing polymerization of sodium acrylate. Silk fibers were further modified by sodium acrylate polymerization in $Ru(bpy)_3^{2+}$/APS system via two methods. The crosslinking effect on these modified silk fibers also existed as observed under optical microscope by

dissolution in 9.3 M LiBr. Meanwhile, FTIR and thermogravimetric results confirmed the chemical and structural changes due to the polymerization of sodium acrylate. These results indicated the co-existence of protein crosslinking and sodium acrylate polymerization in silk fiber. These silk fibers were also effectually modified with higher water absorption.

In this thesis, two common textile materials—polyacrylonitrile (PAN) and silk— have been successfully enhanced in water absorption performance.

8.2 Suggestions for future work

Oxidative stabilization and alkaline hydrolysis are both important in production of fast superabsorbent hydrogel from PAN nanofibers. These as-prepared hydrogels are in form of thin film that is useful in many hygienic applications like baby diapers. Compared with the particle or granular form of superabsorbents, the film form is easier to handle and assemble into the product so the preparation methods for commercial products can be explored. Since the thickness of the superabsorbent film is also a key criterion for commercial products, the control of thickness and preparation of thinner film can be further studied.

Furthermore, since the hydrolyzed PAN electrospun web is in film form, its apparent mechanical strength even in swollen state can be measured. However, its mechanical property is poorer than the as-electropsun PAN web. It is desirable

to enhance its mechanical property at swollen state for other applications. Therefore, several enhancement methods such as fine adjustment on alkaline hydrolysis conditions, employment of co-polymers, and addition of inorganic powders or nanoclays can be further examined to improve its mechanical property.

As reported in the literatures, the silk hydrogel is suitable for some biological applications like dermal reconstruction. Since our modified silks are imparted with high water absorbency, they are suitable for preparing some biomedical textiles such as the wound dressing that absorb the exudates from the wounds. Since these modified silks have high potential application in biological fields, more biological tests such as cytotoxicity test and cell proliferation will be conducted to confirm their suitability.

The modified silk shows improvement in its mechanical property in both dry and wet states. Therefore, the modified silk has high possibility to be woven or knitted into fabric form. It will be beneficial in producing the biomedical textiles for further analysis as a product. In addition, all the modification methods have been applied on a single silk yarn or silk fiber only. In order to increase the production scale, there is a need to investigate the modification directly on silk fabric as well. The properties of the silk fabric prepared from modified silk yarn can be further compared with those of the modified silk fabric.

Since the wet resilience of silk is relatively poor, this effect can be

enhanced by crosslinking of the silk fibroin proteins. In this study, the tyrosyl groups on the silk proteins are crosslinked under the $Ru(bpy)_3^{2+}$/APS system. Therefore, the silk can be knitted or woven into a fabric to further examine its wrinkle recovery angle in both wet and dry state. This silk fabric possibly has an improvement in its wet wrinkle recovery.

One important factor for mass production in industry is the production cost. Although visible light photoredox catalysis requires low cost and renewable light source to perform green chemical reactions under mild conditions, the cost for photocatalyst organometallic ruthenium (II) polypyridine complexes like $Ru(bpy)_3^{2+}$ is still high. As discussed in Chapter 6, this photocatalyst displays reversible behavior under darkness. A further study on the reversibility behavior of this $Ru(bpy)_3^{2+}$/APS system will be conducted so that the expensive $Ru(bpy)_3^{2+}$ can be recycled and hence the production cost can be reduced.

Moreover, the property of the photocatalyst $Ru(bpy)_3^{2+}$ will be studied in depth, especially its behavior to initiate the polymerization at room temperature. As the vinyl monomers contain inhibitor to prevent polymerization, this $Ru(bpy)_3^{2+}$/APS system may not be able to initiate the polymerization. Therefore, some vinyl polymers, such as acrylic acid, can be firstly purified to remove the inhibitor and the observe its polymerization under $Ru(bpy)_3^{2+}$/APS system.